

THESIS

**EVALUATING THE PARAMETER IDENTIFIABILITY AND STRUCTURAL
VALIDITY OF A PROBABILITY-DISTRIBUTED MODEL FOR SOIL
MOISTURE**

Submitted by

Danielle R. Tripp

Department of Civil and Environmental Engineering

In partial fulfillment of the requirements

for the Degree of Master of Science

Colorado State University

Fort Collins, Colorado

Summer 2007

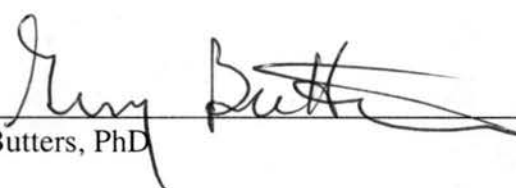
S594
.T775
2007

COLORADO STATE UNIVERSITY

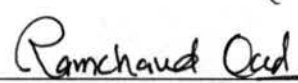
May 18, 2007

WE HEREBY RECOMMEND THAT THE THESIS PREPARED UNDER OUR SUPERVISION BY DANIELLE R. TRIPP ENTITLED EVALUATING THE PARAMETER IDENTIFIABILITY AND STRUCTURAL VALIDITY OF A PROBABILITY-DISTRIBUTED MODEL FOR SOIL MOISTURE BE ACCEPTED AS FULFILLING IN PART REQUIREMENTS FOR THE DEGREE OF MASTER OF SCIENCE.

Committee on Graduate Work




Greg Butters, PhD



Ramchand Oad, PhD



Adviser: Jeff Niemann, PhD



Department Head: Luis Garcia, PhD

ABSTRACT OF THESIS

EVALUATING THE PARAMETER IDENTIFIABILITY AND STRUCTURAL VALIDITY OF A PROBABILITY-DISTRIBUTED MODEL FOR SOIL MOISTURE

Models that use probability distributions to describe spatial variability within a watershed have been proposed as a parsimonious alternative to fully distributed hydrologic models. This study evaluates the performance of a probability-distributed model that simulates local and spatial average soil moisture in a watershed. The model uses well-known expressions for infiltration, evapotranspiration, and groundwater recharge to describe soil moisture dynamics at the local scale. Then, the spatial mean soil moisture is simulated by integrating the local behavior over a probability distribution that characterizes the spatial variability of soil saturation. Ultimately, the model requires time series for precipitation and potential evapotranspiration and calibration of six parameters to simulate the dynamics of the spatial average soil moisture. The model is applied to the Fort Cobb watershed in Oklahoma using one year of data from September 2005 through August 2006. Model performance is evaluated in three main ways. First, the model's ability to reproduce observed local and spatial average soil moisture through calibration is examined. Second, the identifiability and stability of the parameter values are evaluated to assess parameter uncertainty and errors in the mathematical structure of the model. Third, the identifiability and stability of the sensitivities to changes in annual

precipitation and potential evapotranspiration are evaluated to assess the impacts of parameter uncertainty and structural errors on forecasts for unobserved conditions. At the local scale, the calibrated model reproduces the soil moisture with a similar degree of accuracy as a more physically-based model (HYDRUS 1D), and both models exhibit some structural errors. For the spatial average soil moisture, the calibration is acceptable simulating soil moisture with a similar degree of accuracy as the model applied at the local scale. Among all the parameters, the standard deviation of soil saturation is the most stable and identifiable. The probability-distributed model produces a relatively wide range of plausible sensitivities for both the local soil moisture and the spatial mean soil moisture, suggesting that parameter uncertainty and model structural errors produce significant uncertainty for unobserved conditions.

Danielle R. Tripp
Civil and Environmental Engineering Department
Colorado State University
Fort Collins, CO 80523
Summer 2007

ACKNOWLEDGMENTS

The financial support of the U.S. Army Research Office Terrestrial Sciences Program is gratefully acknowledged. Dr. Jeff Niemann provided insight, encouragement, and guidance for this research and for this I am very grateful. I would also like to thank my committee members for taking the time to meet with me and for providing practical insight for this research.

TABLE OF CONTENTS

Signature Page.....	ii
Abstract.....	iii
Acknowledgements.....	v
1 Introduction.....	1
2 Study Area.....	7
3 Model Descriptions.....	11
3.1 Probability-Distributed Model.....	11
3.2 HYDRUS 1D.....	18
4 Results.....	22
4.1 Results for Local Scale.....	22
4.2 Results for Spatial Average.....	36
5 Conclusions.....	47
References.....	49
Appendices.....	53

LIST OF FIGURES

Figure 2.1.....	9
Figure 2.2.....	10
Figure 3.1.....	12
Figure 3.2.....	16
Figure 4.1.....	26
Figure 4.2.....	27
Figure 4.3.....	31
Figure 4.4.....	36
Figure 4.5.....	37
Figure 4.6.....	39
Figure 4.7.....	41
Figure 4.8.....	43
Figure 4.9.....	45
Figure 4.10.....	46

1 Introduction

In recent decades, hydrologic models have become increasingly complex. Prior to the 1980's, hydrologic models were mainly lumped, conceptual models based on water balance. These models typically treat the basin as a single unit using average basin characteristics and ignoring spatial variations. Widely-used examples include the Stanford Watershed Model (Crawford and Linsley, 1964), Sacramento Soil Moisture Accounting Model (Burnash et al., 1973) and the Xinanjiang model (Zhao et al., 1980). Distributed models were introduced in the mid 1980's and account for spatial variability of basin characteristics by dividing a basin into numerous grid cells or other individual units. Basin attributes are then specified for each of these units. A few widely-used examples of distributed models include the SHE model (Abbott et al., 1986; Abbott et al., 1986), THALES (Grayson et al., 1992), and GSSHA (Downer and Ogden, 2002).

The increased complexity of distributed models does not necessarily improve their performance for unobserved conditions due to uncertainty in the values of the model parameters. An increase in complexity may improve the calibration performance due to the increased flexibility in the model behavior, but the ability to identify correct parameter values is typically reduced (Bastidas et al., 1999; Wagener et al., 2004). Parameter sets are typically evaluated by how well they reproduce an observed series of discharges or other variables of interest, and the final parameter values are selected to minimize some measure of disagreement between the simulations and observations. However, it is possible that many parameter sets can reproduce the observations with

similar accuracy. Generalized Likelihood Uncertainty Estimation (GLUE) is a method that aims to assess parameter uncertainty within a model (Beven and Binley, 1992). GLUE assigns a likelihood measure to each parameter set and then plots the likelihood as a function of the individual parameter values. Parameters that are constrained well by the calibration data show high likelihoods over small ranges of the parameter value. Another method for assessing parameter uncertainty is the Regional Sensitivity Analysis (RSA) (Spear and Hornberger, 1980; Hornberger and Spear, 1981), which analyzes the sensitivity of model simulations to changes in the parameter value. This analysis partitions parameter sets into behavioral and non-behavioral sets. Behavioral sets are defined as those that produce model responses similar to the observations. The cumulative distribution of each behavioral set is then plotted as a function of the parameter value. If the cumulative distribution has a uniform gradient over the parameter space, the parameter is not considered important for determining the model's ability to reproduce the observations. Vrugt et al. (2003) proposed the Shuffled Complex Evolution Metropolis (SCEM-UA) algorithm which is a modification of the Shuffled Complex Evolution (SCE-UA) algorithm proposed by Duan (1992). SCEM-UA is a Markov chain Monte Carlo sampler that periodically updates the distribution of the parameters in an effort to identify a global optimum. With a single optimization run, this method simultaneously obtains both the most likely parameter set and its underlying posterior parameter distribution, thus providing insight about parameter uncertainty.

Another issue that affects the reliability of a model is the adequacy of the model's mathematical structure. Most models rely on assumptions to simplify the mathematical description of the physical processes. These assumptions produce errors in the structure

of the equations that are used to simulate the processes. To evaluate structural errors, Wagener et al. (2003) introduced Dynamic Identifiability Analysis (DYNIA), which is based on the GLUE and RSA methodologies. DYNIA divides a calibration time series into a sequence of small windows. For each window, it identifies parameter sets that allow the model to adequately reproduce the observations and then plots the distributions of the preferred parameter values as a function of time. If the preferred values change through time, it suggests that the parameters are being adjusted to overcome shortcomings in the model structure. Wilby (2005) also analyzed parameter stability through time and showed that parameter identifiability and model performance can depend on the period (wet/dry) used for calibration.

Many studies have considered whether the increased complexity of a distributed model allows it to outperform lumped models (Refsgaard and Knudsen, 1996; Boyle et al., 2001; Reed et al., 2004; Carpenter and Georgakakos, 2006). The results of these studies are mixed. For example, Reed et al. (2004) studied 12 distributed models and compared them to the lumped Sacramento Soil Moisture Accounting (SAC-SMA) model. They found that the lumped model performed better than the distributed models in a majority of the cases for simulating streamflow. These results suggest that the additional complexity of distributed models can create parameter identifiability issues that sometimes outweigh the improved descriptions of physical processes.

Probability-distributed models have been proposed as a way to include spatial variability while requiring relatively few parameters. Probability-distributed models are an extension of lumped models that use some kind of probability distribution to describe spatial variation in a watershed. The probability-distributed approach was introduced by

Moore and Clarke (1981) then improved by Moore (1985; 1999; 2007). This model regards soil storage capacity as a stochastic variable to determine the runoff from precipitation events. TOPMODEL shares a certain similarity with this approach. It is a semi-distributed hydrological model that uses a distributed topographic-based index to describe the spatial distribution of runoff production (Beven and Kirkby, 1979). The model can use this index in a spatially-explicit framework or in a frequency-of-occurrence framework that is similar to the probability-distributed approach (Wolock, 1993). Famiglietti and Wood (1994) developed TOPLATS, which uses the TOPMODEL framework to account for spatial variations in a soil-vegetation-atmosphere water-energy balance. Entekhabi and Eagleson (1989) also used probability distributions of precipitation and soil moisture to account for variability within the grid cells of a general circulation model. Niemann and Eltahir (2004; 2005) used probability density functions for soil moisture, precipitation, and potential evapotranspiration (or wet-environment evapotranspiration) to include spatial and temporal variability in a regional water balance model and used the model to assess sensitivity to climate changes.

Parameter uncertainty also affects models that simulate soil moisture, although it has received much less attention in this context. Soil moisture is a key hydrologic variable for understanding land-atmosphere interactions (Entekhabi and Eagleson, 1989), persistence of droughts (Findell and Eltahir, 1997), flood production (Kitanidis and Bras, 1980), etc. Many rainfall-runoff models simulate soil moisture, but most studies do not verify the simulated soil moisture due to the lack of observations. Other studies have focused on simulating local soil moisture using models based on the Richards' equation (Richards, 1931) such as HYDRUS 1D and 1D MIKE SHE (Vrugt et al., 2003; Mertens

et al., 2004; Mertens et al., 2005; Mertens et al., 2006). Some of these studies have also considered the importance of individual parameters for producing soil moisture using the RSA methodology (Mertens et al., 2004; Mertens et al., 2005; Mertens et al., 2006). Similarly, Vrugt et al. (2003) used the SCEM-UA algorithm in order to analyze the probability distributions of the parameter values. All of these studies assessed parameter uncertainty, but they implicitly assume that the model structure is correct.

The main objective of this research is to evaluate the suitability of a simple, probability-distributed model (PDM) to simulate local and spatial mean soil moisture. The model simulates local, depth-averaged soil moisture dynamics using empirical expressions for infiltration, evapotranspiration, and groundwater recharge. The spatial mean soil moisture is determined by integrating the local behavior over a probability distribution that characterizes the spatial variability of soil saturation. A similar version of this model has already been applied to the Illinois River basin to examine the basin's water balance and sensitivity to climate changes (Niemann and Eltahir, 2004; Niemann and Eltahir, 2005). In that case, the model could not be thoroughly tested due to data limitations. Here, a similar model is applied to the Fort Cobb watershed in Oklahoma, which has soil moisture observations available at a 30-minute resolution since September 2005. The model results for both local soil moisture and spatial mean soil moisture are analyzed in three main ways. First, the PDM is assessed in its ability to be calibrated to simulate the observations. Second, the model is assessed for parameter uncertainty and model structural errors using DYNIA. Third, the sensitivities to changes in annual precipitation and potential evapotranspiration (PET) are evaluated in a framework similar to DYNIA in order to assess the impacts of parameter uncertainties and structural errors

on the model's performance for unobserved conditions. At the local scale, the results are also compared to those from a more detailed, process-based model that numerically solves Richards' equation for one-dimensional vertical flow (HYDRUS 1D).

The outline of the paper is as follows. Section 2 describes the Fort Cobb watershed and the available data. Section 3 describes the PDM (Section 3.1) as well as HYDRUS 1D (Section 3.2). Section 4 describes the results first for the local soil moisture (Section 4.1) and then for the spatial mean soil moisture (Section 4.2). Finally, Section 5 summarizes the main conclusions.

2 Study Area

The 813 km² Fort Cobb watershed in southwest Oklahoma is used to evaluate the model. The climate of Fort Cobb is dry sub-humid with an annual precipitation of approximately 820 mm and an annual PET of approximately 1850 mm. The Fort Cobb watershed contains three major subcatchments: Cobb Creek, Lake Creek, and Willow Creek. These subcatchments drain to the 16 km² Fort Cobb reservoir. This reservoir and many of the streams in the watershed have experienced an increase in sediments, nutrients, and pesticides from row cropping and livestock, which makes it a widely studied area (Storm et al., 2003; Fairchild et al., 2004; Geza et al., 2004). The maximum topographic relief of the basin is 182 m. The land cover is approximately 51% cropland, 40% pasture, and 7% forest. The remaining percentage is urban, water, and bare soil (Storm et al., 2003). The unconfined Rush Springs aquifer underlies the watershed. The water table is always more than 2 m below the ground surface, but its depth fluctuates considerably from year to year due to varying irrigation practices (Abbott et al., 2003).

The USDA Agricultural Research Service's (ARS) Grazinglands Research Laboratory collects meteorological and soil moisture data at 15 Micronet stations in the Fort Cobb watershed. Cumulative rainfall, relative humidity, air temperature, and solar radiation are collected at 5 minute increments and volumetric water content measurements for soil moisture at 3 depths (5, 25, and 45 cm) are collected at 30 minute increments. The soil moisture data collection began in September of 2005 and is updated with new data daily. Soil samples were taken during installation of the soil moisture

instruments for calibration purposes. Nearly all the samples were determined to be predominately sand, a few samples were found to be predominately silt, and one sample was predominately clay (Martinez, 2006). Meteorological data are also collected by the Oklahoma Mesonet at 3 stations near or in the Fort Cobb watershed (Fort Cobb, Weatherford, and Hinton).

One year (September 2005 through August 2006) of precipitation, PET, and soil moisture measurements are used to evaluate the model. The precipitation and PET will be used as model inputs (see below), and the soil moisture observations will be used for calibration and evaluation purposes. From the meteorological data, PET was calculated using the ASCE standardized equation (Allen et al., 2005). Short grass is the vegetation type most applicable to the area directly surrounding the stations and was used for simplicity at all 15 stations. Wind speed data is only available at the three Mesonet stations. Wind speeds at the Micronet stations were estimated using a weighted distance approach with the Mesonet data. Then, the spatial average precipitation, PET, and soil moisture were determined using a Thiessen polygon method with the local data from the Micronet stations (Figure 2.1). Among these variables, only the soil moisture exhibited significant spatial variations within the watershed. Thus, precipitation and PET are treated as spatially constant in the analysis, whereas the soil moisture is treated as spatially variable. When the model was previously applied to the much larger (69,000 km²) Illinois River basin, all three variables were treated stochastically (Niemann and Eltahir, 2004). The spatial averages of precipitation, PET, and soil moisture are shown in Figure 2.2. The figure shows that precipitation events were less common during the winter when the PET was also low. As a result, the spatial average soil moisture depends

primarily on the time since the most recent precipitation event. The behaviors at the 5 cm and 25 cm depths are relatively similar, but the soil moisture at 5 cm tends to be more variable through time. Only the soil moisture at the 5 and 25 cm depths are used in this study because the 45 cm data had missing measurements for long periods of the year at multiple stations. At the 5 and 25 cm depths, some of the stations had missing data or unexpectedly high values for soil moisture at certain times (e.g., values between 0.6 and 1.0). Such high values could be a result of the improper instrument calibration or instrument installation errors. These values were excluded when calculating the spatial averages.

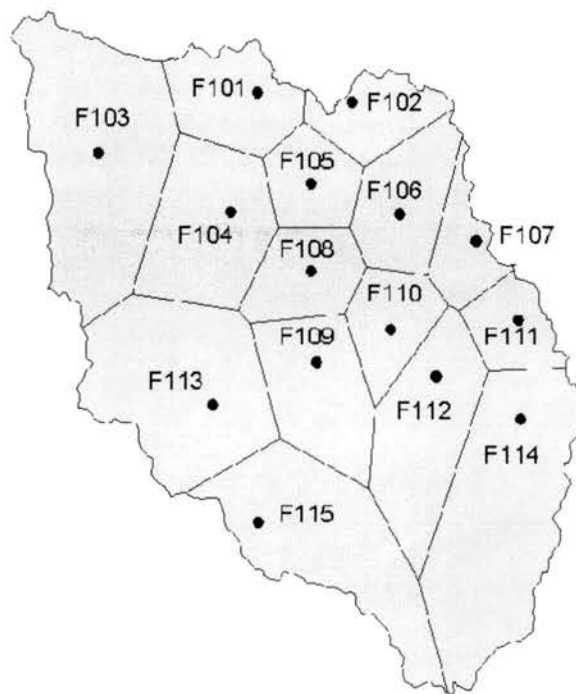


Figure 2.1. Fort Cobb watershed with the thiessen polygons used to calculate the spatial average measurements.

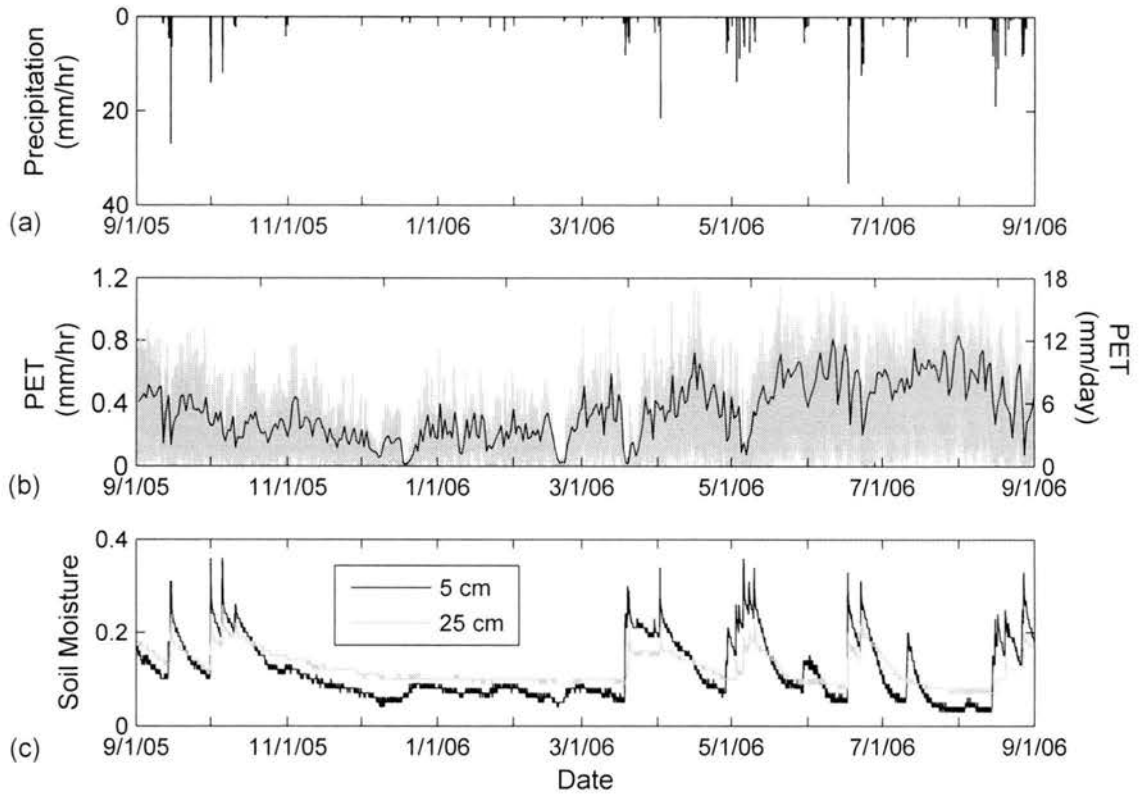


Figure 2.2. Spatial average (a) precipitation, (b) PET, and (c) soil moisture calculated using the local measurements at the Fort Cobb watershed. In part (b), the gray curve shows hourly PET, while the black curve shows the daily total PET. In part (c), the gray curve shows the soil moisture at the 25 cm depth and the black line shows the soil moisture at the 5 cm depth.

3 Model Descriptions

3.1 Probability-Distributed Model

The PDM simulates local, depth-averaged soil moisture by applying a simple water balance. In this model, soil moisture is considered constant with depth in the vadose zone. The model considers two types of locations as shown in figure 3.1: recharge and discharge locations (Niemann and Eltahir, 2004). At recharge locations, the soil may or may not be saturated. Precipitation is partitioned between surface runoff and infiltration, and groundwater recharge can occur. At discharge locations, the soil is assumed to be saturated, and the hydraulic gradient is assumed to be oriented to produce groundwater discharge. No infiltration occurs at these points. Discharge locations are considered to be wetlands and water bodies, such as creeks or reservoirs, where saturated soil conditions are always present. All the soil moisture stations in the Fort Cobb watershed would be considered recharge locations, so these locations are the focus of the analysis. At a recharge location, the soil moisture balance is described as follows:

$$s_t = s_{t-1} + \frac{\Delta t}{\delta \phi} (F - E - G) \quad (1)$$

where s is the depth-averaged degree of soil saturation (volume of water per volume of voids), δ is the depth of the soil for which soil saturation is being calculated, ϕ is the porosity, F is the infiltration rate, E is the evapotranspiration rate, and G is the recharge to groundwater (or drainage from the base of the soil layer). This soil moisture balance can be written in terms of volumetric soil moisture θ as well, where $\theta = s\phi$. For our purposes, δ is selected to be twice the depth of the soil moisture measurement that the

model is used to simulate so that the simulated soil moisture is at the midpoint of the soil column. For example, when comparing to soil moisture at a 5 cm depth, δ is set to 10 cm. Any variations in s within this δ are neglected by the model.

Recharge Location

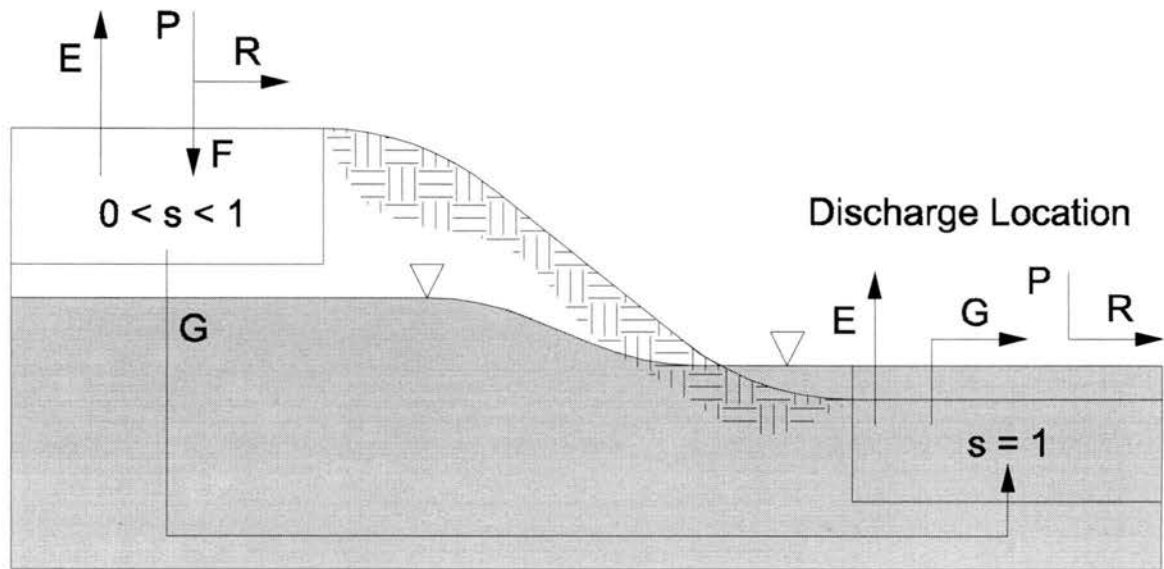


Figure 3.1. Diagram of the PDM framework.

The infiltration rate is determined by the smaller of the infiltration capacity and the precipitation rate. Specifically:

$$F = \begin{cases} F_c & \text{If } F_c < P \\ P & \text{If } F_c \geq P \end{cases} \quad (2)$$

where F_c is the infiltration capacity. The infiltration capacity is defined as $F_c = \alpha(1-s) + K_h$ where α is an infiltrability parameter and K_h is the saturated hydraulic conductivity (Niemann and Eltahir, 2004). Notice that $F_c = K_h$ when the soil

is saturated ($s = 1$), and F_c increases linearly to $F_c = \alpha + K_h$ when the soil is completely dry ($s = 0$).

Evapotranspiration is described as a function of water availability and the PET. Empirical relationships between evapotranspiration efficiency and soil moisture vary depending on the vegetative cover and soil characteristics of the area (Lowry, 1959; Entekhabi et al., 1991). Following Rodriguez-Iturbe et al. (1991) and Entekhabi et al. (1991), E can be written as:

$$E = E_p s^\beta \quad (3)$$

where E_p is the PET and β is the evapotranspiration exponent, which depends on the vegetation characteristics. Lowry (1959) summarized the results of several field studies addressing the relationship between evapotranspiration and soil saturation. In a fully vegetated area, the evapotranspiration rate was closer to the PET rate for all values of s . The model in Equation (3) represents this condition if $\beta < 1$. Entekhabi et al. (1991) set $\beta = 0.5$ for a semi-humid climate in order to represent vegetation. For bare soil conditions, deep rooted plants, or dead vegetation, Lowry (1959) found that the evapotranspiration rate decreases more rapidly from the PET rate as the soil moisture decreases. The model represents this case if $\beta > 1$.

Groundwater recharge is controlled by numerous factors including soil type, soil saturation, water table level, and topography. In this model, recharge to groundwater is described using the well-known percolation model, which assumes that the hydraulic head in Darcy's Law is dominated by the change in elevation. Under this assumption, $G = K_u$, where K_u is the unsaturated hydraulic conductivity. Campbell (1974) wrote

unsaturated hydraulic conductivity as $K_u = K_h s^\gamma$, which implies that the recharge can be written as:

$$G = K_h s^\gamma \quad (4)$$

where γ is the recharge exponent parameter, which depends on the soil texture. Lower values of γ typically correspond to coarser soils such as sands (Clapp and Hornberger, 1978; Wetzel and Chang, 1987). The equations described above control how the PDM simulates depth-averaged soil moisture at the local scale for a recharge location. For a given δ , the parameters α , β , γ , K_h , and ϕ must be calibrated to use the model.

The PDM is also used to simulate the spatial average soil moisture for the watershed. To include some aspects of spatial variability, a gamma distribution is used to describe the spatial variation of soil saturation. Entekhabi and Eagleson (1989) described the spatial variability of soil moisture using a gamma distribution, however they did not test this assumption. The Erlang distribution, a special form of the gamma distribution in which the shape parameter is an integer, was found to describe the spatial variability of soil saturation in the Illinois River basin by Niemann and Eltahir (2004). The assumption of a gamma distribution was also tested for the Fort Cobb watershed. Soil saturation values were calculated by dividing the soil moisture observations by the porosity values that were determined during the model calibration at each station. In particular, the porosity used at each station is the average of the porosities in the 1% of the simulated parameter sets that produce soil moisture with the most accuracy (see details later). The gamma distribution was then tested by applying the Kolmogorov-Smirnov test (Salas et al., 2004). For the 5 cm depth, the gamma distribution is accepted at the 10% significance level for 98.9% of the time periods in the dataset. For the 25 cm depth, the

gamma distribution is accepted at the 10% level for 96.0% of the time periods. The gamma distribution is written:

$$f_s = \frac{k}{\bar{s}\Gamma(k)} \left(\frac{ks}{\bar{s}}\right)^{k-1} e^{-ks/\bar{s}} \quad 0 \leq s < \infty. \quad (5)$$

In this equation, \bar{s} is the spatial mean soil saturation, Γ is the gamma function, and k is the squared inverse of the coefficient of variation ($k \equiv \bar{s}^2 / \sigma^2$), where σ is the spatial standard deviation of soil saturation. Notice that the gamma distribution allows values of soil saturation to be greater than one. When the distribution is used in the model, this portion of the distribution is treated as a probability mass at $s=1$, and this mass is assumed to correspond to the groundwater discharge locations.

To constrain the behavior of the spatial variation of soil saturation, Niemann and Eltahir (2004) proposed that k is constant at all times and found that this was approximately the case for the Illinois River dataset. Here, both k and σ and were examined to determine if either of these can be approximated as a constant. Figure 3.2 plots σ as a function of the spatial average soil saturation for the 12 month period of observation at the 5 cm depth. If σ were exactly constant, the data would plot as a horizontal line. If k was exactly constant, the data would plot along a line through the origin because $1/\sqrt{k} = \sigma / \bar{s}$. This plot shows that neither σ nor k is truly constant for this dataset, but it is better to assume that σ is constant. Note that the most common values of σ are between about 0.05 and 0.15 with lower values occurring when the spatial average soil saturation is moderate to low. A similar behavior is observed for the 25 cm data, so σ is also assumed to be constant at this depth for consistency.

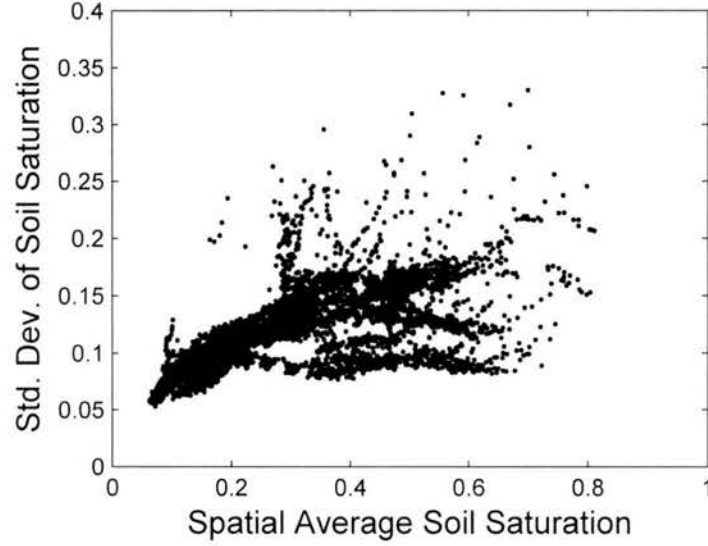


Figure 3.2. A plot of the spatial standard deviation of soil saturation against the spatial average soil saturation for the 12 month period of observation. Soil saturations are calculated by dividing the observed soil moisture values by the average porosity calculated from the 1% of the simulations with the most accuracy.

To determine the spatial mean fluxes, the local fluxes are integrated over the spatial distribution of soil saturation. Locally, the surface runoff is the portion of the precipitation that does not infiltrate into the soil. The spatial mean runoff \bar{R} is then found by integrating the local surface runoff over the spatial distribution of soil saturation. In particular,

$$\bar{R} = \int_{s=0}^1 [P - F_c] f_s ds + \int_{s=1}^{\infty} P f_s ds. \quad (6)$$

where P is the precipitation rate, which is considered to be spatially constant due to the scale at which the model is applied. The first term represents the recharge locations where infiltration can occur, and the second term represents the discharge locations where no infiltration occurs. Evaluating the integrals in Equation (6), one obtains an analytical expression for the spatial mean surface runoff:

$$\bar{R} = P - (\alpha + K_h) \Gamma(k/\bar{s}, k) + \alpha \bar{s} \Gamma(k/\bar{s}, k+1). \quad (7)$$

The spatial mean evapotranspiration \bar{E} can be determined by integrating the local evapotranspiration expression (Equation (3)) over the distribution of soil saturation:

$$\bar{E} = \int_{s=0}^1 E f_s ds + \int_{s=1}^{\infty} E_p f_s ds. \quad (8)$$

Notice that the portion of the gamma distribution with $s \geq 1$ is treated as a probability mass at $s = 1$, so the evapotranspiration rate is equal to the PET. Equation (8) can be analytically solved to obtain an expression for the spatial mean evapotranspiration:

$$\bar{E} = E_p (\bar{s}/k)^\beta \frac{\Gamma(k+\beta)}{\Gamma(k)} \Gamma(k/\bar{s}, k+\beta) + E_p (1 - \Gamma(k/\bar{s}, k)). \quad (9)$$

Similarly, the local groundwater recharge (Equation (4)) can be integrated over the spatial distribution of soil saturation to determine the spatial mean groundwater recharge \bar{G} . In particular:

$$\bar{G} = \int_{s=0}^1 G f_s ds. \quad (10)$$

The integral does not include the part of the gamma distribution where $s > 1$ because this portion represents groundwater discharge locations. Equation (10) can be solved analytically to obtain an expression for the spatial mean groundwater recharge:

$$\bar{G} = K_h (\bar{s}/k)^\gamma \frac{\Gamma(k+\gamma)}{\Gamma(k)} \Gamma(k/\bar{s}, k+\gamma). \quad (11)$$

With these expressions describing \bar{R} , \bar{E} , and \bar{G} , one can apply a water balance to the region, which implies:

$$\bar{s}_t = \bar{s}_{t-1} + \frac{\Delta t}{\delta \phi} [\bar{P} - \bar{R} - \bar{E} - \bar{G}]. \quad (12)$$

Notice that the PDM requires one additional parameter (σ) to simulate the spatial mean soil moisture.

3.2 HYDRUS 1D

HYDRUS 1D is a widely-used, physically-based model for soil moisture simulation. Here, the model is used as a point of comparison when evaluating the performance of the PDM at the local scale. HYDRUS 1D has various options within its framework that allow one to control the complexity of the resulting model (Simunek et al., 2005). Here, the model is applied in a way that requires as few parameters as possible. The governing equation for HYDRUS 1D is Richards' equation (Richards, 1931), which can be written:

$$\frac{\partial \theta}{\partial t} = \frac{\partial}{\partial z} \left[K_u \left(\frac{\partial h}{\partial z} + 1 \right) \right] - R \quad (13)$$

where θ is the volumetric water content, t is time, z is the vertical coordinate (positive upward), K_u is the unsaturated hydraulic conductivity, h is the pressure head (negative if unsaturated), and R is a sink term that is used to account for root water uptake. In this application, the lower boundary condition is assumed to be free drainage because the water table is relatively deep below the root zone. HYDRUS 1D numerically solves Richards' equation to estimate one dimensional vertical saturated or unsaturated water flow.

The sink term R defines the amount of water that is extracted by plant roots at any soil depth to supply transpiration. In this application of HYDRUS, all evapotranspiration is assumed to be transpiration for simplicity, which was also assumed by Skaggs et al. (2006). This assumption was evaluated by using seasonal variations in leaf area index from a similar site in Oklahoma (Gu et al., 2006) to partition the PET into potential

evaporation and potential transpiration using the method from Hupet et al. (2003). Although this partitioning obviously increases the model's complexity, it was found that it does not improve the model's performance at the Fort Cobb watershed. With the additional complexity in separating the evapotranspiration, more parameters would be required making the parameters less identifiable. The sink term R is based on the pressure head, root characteristics, and atmospheric conditions (Skaggs et al., 2006) and can be written as:

$$R = wbE_p \quad (14)$$

where w describes the vegetation's response to water stress, b describes the distribution of water uptake as a function of depth in the soil, and E_p is the potential evapotranspiration, which is assumed to be equivalent to the potential transpiration rate. The van Genuchten (1987) S-shaped function is used to define w . When the plants are not experiencing water stress (i.e. $h = 0$), $w = 1$, and the root water uptake is occurring at the PET rate. As h becomes more negative, w approaches zero causing the root water uptake to decrease from the potential rate. Specifically, this function is written:

$$w = \frac{1}{1 + \left(\frac{h}{h_{50}} \right)^p} \quad (15)$$

where h_{50} represents the pressure head where the transpiration is half of the potential rate and p determines how gradually w changes as h changes. In the literature, p is documented to be 1.5 to 3.0 (Skaggs et al., 2006). Smaller values of p indicate a more gradual transition from potential to reduced root water uptake as a function of h . h_{50}

ranges from -10 to -50 m in the literature (Skaggs et al., 2006). More negative values of h_{50} force h to become more negative in order to reduce the uptake from the potential rate.

The normalized root water uptake distribution b describes the variation of the water uptake within the root zone, which is controlled by the distribution of roots within the root zone. The root distribution is highly dependant on the type of biome in which the plant is located (Jackson et al., 1996). However, nonlinear functions have been found to be more accurate in matching measured root distribution data than the traditional linear functions (Li et al., 2006). As a result, an exponential distribution is used for b , which is similar to the distributions used in previous studies (Raats, 1974; Arora and Boer, 2003; Mertens et al., 2006). Specifically:

$$b = ae^{-a(L-z)} \quad (16)$$

where a is a positive parameter that describes the decrease in root density and water uptake with depth and L is the z coordinate of the ground surface above an arbitrary datum. A larger a value indicates less root water extraction deep in the soil.

The Brooks and Corey expressions are used to describe soil water retention and unsaturated hydraulic conductivity (Brooks and Corey, 1966). These expressions are selected because, when coupled with the free drainage boundary condition, they produce a drainage rate at the bottom of the soil column that is similar to G in the PDM. Using Brooks-Corey, the soil water retention is defined as:

$$s_e = \begin{cases} |vh|^{-n} & h < -1/v \\ 1 & h \geq -1/v \end{cases} \quad (17)$$

where s_e is the effective soil saturation, ν is the inverse of the air-entry pressure, and n is the pore size distribution index. s_e is the amount of the pore space that contributes to the flow of water and is defined as:

$$s_e = \frac{\theta - \theta_r}{\phi - \theta_r} \quad (18)$$

where θ_r is the residual water content. The inclusion of θ_r is the main difference between the Brooks-Corey and Campbell (1974) formulations. The Brooks-Corey unsaturated hydraulic conductivity is written:

$$K_u = K_h s_e^{2/n+l+2} \quad (19)$$

where l is the pore conductivity parameter. In this application, $l = 0.5$ is used, which is the average among many soil types. Specifying this value provides no loss of generality in the model (Mualem, 1976; Assouline, 2005).

The implementation of HYDRUS described above represents the processes with relatively few parameters. Eight parameters must be calibrated including θ_r , θ_s , ν , K_h , n , p , h_{50} , and a . The main difference between the local formulation in the PDM and this formulation of HYDRUS is that HYDRUS explicitly allows and simulates vertical variations in soil moisture.

4 Results

4.1 Results for Local Scale

First the PDM is analyzed in how well it can be calibrated to reproduce observed local soil moisture at the 5 cm and 25 cm depths. Since the PDM does not allow variation in soil moisture with depth, it must be separately applied and calibrated for each depth. The results will be compared to those of HYDRUS 1D. The soil depth in HYDRUS 1D is set to 0.5 m, so it actually simulates both the 5 cm and 25 cm soil moisture values simultaneously. In some applications, this may be a significant advantage over the PDM. However, for purposes of comparison, it is also calibrated separately to reproduce either the 5 cm or the 25 cm soil moisture. The initial soil moisture values supplied to HYDRUS 1D and the PDM are the first observed soil moisture values at the appropriate depth.

To calibrate the PDM, 1000 parameter sets were generated from a uniform joint distribution within independent ranges specified for each parameter. Given the uncertainty regarding the soil characteristics within the watershed, relatively large ranges of parameter values were considered. Specifically, porosity ϕ was allowed to range from 0.25 to 0.60, which is appropriate for most soil types including silts and sands (McWhorter and Sunada, 1985). K_h is sampled from the range 0.001 to 2.0 m/hr, which encompasses most sandy soils. For silt and clay materials, K_h can sometimes be lower than this range (McWhorter and Sunada, 1985). Little information is available about the dependence of the infiltrability parameter α on the soil type. Niemann and Eltahir

(2004) used a value of 0.0036 m/hr for their analysis of the Illinois River basin. Here, this parameter is sampled from the same range as K_h . β is allowed to range from 0.5 to 3, which permits the evapotranspiration equation to represent a broad range vegetative covers. γ spans from 4 to 30, which represents a broad range of soil types. Sands and silts typically have values in the range of 10 to 14. Sands are usually in the lower portion of this range, while finer material, such as clays, can be represented by values from 20 to 30 (Clapp and Hornberger, 1978; Wetzel and Chang, 1987).

To the extent possible, equivalent parameter ranges were used for HYDRUS 1D. ϕ in HYDRUS 1D was allowed to vary from 0.3 to 0.6, where the lower bound is a bit higher than the one used for the PDM. θ_r was allowed to range from 0.001 to 0.10, which encompasses the average values provided for all soil types from Carsel and Parrish (1988). Sands and silts tend to have average values in the range of 0.03 to 0.05. For very fine materials such as clays, θ_r often takes values near 0.10 (Carsel and Parrish, 1988) but can range up to 0.19 (Isrealson et al., 1962; van Genuchten et al., 1989). The inverse of the air entry pressure ν was allowed to vary from 1 to 20 m⁻¹ encompassing the range of values representing most soil types (Dingman, 2002; Scanlon et al., 2002). Soils containing especially coarse material such as gravel can have much higher values of ν . The pore size distribution index n is allowed to vary from 0.1 to 0.6, which allows the exponent for the unsaturated hydraulic conductivity function to span approximately the same range as γ in the PDM. Saturated hydraulic conductivity K_h is sampled from 0.001 to 2.0 m/hr. The range is the same as the one used for the PDM. The root water uptake parameter p has a range from 0.25 to 3.0, and h_{50} spans a range from -30 to -0.01 m. These ranges are slightly different than the root water uptake values reported in the

literature where p spans from 1 to 3 and h_{50} spans from -50 to -10 to m (Skaggs et al., 2006). These reported values cause the root water uptake to occur at the PET rate, then decrease rapidly to essentially zero when s_e approaches zero. Smaller values of h_{50} allows reduced root water uptake to occur with a less negative value of h . This range allows inclusion of the behavior simulated by the PDM, which can produce an immediate reduction from potential uptake with reduced water availability. Lower values of p allow a more gradual transition from potential to reduced uptake, which is another effect the PDM allows. The root distribution parameter a has a range of 2.5 to 10. This range was determined by comparing the cumulative root water uptake distribution with the cumulative distributions of roots for similar biomes as estimated by Jackson et al. (1996).

The performance of each parameter set for a given depth was evaluated using the root mean square error (*RMSE*):

$$RMSE = \sqrt{\frac{1}{N} \sum_{t=1}^N (\theta_{t,obs} - \theta_{t,sim})^2} \quad (20)$$

where N is the number of time steps, $\theta_{t,obs}$ is the observed soil moisture value at that time step, and $\theta_{t,sim}$ is the simulated soil moisture value at that time step. The best parameter sets are those that produce the minimum *RMSE* for a given depth. Other objective functions such as the coefficient of efficiency (Legates and McCabe, 1999), absolute error, and relative error were considered, but the preferred parameters sets were relatively insensitive to this choice.

Figure 4.1 compares the soil moisture simulated by the two models with the observations for station F103 at 5 cm and 25 cm. In all cases, the parameter sets with the lowest *RMSE* are used. All stations were calibrated and produce similar results except as

explicitly noted in this paper, but only station F103 was selected to be described in detail for brevity. Both the PDM and HYDRUS 1D produce soil moisture dynamics that are comparable to the observations. For the 5 cm depth, the minimum *RMSE* is 0.022 for the PDM and 0.028 for HYDRUS. For 25 cm depth, the minimum *RMSE* is 0.020 for the PDM and 0.021 for HYDRUS. These calibrations were performed with the entire year of data, however both HYDRUS and the PDM can be calibrated with the first few months of data and similar results will be reached for simulating soil moisture for the remainder of the year. The soil moisture dynamics simulated by both models are similar, however a closer inspection of the models indicates that they rely on a different partitioning of infiltration into evapotranspiration and groundwater recharge. As described in the previous section, the PDM determines the evapotranspiration and groundwater recharge as functions of soil saturation. In HYDRUS, such explicit relations are not used. Figure 4.2 evaluates the dependence of these two fluxes on soil saturation by plotting G/K_h and E/E_p as a function of soil saturation. For HYDRUS, E is the total amount of evapotranspiration from the soil column, G is the drainage at the lower boundary, and the soil saturation is s_e at the 25 cm depth. The results from HYDRUS are shown by symbols, and the results from the PDM are shown by solid curves. Each line or symbol corresponds to one of the top 5 parameter sets in terms of minimum *RMSE* for the respective model. The first interesting observation is the relatively narrow scatter in most plots from HYDRUS. This result suggests that the explicit dependence of evapotranspiration and recharge on soil saturation in the PDM is consistent with the behavior of HYDRUS in most cases. However, the functional relationships produced by HYDRUS can be very different than those produced by the PDM. This result suggests

that the two models partition infiltration differently. Finally, it is interesting to note that the evapotranspiration results produced by the different parameter sets in HYDRUS are considerably different from each other. Some of these functions are s-shaped and seem to identify the transition between water and energy limited evapotranspiration. Others have a straighter shape that is more similar to the calibrated relationships from the PDM. All of these parameter sets produce similar soil moisture dynamics, but they achieve these results by rather different means. The PDM was also used to simulate soil moisture at the 5 cm and 25 cm depths for the rest of the stations. At the 5 cm depth, the *RMSE* ranged from 0.015 to 0.066 among the stations. At the 25 cm depth, the *RMSE* ranged from 0.015 to 0.055.

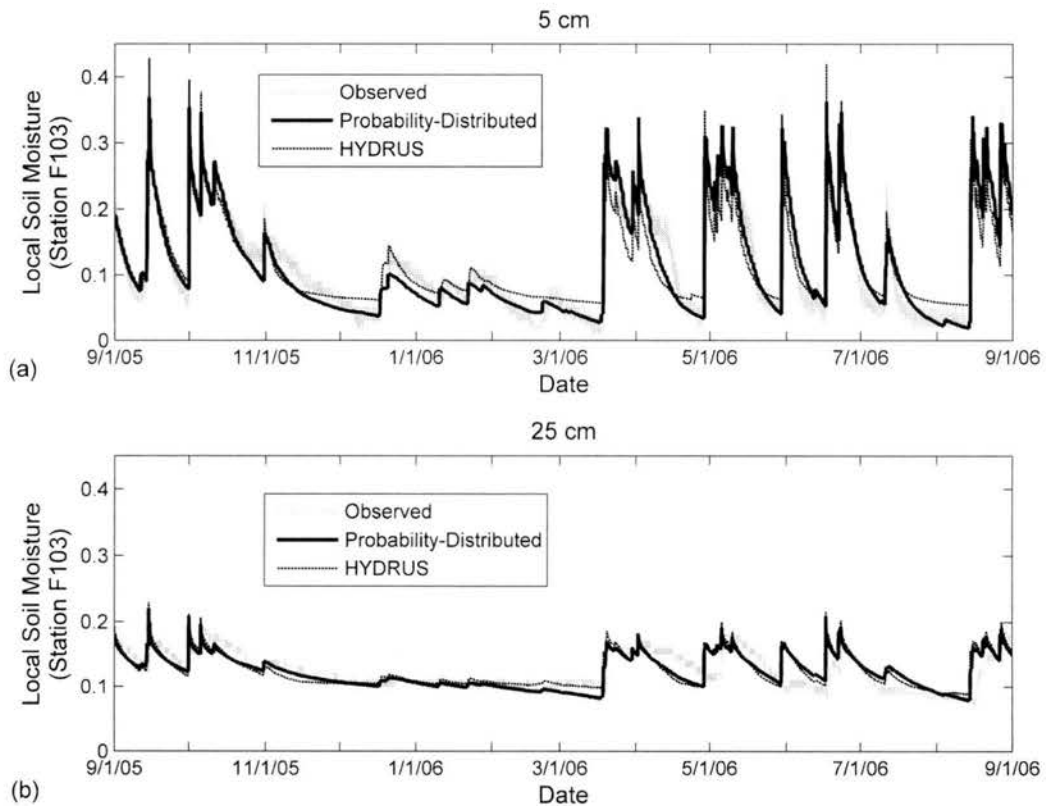


Figure 4.1. Observed and simulated soil moisture at (a) 5 cm and (b) 25 cm depths for Station F103 using the parameter sets with the lowest *RMSE* for both models.

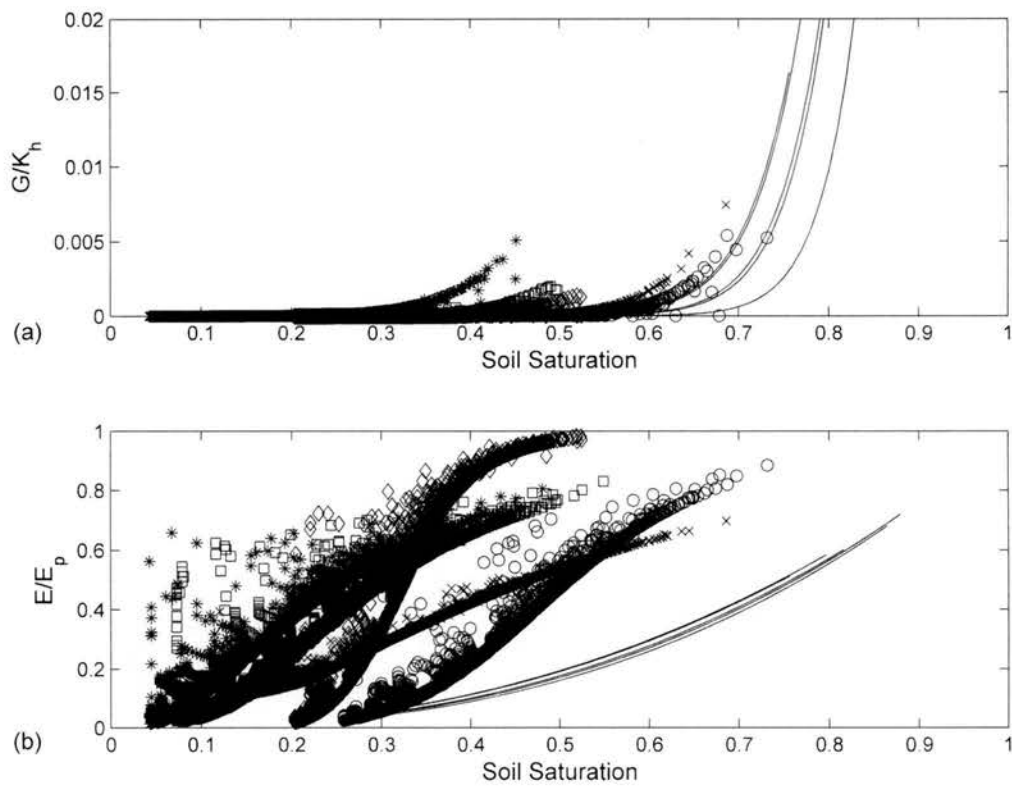


Figure 4.2. Comparison of (a) groundwater and (b) evapotranspiration fluxes as a function of soil saturation for HYDRUS 1D (symbols) and the PDM (solid curves). For each model, the figure shows the results calculated with the 5 parameter sets that produce the lowest *RMSEs*. G/K_h extends up to 0.11 for the PDM during the 12 month simulations, but this is not shown for clarity.

Although both models are capable of reproducing the observed soil moisture after calibration, this tendency does not ensure that the models will produce reliable predictions of soil moisture for unobserved conditions. In particular, the parameter values may be poorly constrained, and the model may have structural errors that become important during unobserved periods. DYNIA (Wagener et al., 2003) is used to evaluate these issues. This method examines how identifiable and stable the preferred parameter values are through time. The underlying argument of this method is that the same parameter values should be selected to reproduce sub-portions of a calibration dataset if

the model structure is correct. If the preferred parameter values change with time, then the parameters are likely being adjusted to overcome deficiencies in the model structure. This procedure utilizes parts of the GLUE framework (Beven and Binley, 1992) and RSA (Spear and Hornberger, 1980; Hornberger and Spear, 1981).

The DYNIA procedure begins with the same 1000 parameter sets that were used in the calibration above. For each parameter set, the soil moisture is simulated for the entire calibration period (1 year). Then, the results of the simulation are evaluated by dividing the calibration record into a series of small windows of time. The windows should be large enough that data fluctuations, diurnal effects, and measurement errors do not affect the results but small enough that wet and dry periods occur in different windows. A window of 2 days was used for this analysis. For each window, the mean absolute error (*MAE*) is calculated for every one of the 1000 parameter sets as:

$$MAE = \frac{1}{N} \sum_{t=1}^{N_t} |\theta_{t,obs} - \theta_{t,sim}| \quad (21)$$

where N represents the number of measurements in the specified window. A likelihood value L is derived for each parameter set by calculating an initial likelihood L_i as $L_i = 1 - MAE$ and then calculating a final normalized likelihood as $L = L_i / \sum L_i$. The most likely parameter sets are those with the lowest *MAE*. For each window, the top 10% of parameter sets in terms of their likelihood are identified, and the likelihoods are again normalized so that they sum to unity in each window. The cumulative distribution of the normalized likelihood is then plotted as a function of the parameter value. The parameter space is divided into 20 bins of equal size, and the gradient of the cumulative distribution within each bin is calculated. A larger gradient indicates the parameter value

is more likely to be contained in that bin. For visualization, the gradient is transformed into shading, with darker shading representing steeper gradients or more likely bins. In the end, the results of DYNIA can be thought of as histograms of the most likely parameter values for small windows of time in the calibration record. It is important to note that the DYNIA analysis draws parameter values from a uniform distribution within the specified ranges for each parameter, so it neglects the possibility of parameter dependence in identifying the likelihood histograms. It also assumes that the observations are correct. A more detailed description of the DYNIA procedure can be found in the MCAT toolkit (Wagener et al., 2004) or in Wagener et al. (2003).

Figure 4.3 shows DYNIA results for selected parameters of the PDM and HYDRUS for the 5 cm depth. Although the results from the entire year were generated, only the first 4 months (fall) are shown for clarity. This period contains a range of wet and dry conditions that is representative of the entire year. The solid black curves in each part of the figure shows the soil moisture dynamics for reference. The gray shading shows the results of the DYNIA analysis. For a selected time, darker shading at a particular value of the parameter indicates that that parameter value is more likely based on the soil moisture observations in that window. The dotted lines show the 90% confidence limits for the parameter value, meaning that there is a 90% likelihood that the parameter falls within these bounds. Figures 4.3a and 4.3b show the DYNIA results for ϕ from the PDM and HYDRUS, respectively. For the PDM, relatively well-defined dark areas are present in the figure, particularly during wet periods, which suggests that the porosity is relatively well-constrained by the calibration data. However, it also suggests that the preferred porosity (indicated by a darker shading at that parameter value) is

around 0.45 for wet periods and drops to about 0.3 during the driest periods. Because porosity is time invariant in reality, this transition most likely suggests that the model exhibits structural errors with the preferred value for porosity changing to compensate for the shortcomings in the equations describing the soil moisture dynamics. For HYDRUS (Figure 4.3b), the porosity is less well-constrained than it is for the PDM because less obvious dark areas are visible in the figure and the 90% confidence limits encompass the entire parameter space during most periods. A weak preference is observed for values around 0.55 during wet periods, while values around 0.30 are preferred in certain dry periods. Overall, however, it is difficult to identify a strong preference for ϕ at any time. Figure 4.3c examines the groundwater recharge exponent γ in the PDM. The figure suggests that γ is not as identifiable as ϕ . During all periods of the year, γ values are constrained to be greater than 10. However, during wet periods, a slight preference is visible for values between 15 and 20. The pore size distribution index n in HYDRUS is similar to the inverse of γ in the PDM. Figure 4.3d shows the DYNIA results for n . Lower n values are considered more likely in wet periods, whereas higher n values are considered more likely in dry periods. Note the dashed lines in the figure which identify the range of the parameter that includes 90% of likelihood changes substantially through time, which suggests that there are significant structural errors because n is a time invariant parameter. Such structural errors could arise from various sources. It is possible that the soil moisture observations contain errors that are related to the level of wetness (e.g., due to the calibration of the instrument). Alternatively, it is possible that some of the simplifying assumptions used in constructing the HYDRUS model are

invalid (e.g., uniform hydraulic parameters with depth, water stress functions, root distribution functions, etc.).

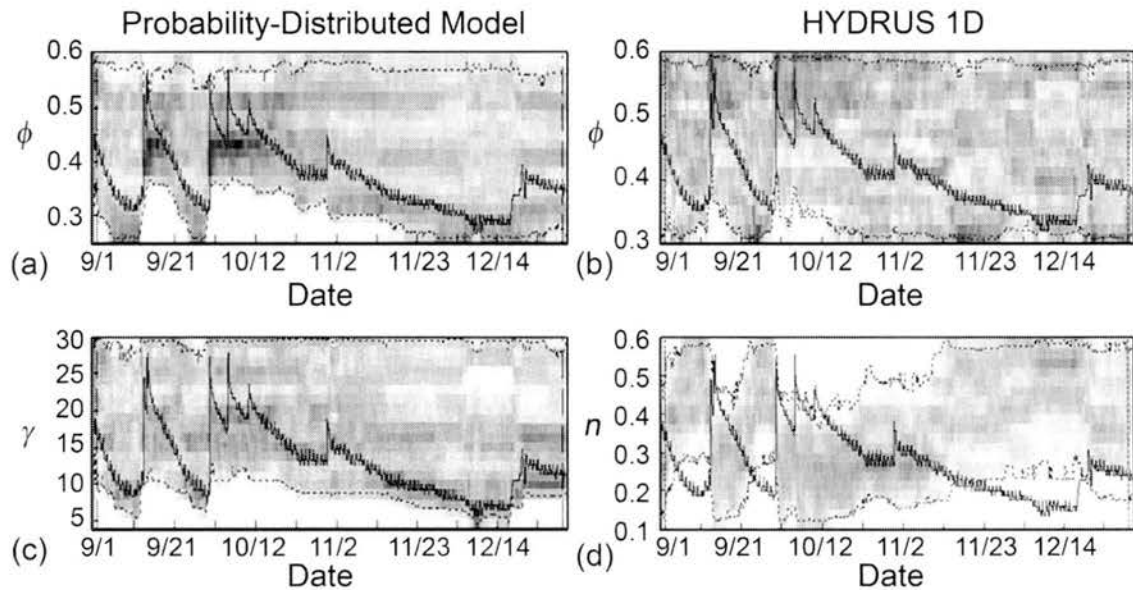


Figure 4.3. DYNIA results for a 4 month period (September 2005 through December 2005) at station F103 at the 5 cm depth. The gray shading shows the likelihood histograms of porosity for (a) the PDM and (b) HYDRUS 1D. Similarly, the shading shows the likelihood histograms of (c) the groundwater discharge exponent for the PDM and (d) the pore size distribution index for HYDRUS 1D. The dashed black lines are the 90% limits of the parameter histograms (i.e. 90% of the likelihood falls within these bounds). The solid black curves show the soil moisture values. The y-axis numbering refers to the parameter values, not the soil moisture values.

Similar results were observed for the parameters that are not shown in Figure 4.3. The parameters α and K_h in the PDM exhibit some variation through time, and the confidence interval spans nearly the entire parameter space. β is relatively identifiable during dry periods with preferred values occurring between 1.0 and 1.5. The DYNIA results for the 25 cm depth at station F103 are similar to the 5 cm results. The only parameter showing a significant difference is ϕ , which tends towards a lower value during all periods and does not show the structural errors that were visible in the 5 cm

results. This result makes sense intuitively because one expects porosity to decrease with depth in the soil. When the PDM is applied to other stations in the watershed, similar results for parameter identifiability and structural errors were obtained. Appendices A and B contain complete DYNIA results for all parameters over the entire year for the PDM at the 5 cm depth and 25 cm depth, respectively. Also DYNIA results for station F113 are included in Appendix C. Most of the remaining HYDRUS parameters were found to be unidentifiable through the year including K_h and ν . θ_r is unidentifiable during wet periods, but shows a concentration of preferred values shifting from 0.08 to approximately 0.03 during moderate to dry periods, respectively. This shift also suggests that structural errors occur in the model. The root water uptake parameters h_{50} and a are relatively unidentifiable as well. The exponent p shifts values suggesting some structural error but is stable and identifiable as a low value during dry periods. DYNIA results for HYDRUS at the 25 cm depth typically indicate similar identifiability issues and structural inadequacies as those observed for the 5 cm depth, but the results are less pronounced. Appendices D and E contain complete DYNIA results for all parameters over the entire year for HYDRUS at the 5 cm depth and 25 cm depth, respectively.

In the end, the calibration and identifiability results suggest that the inclusion of vertical dynamics in HYDRUS do not significantly improve the simulation of soil moisture dynamics (Figure 4.1) or improve parameter identifiability or structural errors (Figure 4.3) when applied to this watershed. Among the two models, only HYDRUS is able to simulate vertical variations of soil moisture, but the simplified structure of the PDM appears adequate if soil moisture is only required for a single depth or averaged over the root-zone. It is important to note that a different conclusion might have been

reached if additional data were available to constrain variations in hydraulic properties with depth and other details in HYDRUS.

While DYNIA is a valuable tool for assessing parameter uncertainty and model structural errors, it does not evaluate the impact of these issues on the model's predictions for unobserved conditions. For example, it is possible that a parameter is poorly constrained but that all plausible values of that parameter produce the same results for unobserved conditions. In such a case, the lack of identifiability may not matter. To qualitatively assess the impacts of parameter identifiability and model structural errors on unobserved conditions, an extension of DYNIA is proposed called Dynamic Sensitivity Analysis (DYNSA). The DYNSA procedure starts by generating 1000 parameter sets from a joint distribution within specified limits on the parameter values. Each parameter set is then used to simulate the observed soil moisture record. For small windows of time, the likelihood of a parameter set is calculated based on the *MAE*. Up to this point, the method is identical to DYNIA. However, rather than plotting the likelihood histogram for each parameter value in each window, the likelihood histogram of a sensitivity is plotted for each window. The sensitivity is calculated by perturbing an input variable (in this case, either precipitation or PET) by a fixed percentage at all times during the calibration period. Here, precipitation and PET are individually increased by 10%. The model is then run for each parameter set using the perturbed input to obtain the resulting soil moisture values. The sensitivity is calculated as:

$$\Psi_p = \frac{\Delta E[s] / E[s]}{\Delta E[P] / E[P]} \quad (22)$$

or

$$\Psi_{E_p} = \frac{\Delta E[s]/E[s]}{\Delta E[E_p]/E[E_p]} \quad (23)$$

depending on whether the precipitation or PET is perturbed. In these equations, $\Delta E[s]/E[s]$ is the change in temporal average soil saturation relative to the temporal average in the calibration dataset. Similarly, $\Delta E[P]/E[P]$ is the relative change in temporal average precipitation, and $\Delta E[E_p]/E[E_p]$ is the relative change in temporal average PET. If the absolute value of a sensitivity is greater than one, then the perturbation is augmented in the soil moisture. If the absolute value of the sensitivity is less than one, the perturbation is dampened in the soil moisture. Once the sensitivity is calculated for each parameter set, the likelihood histogram of the sensitivities are plotted for each window. In this analysis, the sensitivity is used as a measure of the change in model behavior as one moves to unobserved conditions. An infinite number of unobserved cases can occur and the perturbation represents only one of the possible unobserved cases. Yet, the peakedness of the sensitivity histograms gives qualitative insights about how well constrained the sensitivity is with respect to the parameter uncertainty. In addition, time variations in the sensitivity histograms indicate how much the structural errors impact the predictions for this unobserved case.

Figures 4.4a and 4.4b show the DYNOSA results for the PDM at a 5 cm depth for station F103 when precipitation and PET are perturbed, respectively. For the sensitivity to precipitation (Figure 4.4a), the shading indicates that the histograms have a clear peak value. During the wet periods, two distinct bands of preferred values are observed at about 0.12 and 0.22. During the dry periods, one band is preferred between about 0.10 and 0.20, with more preference towards higher values in this range. No consistent band

of preferred sensitivity persists through all of the time windows. Recall that the sensitivity that is being plotted is the average sensitivity calculated from the entire record, not the sensitivity within the individual windows of time. Thus, the observed variations in the sensitivity do not represent actual temporal variations in the response of soil moisture to precipitation but rather changes in the long-term sensitivity that arise due to variations in the most likely parameter values. It is interesting to note, however, that the 90% limits remain relatively stable with time. A similar behavior is observed in the sensitivity to PET shown in Figure 4.4b. In this case, the preferred sensitivities range from about -0.2 to -0.45. Higher sensitivities are observed for drier parts of the record. Overall, these results suggest that parameter uncertainty and structural errors can result in a relatively wide range in sensitivities. Consequently, these issues are expected to be important sources of error when applying the model to simulate unobserved conditions. Appendices F and G contain complete DYNSA results for the entire year for the PDM at the 5 cm depth and 25 cm depth, respectively.

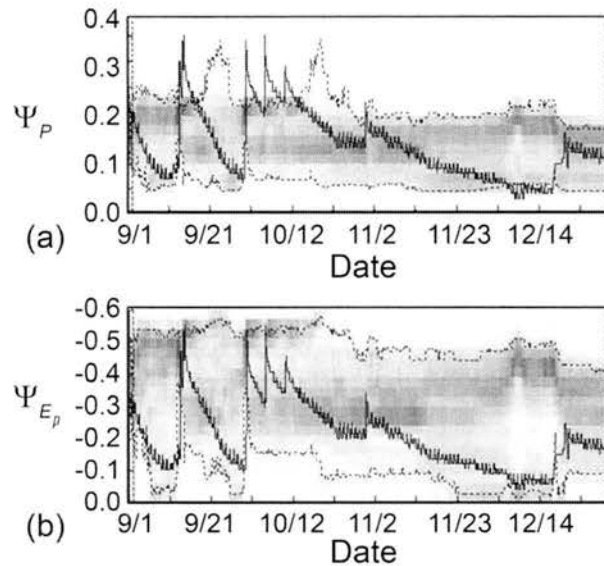


Figure 4.4. DYNSA results for the local soil moisture simulated with the PDM for station F103 at the 5 cm depth using a 4 month period. The gray shading shows the likelihood histogram of sensitivity obtained by increasing (a) precipitation and (b) PET by 10%. The dashed black lines show the 90% confidence limits on the sensitivity, and the solid black lines show the observed soil moisture for reference. Note that the y-axis numbers refer to the sensitivity values, not the soil moisture values.

4.2 Results for Spatial Average

Attention is now focused on the use of the PDM to simulate the spatial mean soil moisture. The analysis in this section is the same as the previous section, except it considers the spatial mean rather than local soil moisture. The model will be evaluated by how well it can reproduce the observed spatial average soil moisture through calibration, how identifiable and stable its parameters are through time, and how stable the sensitivities are to changes in precipitation and PET. It is important to note that the spatial average soil moisture exhibits different behavior from soil moisture at individual stations. For example, Figure 4.5 plots the local soil moisture at two stations (F113 and F110) against the spatial average. As the spatial average soil moisture becomes large, the

soil moisture at one of these stations becomes even larger, while the soil moisture at the other one remains low. This behavior suggests that even though only 15 stations are available in the dataset, the spatial average is determined from a relatively dynamic spatial pattern of soil moisture. Also visible in Figure 4.5 are some of the surprisingly high soil moisture values that occasionally occur in the dataset, but these points are excluded when calculating the spatial average.

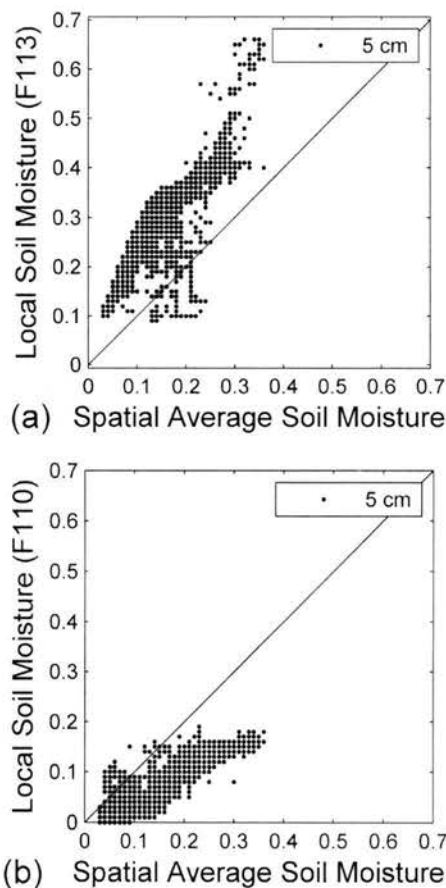


Figure 4.5. Local soil moisture at stations (a) F113 and (b) F110 plotted against the spatial average soil moisture for the 5 cm depth.

To calibrate the model, 1000 parameter sets were generated from a uniform sampling of the parameter space. The model requires one additional parameter σ to simulate the spatial mean soil moisture because the spatial distribution of soil saturation now plays a role. The allowable range for this parameter was selected to be 0.04 to 0.15 based on the field data shown in Figure 3.2. Similar to the analysis of local soil moisture, the model for the spatial mean is calibrated by choosing the parameter set with the lowest *RMSE*. Figure 4.6 shows the spatial mean soil moisture at the 5 cm and 25 cm depths from the calibrated model. At the 5 cm depth, the recession of the mean soil moisture after events appears to be a bit more nonlinear in the model than in the observations. For both depths, the *RMSE* of the model results is similar to that obtained in the analysis of local soil moisture.

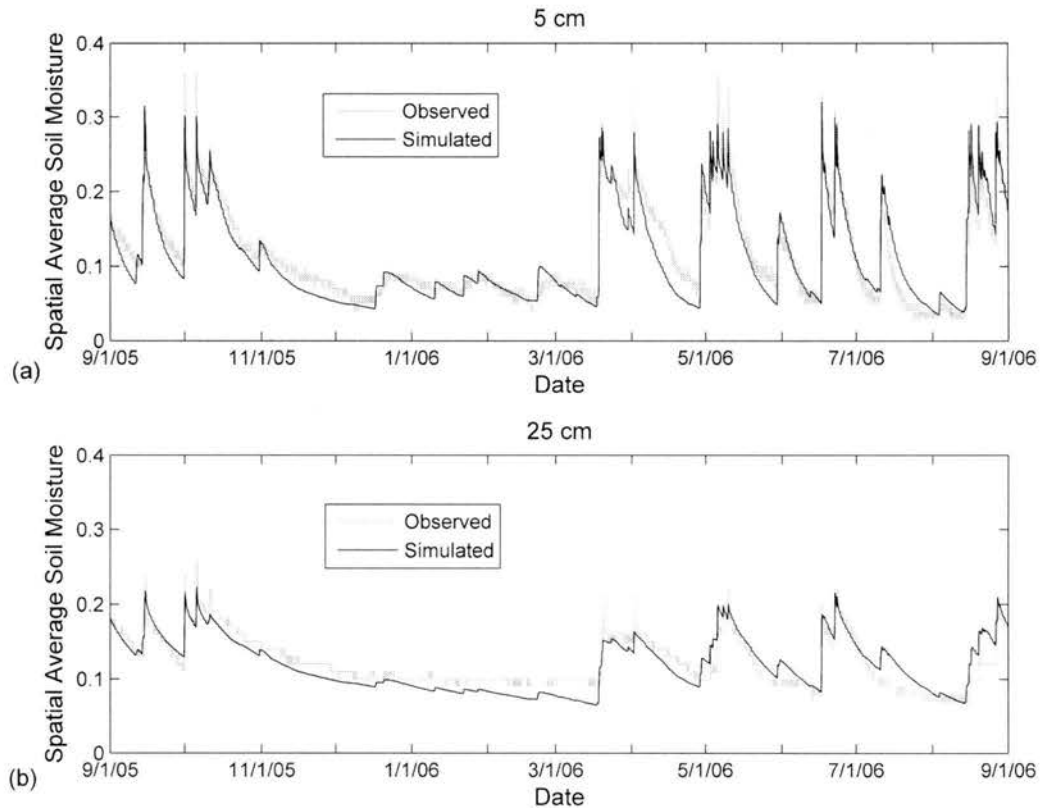


Figure 4.6. Comparison of the observed spatial average soil moisture and the spatial mean soil moisture simulated by the PDM using the parameter set with the lowest RMSE at the (a) 5 cm and (b) 25 cm depths.

So far, the model has been separately applied and calibrated to simulate either the local or spatial mean soil moisture. However, when the model is applied to the spatial mean, it implicitly simulates local soil moisture as well. The model structure implicitly assumes that a single parameter set can apply to both scales. The only distinction between the two scales is that a distribution of soil saturation is included when simulating the spatial mean. To test this assumption, the *RMSE* obtained at each station is examined when using the top 1% of the parameter sets from the calibration against the spatial average soil moisture. This range of *RMSE* should be similar to the range obtained using a local calibration if the model approach is correct. Figure 4.7 shows this comparison.

At most stations, the parameters from the spatial mean are less efficient at simulating the local soil moisture than the parameters determined from the local calibration at each station. For example, the *RMSE* is typically 2 to 3 times larger when using the parameters from the spatial mean at the 5 cm depth. This result is not surprising because spatial variability in a region arises from much more than simply variations in soil saturation as assumed by the model. Thus, the model can be successfully calibrated to simulate either the local or the spatial mean soil moisture, but a single calibration does not reliably simulate both simultaneously.

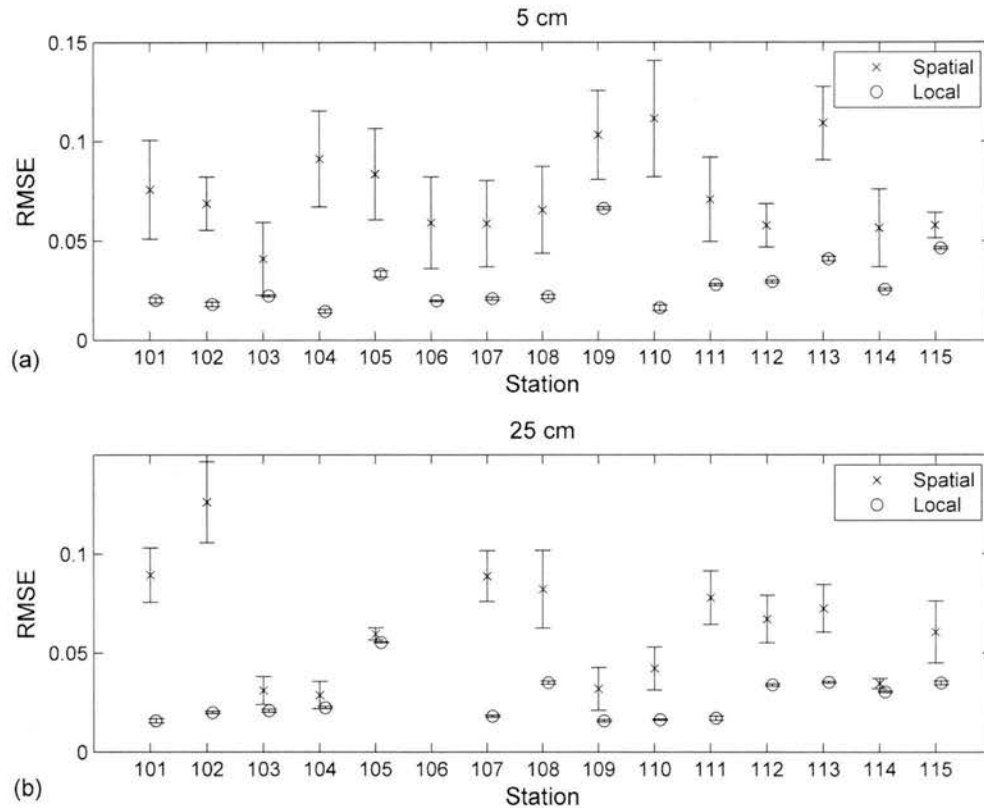


Figure 4.7. A comparison of the ranges of *RMSE* for local soil moisture when simulated with the top 1% of parameter sets from calibrations to the spatial average and to each local gage. The ranges labeled “Local” were calculated by calibrating the local soil moisture in the PDM to reproduce the observed local soil moisture at each station. The ranges labeled “Spatial” were calculated by calibrating the spatial mean soil moisture to the observed spatial average and then applying these parameter sets to simulate the local soil moisture at individual gages. Parts (a) and (b) show the same analysis at the 5 cm and 25 cm depths, respectively.

The DYNIA procedure is also used to evaluate parameter identifiability and model structural errors when simulating the spatial mean. Figure 4.8 shows the results for all six parameters for the first 4 months of the calibration record at the 5 cm depth. The entire year was evaluated but only the first 4 months are shown for clarity. In Figure 4.8a, the porosity ϕ is relatively identifiable at all times but more identifiable during the wet periods. Three stable bands of likely values are visible during the drier calibration period, but only the bands at about 0.45 and 0.55 are observed at all time periods. This

result is similar to the one observed for the local soil moisture in Figure 4.3a. The saturated hydraulic conductivity K_s in Figure 4.8b is only weakly identifiable but shows several distinct bands of likely values. The lowest band (between 0 and 0.5) appears in all conditions, while the bands at higher values tend to appear and disappear during wet and dry conditions. Figure 4.8c shows the results for the infiltrability parameter α . The confidence limits on this parameter span nearly the entire allowable range, which suggests this parameter is mostly unidentifiable. A weak preference for low values is observed during the recession parts of the record. α influences infiltration rates, so it makes sense that this parameter is more identifiable from the recessions immediately after precipitation events than during prolonged periods without precipitation. The evapotranspiration exponent β in Figure 4.8d is more identifiable during drier conditions. This parameter tends to decrease from 2.5 to 1.8 as the soil dries, which suggests some structural errors in the model. The groundwater recharge exponent γ in Figure 4.8e is more identifiable during wetter periods when its most likely values are between about 20 and 25. It is interesting to note that the models for evapotranspiration and recharge are very similar to each other in their mathematical form. The main difference is that the evapotranspiration depends on the observed PET, whereas the groundwater recharge relies on a constant parameter (saturated hydraulic conductivity) instead. Loosely speaking, the model can only distinguish these two fluxes by identifying a correlation between PET and changes in spatial mean soil moisture. The low identifiability in Figures 4.8d and 4.8e suggests that the relationship between these two variables is weak. Figure 4.8f evaluates the standard deviation σ . This parameter is identifiable during the entire calibration period, particularly during dry periods. The most

likely values are around 0.07. Notice that the actual standard deviation data from Figure 3.2 indicates a similar value for the standard deviation during dry periods. It is interesting that the model for the spatial mean identifies this parameter value because it is given no information about the spatial variation in soil moisture aside from the gamma distribution.

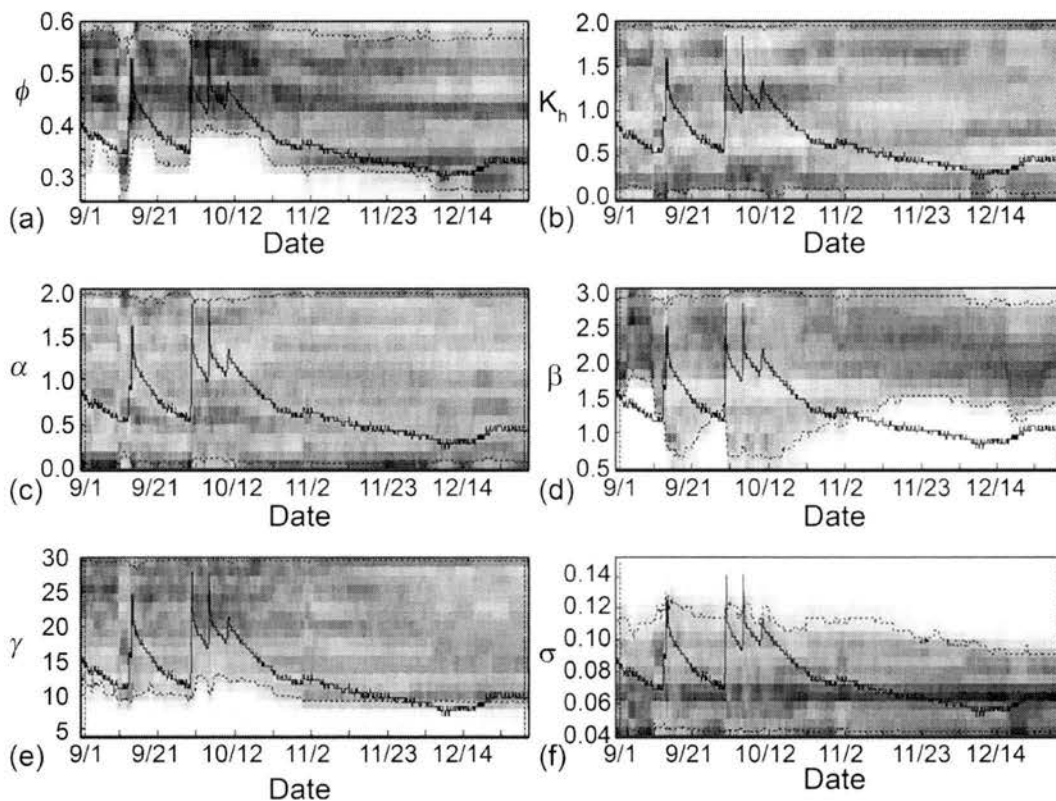


Figure 4.8. DYNIA results for the parameters of the PDM applied to the spatial mean soil moisture at the 5 cm depth. The individual plots consider the following parameters: (a) porosity, (b) saturated hydraulic conductivity, (c) infiltrability, (d) evapotranspiration exponent, (e) groundwater recharge exponent, and (f) standard deviation of soil saturation. The solid black curves show the spatial average soil moisture for reference, and the dashed black curves show the 90% limits on the parameter values. Only the first 4 months of the analysis are shown for clarity.

Similar results are obtained when applying the DYNIA procedure to the spatial mean soil moisture at the 25 cm depth. α is the only parameter indicating significant

differences between the two depths. At 25 cm, α is not identifiable at all. This result makes intuitive sense because it suggests that the soil moisture at a greater depth is less indicative of the infiltration characteristics at the ground surface. Appendices H and I contain DYNIA results for the entire year for the PDM applied spatially at the 5 cm and 25 cm depths, respectively.

The DYNOSA analysis was also performed using the spatial mean soil moisture to assess the impact of parameter uncertainty and model structural errors on model predictions for unobserved conditions. In this analysis, the precipitation or PET is perturbed by 10% and the resulting sensitivities of the spatial mean soil moisture are calculated for each parameter set. Figure 4.9 shows the histograms of the sensitivities to precipitation and PET from the DYNOSA analysis. The histograms of both sensitivities are relatively stable through time, although larger values are considered more likely during drier periods. It is interesting to compare the sensitivities in Figure 4.9 to the sensitivities of local soil moisture in Figure 4.4. In general, the changes in the most likely sensitivities are more gradual for the spatial mean than the local soil moisture. Also, the most likely sensitivities to precipitation tend to increase during dry periods for the local and spatial mean soil moisture. For the local soil moisture, the most likely sensitivities to precipitation are usually between 0.10 and 0.20. For the spatial mean soil moisture, the most likely sensitivities are usually between 0.10 and 0.15. The lower sensitivity for the spatial mean indicates that the perturbation is softened by including a range of soil saturations through the probability distribution. For both the local and spatial mean, the most likely sensitivities to PET are between about -0.25 and -0.45, with a preference toward the more negative sensitivities during the drier periods.

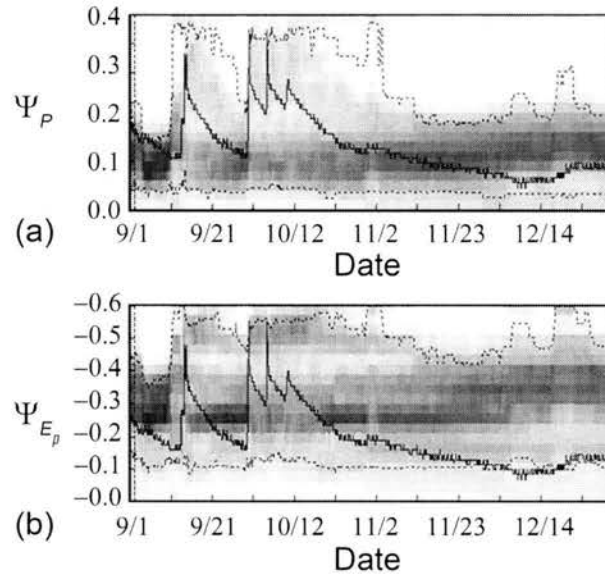


Figure 4.9. DYNOSA results for the spatial mean soil moisture simulated with the PDM at a 5 cm depth using a 4 month period. The gray shading shows the histogram of sensitivity obtained by changing (a) precipitation and (b) PET by 10%. The dashed black lines show the 90% limits on the sensitivity, and the solid black lines show the observed spatial average soil moisture for reference. Note that the y-axis numbers refer to the sensitivity values not the soil moisture values.

Recall that the sensitivity plotted in the DYNOSA analysis is the sensitivity for the entire record, not the sensitivities within the individual windows of time. Thus, the observed variations in the sensitivity represent changes in the long-term sensitivity that arise due to variations in the most likely parameter values. For comparison, Figure 4.10 plots the sensitivity to PET that is calculated within each window. In particular, it shows:

$$\psi_{E_p}(i) = \frac{\Delta \bar{s}(i) / \bar{s}(i)}{\Delta E_p(i) / E_p(i)} \quad (24)$$

where $\Delta \bar{s}(i) / \bar{s}(i)$ is the relative change in the spatial mean soil moisture for each time step i that results from the specified relative change in PET $\Delta E_p(i) / E_p(i)$, which is 0.10.

For each window, this sensitivity is calculated for the 10% of the parameter sets that

produce the lowest *RMSE* for the entire calibration period of spatial average soil moisture. Histograms of sensitivity are then calculated for each window and plotted in a similar format as the DYNIA and DYNOSA results.

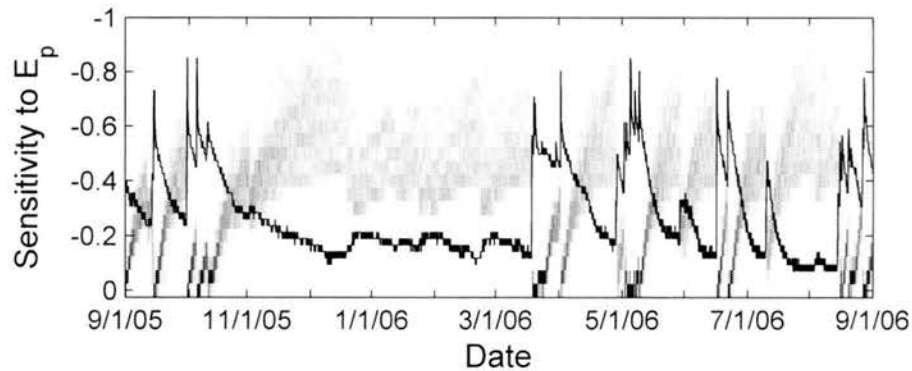


Figure 4.10. Sensitivity of simulated spatial mean soil saturation at each point in time to changes in PET. The gray shading is the histogram of sensitivities at each time for the top 10% of parameter sets in terms of the *RMSE* at that point in time.

Figure 4.10 shows the results of this analysis, which are very different from Figure 4.9. Because the same parameters are used at all times in Figure 4.10, any temporal variations are temporal variations in the sensitivity of the spatial mean soil moisture itself. In the periods immediately after precipitation events, the spatial mean soil moisture is very insensitive to changes in PET because the soil moisture is controlled by the infiltration process. After these periods, the sensitivity of the spatial mean soil moisture increases to a range of values (roughly -0.3 to -0.6) that remains relatively constant through time. The sensitivity plotted in Figure 4.9 is in the lower part of this range because it is essentially a temporal average of the sensitivities shown here. The spread of sensitivities observed in Figure 4.10 is also an indication of the uncertainty that results from the parameter identifiability.

5 Conclusions

The main conclusions of this analysis are as follows:

1. The descriptions that the PDM uses to describe the hydrologic fluxes at the local scale can be calibrated to reproduce local soil moisture with accuracy that would be adequate for many applications. Even though the model relies on only 5 parameters, the identifiability of those parameters is limited. In some cases such as porosity, the most likely parameter values changed depending on the portion of the calibration data that was considered. The most likely explanation of this behavior is that the simple mathematical structure of the model has some deficiencies. It is also possible that the instrument used to observe soil moisture is not correctly installed or ideally calibrated.
2. A simple application of HYDRUS 1D was also calibrated to simulate local soil moisture dynamics. This model has the advantage of including vertical variations in soil moisture that result from simulating Richard's equation and distributed root water uptake. However, the model also requires more parameters (8). After calibration, HYDRUS 1D reproduces the local soil moisture observations with similar accuracy as the PDM. These results support the point made in various other papers, which is that complex models must be supported by additional data in order to produce improvements in performance over simple models. HYDRUS 1D also exhibits relatively low parameter identifiability and temporal variations in the most likely parameter values in some cases (n). These variations may result from errors in the

mathematical structure of the model, variations of the hydraulic properties with depth, or data collection problems.

3. The PDM can also reproduce the spatial average soil moisture after calibration, but it cannot simultaneously simulate both the local and spatial mean soil moisture using the same parameter sets. This result suggests that the use of a probability distribution of soil saturation to treat spatial variations within the watershed has limitations. Many of the parameters are also weakly identifiable when simulating the spatial mean (e.g., α), and some exhibit changes in the preferred values through time (e.g., β). Interestingly, the most stable and identifiable parameter is the standard deviation of soil saturation σ , which actually varies with time in the watershed based an analysis of the spatial variations of soil moisture between stations.
4. A new method, Dynamic Sensitivity Analysis (DYNSA), was developed to assess the impact of parameter identifiability and model structural errors on predictions for unobserved conditions. This method calculates the likelihood distribution of the temporal average sensitivities to changes in precipitation and PET in a framework similar to DYNIA. When applied to either local or spatial mean soil moisture, the method suggests that both parameter uncertainty and structural errors contribute to uncertainty for unobserved conditions.

References

- Abbott, M.B., Bathurst, J.C., Cunge, J.A., Oconnell, P.E. and Rasmussen, J., 1986. An Introduction To The European Hydrological System - Systeme Hydrologique Europeen, She.1. History And Philosophy Of A Physically-Based, Distributed Modeling System. *Journal Of Hydrology*, 87(1-2): 45-59.
- Abbott, M.B., Bathurst, J.C., Cunge, J.A., Oconnell, P.E. and Rasmussen, J., 1986. An Introduction To The European Hydrological System - Systeme Hydrologique Europeen, She.2. Structure Of A Physically-Based, Distributed Modeling System. *Journal Of Hydrology*, 87(1-2): 61-77.
- Abbott, M.M., Tortorelli, R.L., Becker, M.F. and Trombley, T.J., 2003. Overview of water resources in and near Wichita and affiliated tribes treaty lands in western Oklahoma. Water-Resources Investigations Report 03-4024, U.S.G.S., Oklahoma City.
- Allen, R.G. et al., 2005. The ASCE standardized reference evapotranspiration equation. American Society of Civil Engineers, Reston, VA.
- Arora, V.K. and Boer, G.J., 2003. A representation of variable root distribution in dynamic vegetation models. *Earth Interactions*, 7(6).
- Assouline, S., 2005. On the relationships between the pore size distribution index and characteristics of the soil hydraulic functions. *Water Resources Research*, 41(7).
- Bastidas, L.A., Gupta, H.V., Sorooshian, S., Shuttleworth, W.J. and Yang, Z.L., 1999. Sensitivity analysis of a land surface scheme using multicriteria methods. *Journal Of Geophysical Research-Atmospheres*, 104(D16): 19481-19490.
- Beven, K. and Binley, A., 1992. The future of distributed models: Model calibration and uncertainty prediction. *Hydrological Processes*, 6: 279-298.
- Beven, K. and Kirkby, M., 1979. A physically based, variable contributing area model of basin hydrology. *Hydrological Sciences Bulletin*, 24: 43-69.
- Boyle, D.P. et al., 2001. Toward improved streamflow forecasts: Value of semidistributed modeling. *Water Resources Research*, 37(11): 2749-2759.
- Brooks, R.H. and Corey, A.T., 1966. Properties of porous media affecting fluid flow. *Journal of the irrigation and drainage division*, 72(IR2): 61-88.
- Burnash, R., Ferral, R. and RA, M., 1973. A generalized streamflow simulation system: conceptual models for digital computer. Joint Fed-State River Forecast Center, Sacramento, CA.
- Campbell, G.S., 1974. A simple method for determining unsaturated conductivity from moisture retention data. *Soil Science*, 117(6): 311-314.
- Carpenter, T.M. and Georgakakos, K.P., 2006. Intercomparison of lumped versus distributed hydrologic model ensemble simulations on operational forecast scales. *Journal Of Hydrology*, 329(1-2): 174-185.
- Carsel, R.F. and Parrish, R.S., 1988. Developing Joint Probability-Distributions Of Soil-Water Retention Characteristics. *Water Resources Research*, 24(5): 755-769.

- Clapp, R.B. and Hornberger, G.M., 1978. Empirical equations for some soil hydraulic properties. *Water Resources Research*, 14(4): 601-604.
- Crawford, N.H. and Linsley, R.K., 1964. A conceptual model of hydrologic cycle. IAHS Publication No. 63, IAHS Press, Wallingford.
- Dingman, S.L., 2002. *Physical Hydrology*. Prentice-Hall, Inc., Upper Saddle River, New Jersey.
- Downer, C.W. and Ogden, F.L., 2002. Gridded Surface Subsurface Hydrologic Analysis (GSSHA).
- Duan, Q.Y., Sorooshian, S. and Gupta, V., 1992. Effective And Efficient Global Optimization For Conceptual Rainfall-Runoff Models. *Water Resources Research*, 28(4): 1015-1031.
- Entekhabi, D. and Eagleson, P.S., 1989. Land surface hydrology parameterization for atmospheric general circulation models. *Journal of Climate*, 2: 816-831.
- Entekhabi, D., Rodriguez-Iturbe, I. and Bras, R.L., 1991. Variability in large-scale water balance with land surface-atmosphere interaction. *Journal of Climate*, 5: 798-813.
- Fairchild, J. et al., 2004. An integrated assessment of the trophic status of Fort Cobb reservoir, Oklahoma, Final Report. 93, U.S. Bureau of Reclamation.
- Famiglietti, J.S. and Wood, E.F., 1994. Multiscale Modeling Of Spatially-Variable Water And Energy-Balance Processes. *Water Resources Research*, 30(11): 3061-3078.
- Findell, K.L. and Eltahir, E.A.B., 1997. An analysis of the soil moisture-rainfall feedback, based on direct observations from Illinois. *Water Resources Research*, 33(4): 725-735.
- Geza, M., Barfield, B.J. and Huhnke, R.L., 2004. Modeling economic and environmental impact of landuse change in the Fort Cobb basin, ASAE/CSAE Annual International Meeting. ASAE, Ontario, Canada.
- Grayson, R.B., Moore, I.D. and McMahon, T.A., 1992. Physically Based Hydrologic Modeling.1. A Terrain-Based Model For Investigative Purposes. *Water Resources Research*, 28(10): 2639-2658.
- Gu, Y.X., Belair, S., Mahfouf, J.F. and Deblonde, G., 2006. Optimal interpolation analysis of leaf area index using MODIS data. *Remote Sensing Of Environment*, 104(3): 283-296.
- Hornberger, G.M. and Spear, R.C., 1981. An Approach To The Preliminary-Analysis Of Environmental Systems. *Journal Of Environmental Management*, 12(1): 7-18.
- Hupet, F., Lambot, S., Feddes, R.A., van Dam, J.C. and Vanclooster, M., 2003. Estimation of root water uptake parameters by inverse modeling with soil water content data. *Water Resources Research*, 39(11).
- Isrealson, O.W., Vaughn, E. and Hanson, V.E., 1962. *Irrigations Principles and Practice*. John Wiley and Sons, Inc., New York.
- Jackson, R.B. et al., 1996. A global analysis of root distributions for terrestrial biomes. *Oecologia*, 108(3): 389-411.
- Kitanidis, P.K. and Bras, R.L., 1980. Real-Time Forecasting With A Conceptual Hydrologic Model.2. Applications And Results. *Water Resources Research*, 16(6): 1034-1044.
- Legates, D.R. and McCabe, G.J., 1999. Evaluating the use of "goodness-of-fit" measures in hydrologic and hydroclimatic model validation. *Water Resources Research*, 35(1): 233-241.

- Li, K.Y., De Jong, R., Coe, M.T. and Ramakutty, N., 2006. Root-water-uptake based upon a new water stress reduction and an asymptotic root distribution function. *Earth Interactions*, 10(14).
- Lowry, W.P., 1959. The falling rate phase of evaporative soil-moisture loss-A critical evaluation. *Bulletin of the American Meteorological Society*, 40(12): 605-608.
- Martinez, J.E., 2006. Soils at Fort Cobb Micronet. Oklahoma Mesonet, Oklahoma Climatological Survey, Norman, Ok.
- McWhorter, D. and Sunada, D.K., 1985. Groundwater hydrology and hydraulics. Water Resources Publications, Littleton, CO.
- Mertens, J., Madsen, H., Feyen, L., Jacques, D. and Feyen, J., 2004. Including prior information in the estimation of effective soil parameters in unsaturated zone modelling. *Journal of Hydrology*, 294: 251-269.
- Mertens, J., Madsen, H., Kristensen, M., Jacques, D. and Feyen, J., 2005. Sensitivity of soil parameters in unsaturated zone modelling and the relation between effective laboratory and in situ estimates. *Hydrological Processes*, 19: 1611-1633.
- Mertens, J., Stenger, R. and Barkle, G.F., 2006. Multiobjective inverse modeling for soil parameter estimation and model verification. *Vadose Zone Journal*, 5(3): 917-933.
- Moore, R.J., 1985. The Probability-Distributed Principle And Runoff Production At Point And Basin Scales. *Hydrological Sciences Journal-Journal Des Sciences Hydrologiques*, 30(2): 273-297.
- Moore, R.J., 1999. Real-time forecasting systems: Perspectives and prospects. In: R. Casale and C. Marottini (Editors), *Floods and Landslides: Integrated Risk Assessment*. Springer-Verlag, Berlin, pp. 147-189.
- Moore, R.J., 2007. The PDM rainfall-runoff model. *Hydrology and Earth System Sciences*, 11(1): 483-499.
- Moore, R.J. and Clarke, R.T., 1981. A Distribution Function-Approach To Rainfall Runoff Modeling. *Water Resources Research*, 17(5): 1367-1382.
- Mualem, Y., 1976. A new model of predicting the hydraulic conductivity of unsaturated porous media. *Water Resources Research*, 12: 513-522.
- Niemann, J.D. and Eltahir, E.A.B., 2004. Prediction of regional water balance components based on climate, soil, and vegetation parameters, with application to the Illinois River Basin. *Water Resources Research*, 40.
- Niemann, J.D. and Eltahir, E.A.B., 2005. Sensitivity of regional hydrology to climate changes, with application to the Illinois River basin. *Water Resources Research*, 41(7).
- Raats, P.A.C., 1974. Steady Flows Of Water And Salt In Uniform Soil Profiles With Plant Roots. *Soil Science Society Of America Journal*, 38(5): 717-722.
- Reed, S. et al., 2004. Overall distributed model intercomparison project results. *Journal Of Hydrology*, 298(1-4): 27-60.
- Refsgaard, J.C. and Knudsen, J., 1996. Operational validation and intercomparison of different types of hydrological models. *Water Resources Research*, 32(7): 2189-2202.
- Richards, L.A., 1931. Capillary conduction of liquids through porous mediums. *Physics*, 1: 318-333.
- Rodriguez-Iturbe, I., Entekhabi, D. and Bras, R.L., 1991. Nonlinear dynamics of soil moisture at climate scales. *Water Resources Research*, 27(8): 1899-1906.

- Salas, J.D., Smith, R.A., Tabios, G.Q. and Heo, J.-H., 2004. Statistical techniques in water resources and environmental engineering. Dept. of Civil Engineering Colorado State University.
- Scanlon, B.R. et al., 2002. Intercode comparisons for simulated water balance of surficial sediments in semiarid regions. *Water Resources Research*, 38(12).
- Simunek, J., van Genuchten, M.T. and Sejna, M., 2005. The HYDRUS 1D software package for simulating the one-dimensional movement of water, heat, and multiple solutes in variably saturated porous media. Department of Environmental Sciences, University of California Riverside, Riverside, CA.
- Skaggs, T.H., Shouse, P.J. and Poss, J.A., 2006. Irrigating forage crops with saline waters: 2. Modeling root uptake and drainage. *Vadose Zone Journal*, 5: 824-837.
- Spear, R.C. and Hornberger, G.M., 1980. Eutrophication In Peel Inlet.2. Identification Of Critical Uncertainties Via Generalized Sensitivity Analysis. *Water Research*, 14(1): 43-49.
- Storm, D.E., White, M.J. and Stoodley, S., 2003. Fort Cobb Basin- Modeling and Land Cover Classification, Oklahoma Conservation Commission.
- van Genuchten, M.T., 1987. A numerical model for water and solute movement in and below the root zone. 121, U.S. Salinity laboratory, USDA, ARS, Riverside, CA.
- van Genuchten, M.T., Leij, F.J. and Lund, L.J. (Editors), 1989. Indirect methods for estimating the hydraulic properties of unsaturated soils. proceedings of the International Workshop on Indirect Methods for Estimating the Hydraulic Properties of Unsaturated Soils. U.S. Salinity Laboratory, ARS, Riverside, CA.
- Vrugt, J.A., Bouten, W., Gupta, H.V. and Hopmans, J.W., 2003. Toward improved identifiability of soil hydraulic parameters: On the selection of a suitable parametric model. *Vadose Zone Journal*, 2: 98-113.
- Vrugt, J.A., Gupta, H.V., Bouten, W. and Sorooshian, S., 2003. A Shuffled Complex Evolution Metropolis algorithm for optimization and uncertainty assessment of hydrologic model parameters. *Water Resources Research*, 39(8).
- Wagner, T., McIntyre, N., Lees, M.J., Wheater, H.S. and Gupta, H.V., 2003. Towards reduced uncertainty in conceptual rainfall-runoff modelling: Dynamic identifiability analysis. *Hydrological Processes*, 17: 455-476.
- Wagner, T., Wheater, H.S. and Gupta, H.V., 2004. Rainfall-runoff modelling in gauged and ungauged catchments. Imperial College Press, London, UK, 300 pp.
- Wagner, T., Wheater, H.S. and Lees, M.J., 2004. Monte-Carlo analysis toolbox user manual. Penn State University, formerly Imperial College, University Park, PA.
- Wetzel, P.J. and Chang, J.-T., 1987. Concerning the relationship between evapotranspiration and soil moisture. *Journal of Climate and Applied Meteorology*, 26: 18-27.
- Wilby, R.L., 2005. Uncertainty in water resource model parameters used for climate change impact assessment. *Hydrological Processes*, 19(16): 3201-3219.
- Wolock, D., 1993. Simulating the variable-source-area concept of streamflow generation with the watershed model TOPMODEL. Water-Resources Investigations Report 93-4124, U.S. Geological Survey, Lawrence, KS.
- Zhao, R., Zhuang, Y., Fang, L., Liu, X. and Zhang, Q., 1980. The Xinanjiang Model. Hydrological Forecasting, IAHS Publication No. 129. IAHS Press, Wallingford.

Appendix A

DYNIA results for the PDM applied locally at F103 at 5 cm.

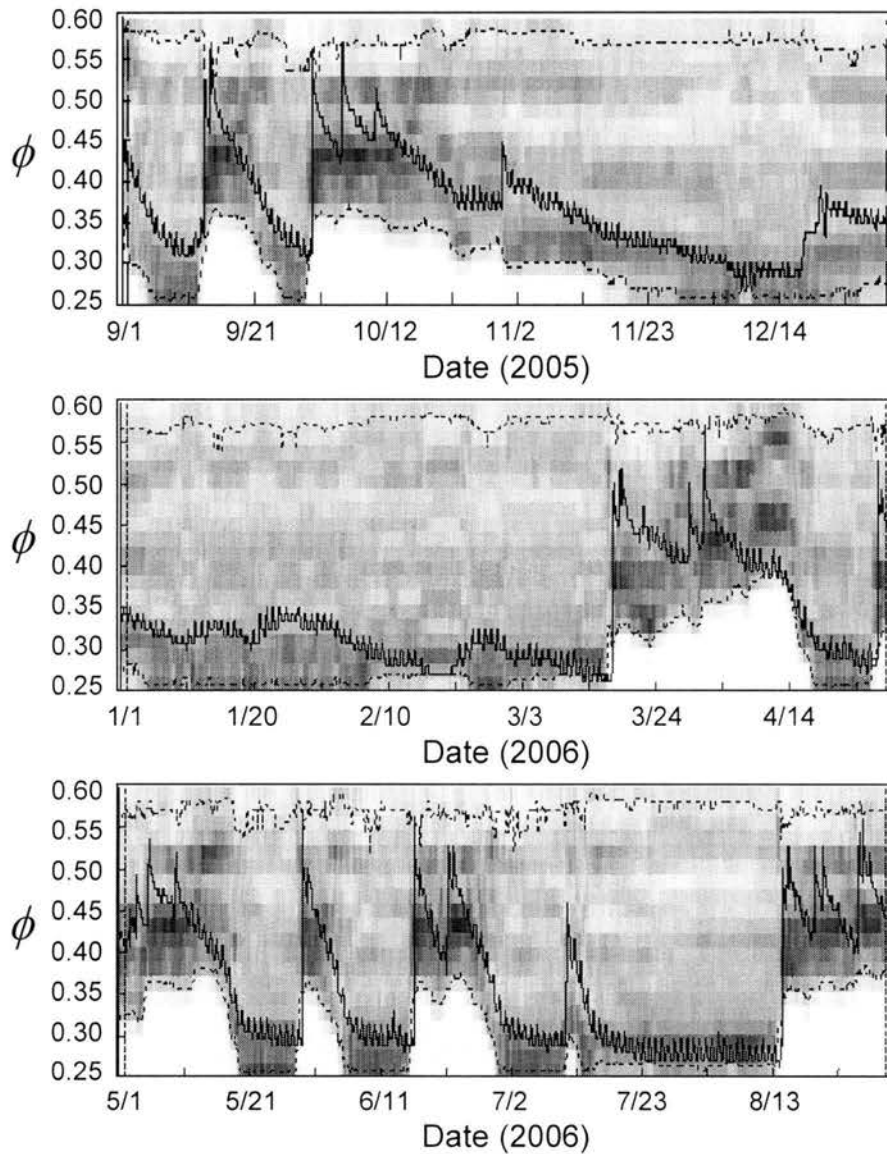


Figure A.1. ϕ parameter DYNIA results for September 2005 through August 2006 for the PDM applied locally at station F103 at 5 cm.

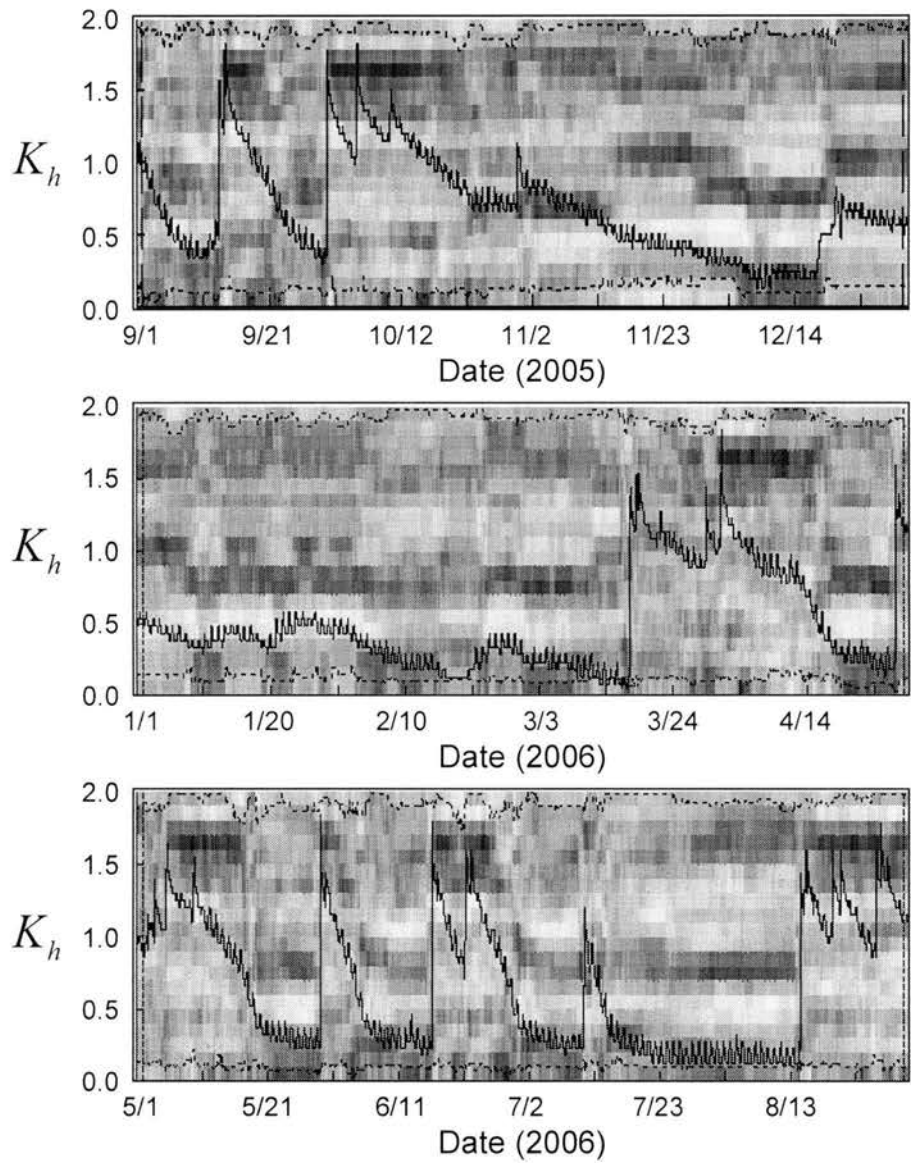


Figure A.2. K_h parameter DYNIA results for September 2005 through August 2006 for the PDM applied locally at station F103 at 5 cm.

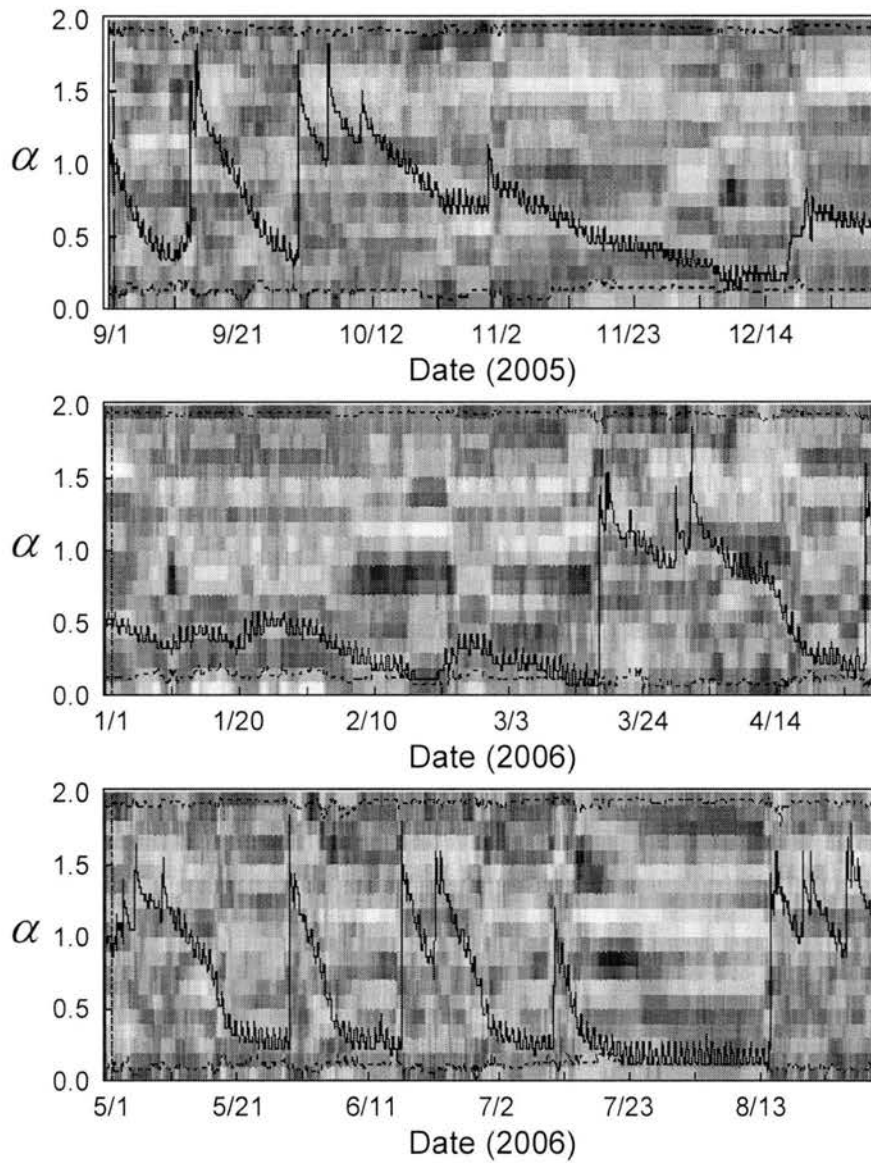


Figure A.3. α parameter DYNIA results for September 2005 through August 2006 for the PDM applied locally at station F103 at 5 cm.

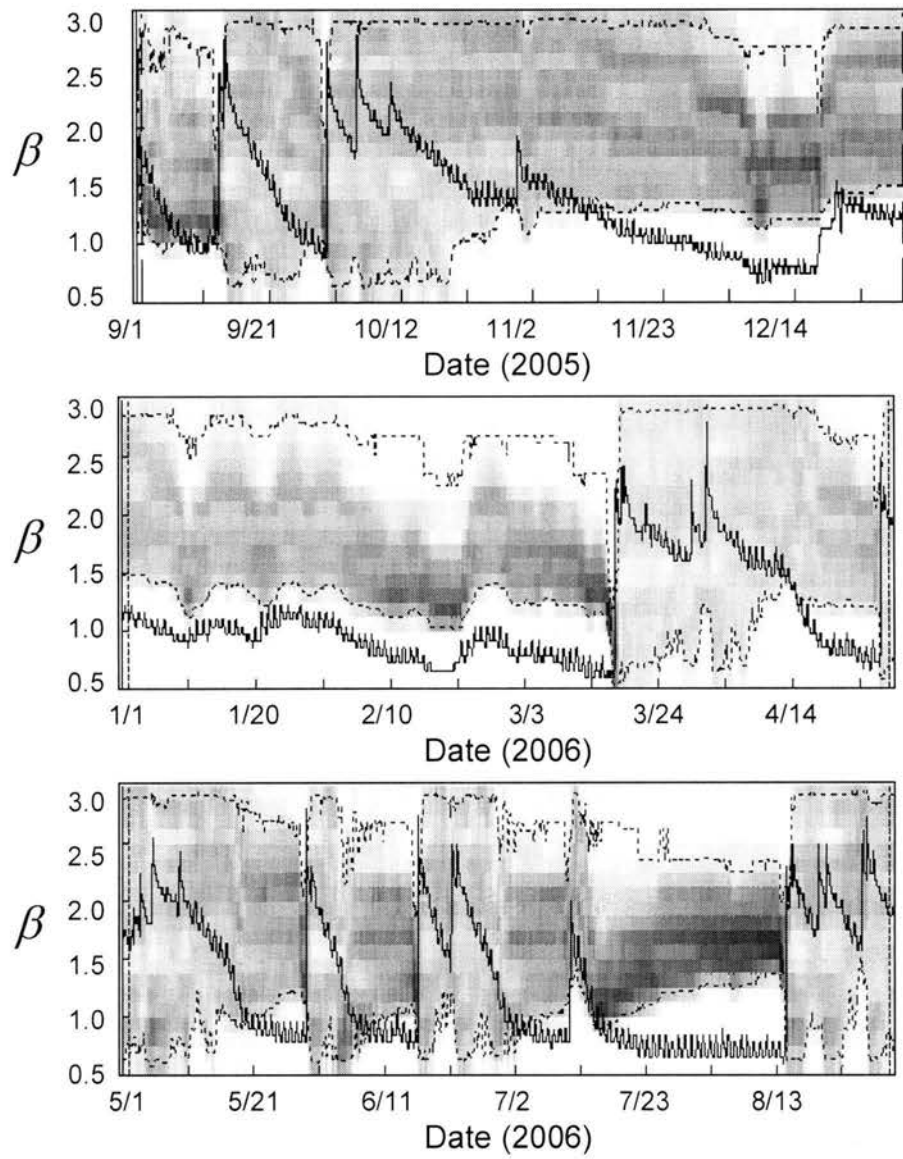


Figure A.4. β parameter DYNIA results for September 2005 through August 2006 for the PDM applied locally at station F103 at 5 cm.

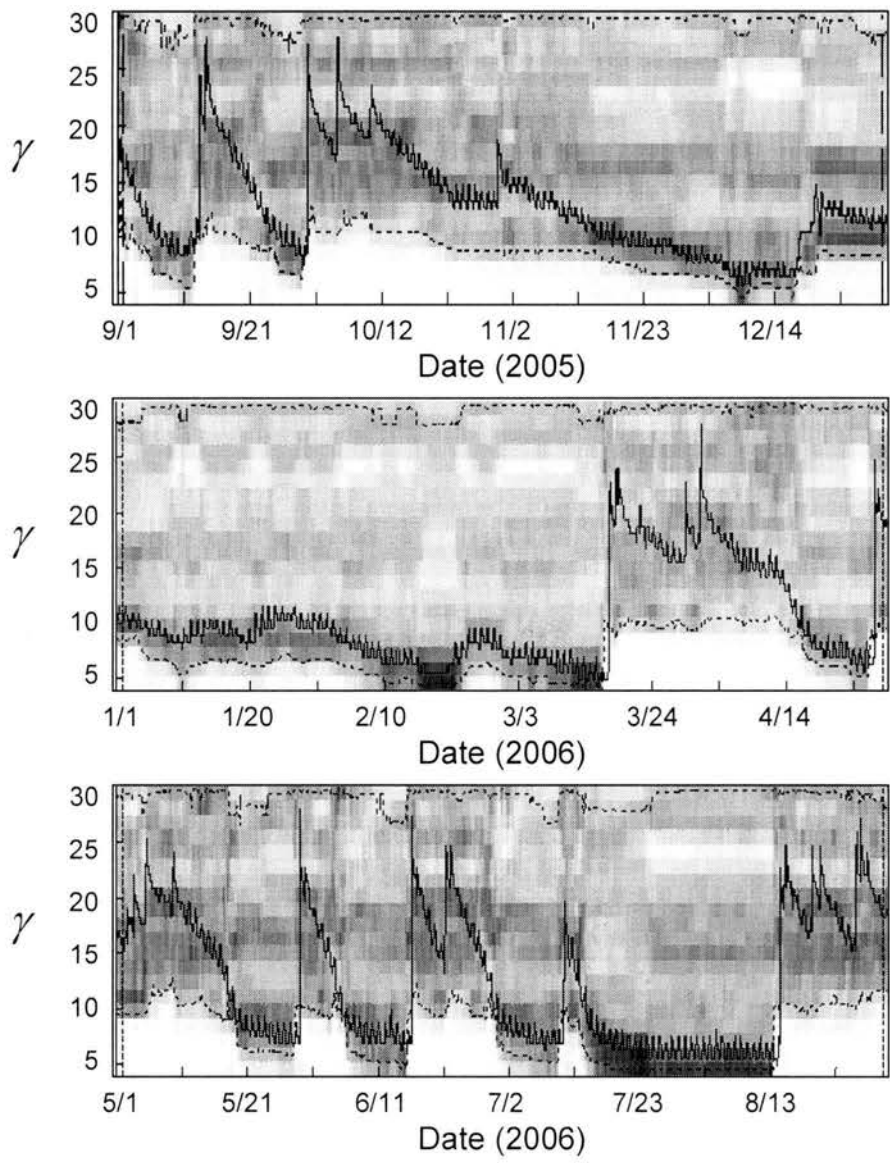


Figure A.5. γ parameter DYNIA results for September 2005 through August 2006 for the PDM applied locally at station F103 at 5 cm.

Appendix B

DYNIA results for the PDM applied locally at F103 at 25 cm.

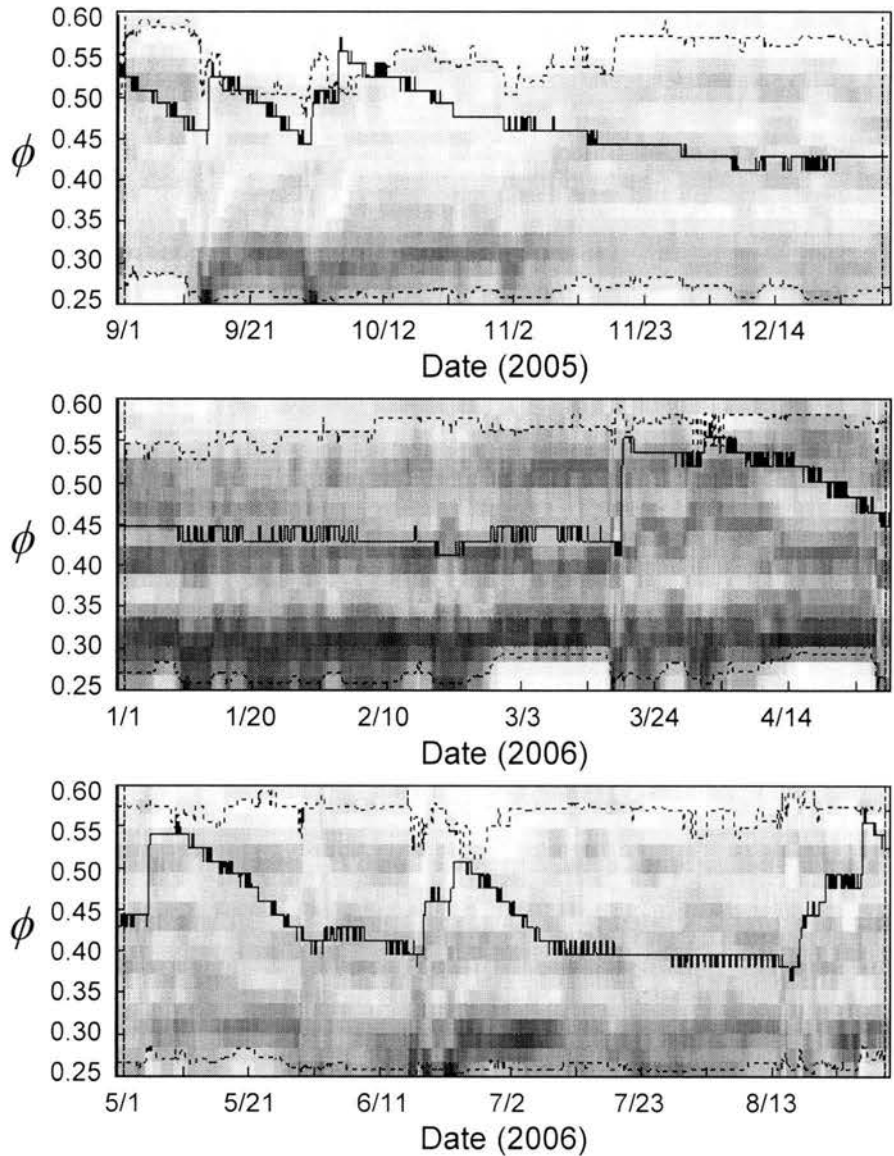


Figure B.1. ϕ parameter DYNIA results for September 2005 through August 2006 for the PDM applied locally at station F103 at 25 cm.

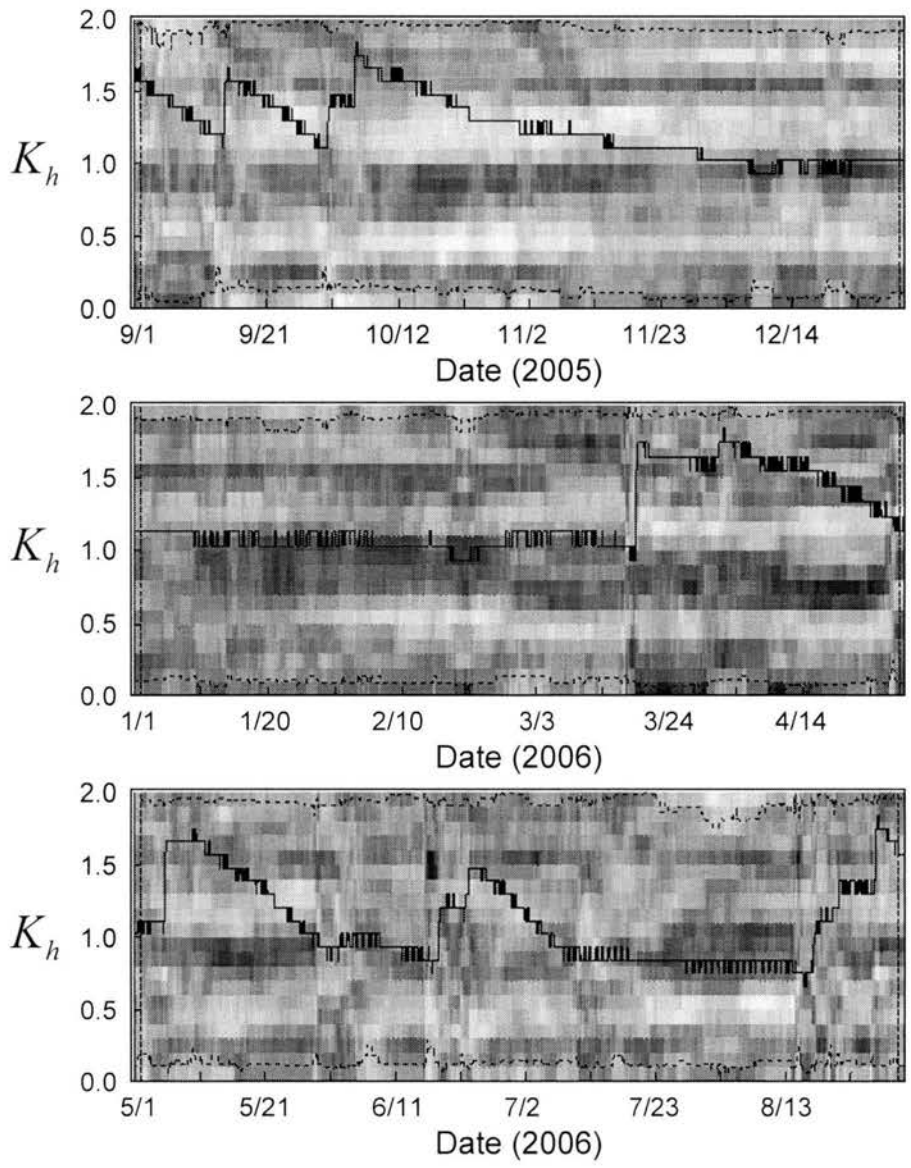


Figure B.2. K_h parameter DYNIA results for September 2005 through August 2006 for the PDM applied locally at station F103 at 25 cm.

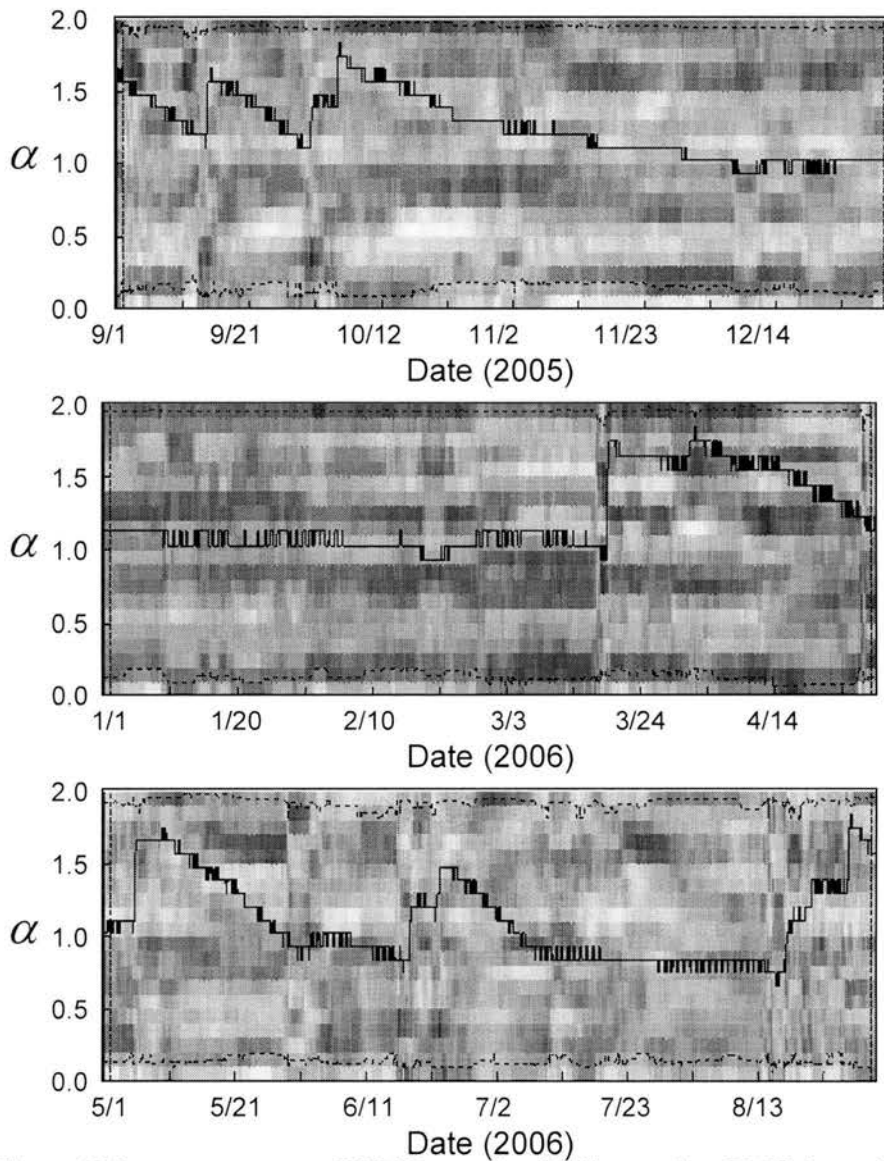


Figure B.3. α parameter DYNIA results for September 2005 through August 2006 for the PDM applied locally at station F103 at 25 cm.

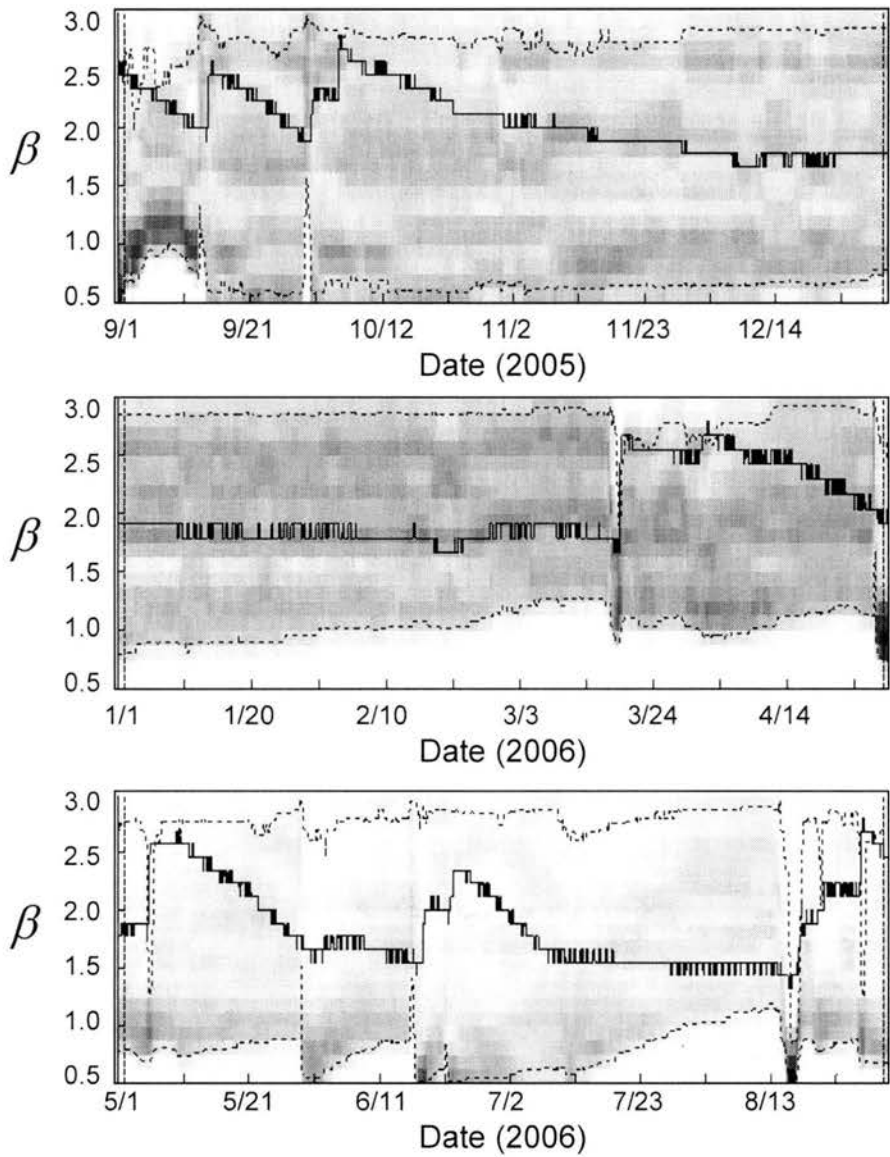


Figure B.4. β parameter DYNIA results for September 2005 through August 2006 for the PDM applied locally at station F103 at 25 cm.

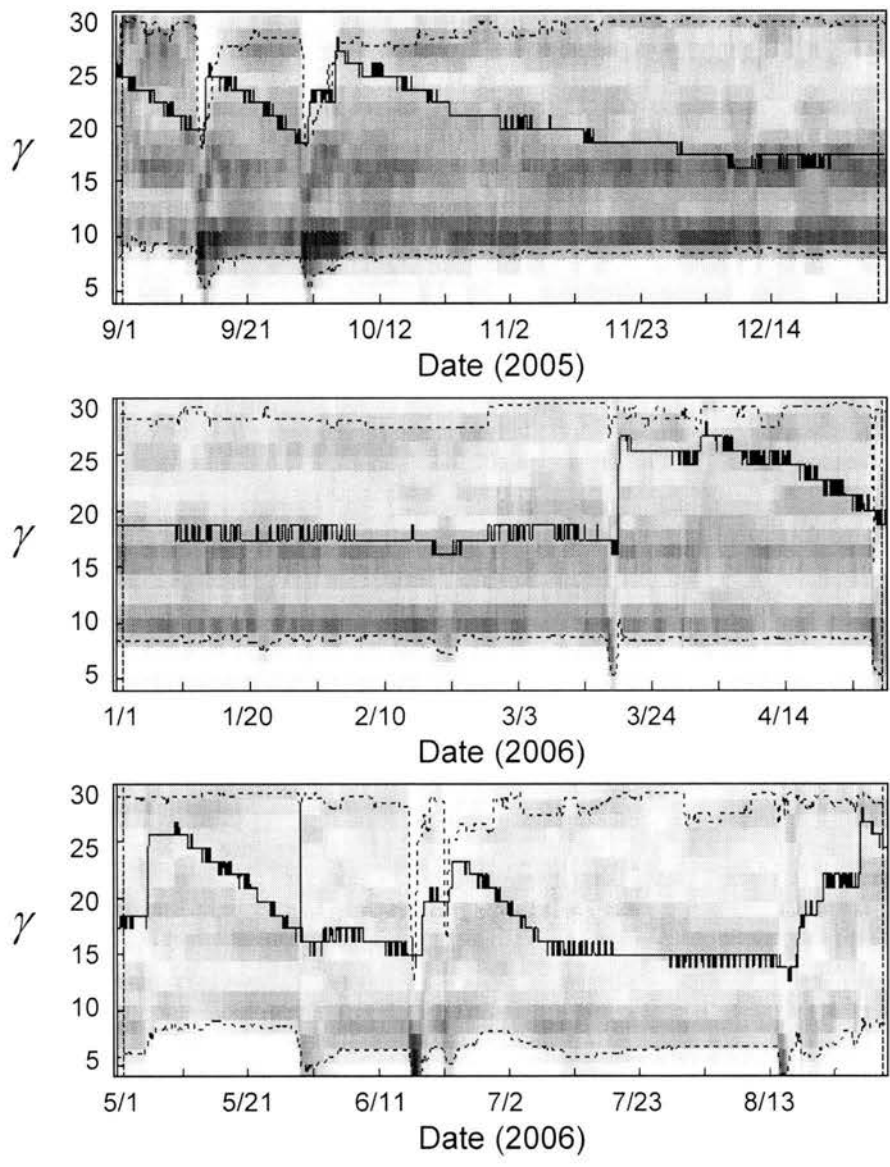


Figure B.5. γ parameter DYNIA results for September 2005 through August 2006 for the PDM applied locally at station F103 at 25 cm.

Appendix C

DYNIA results for the PDM applied at station F113 for the 5 cm depth

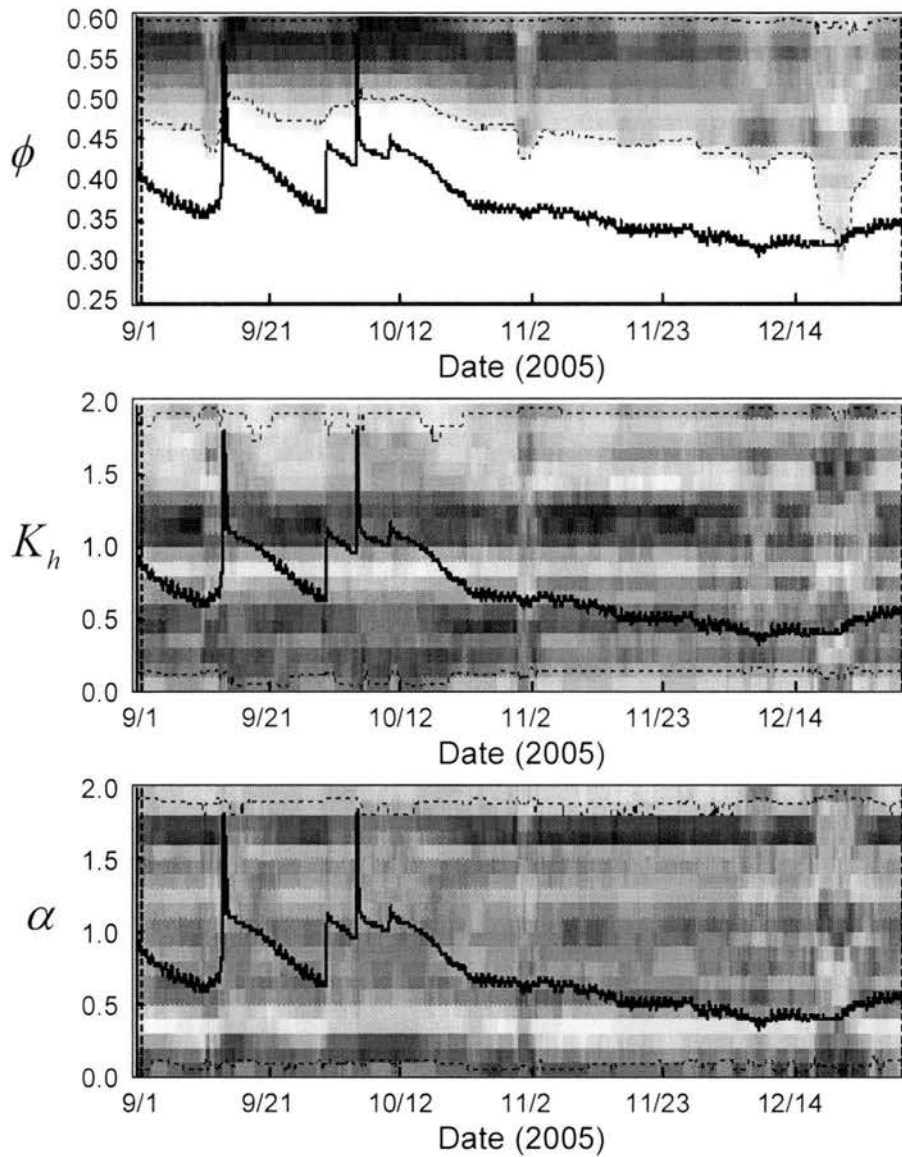


Figure C.1. DYNIA results for porosity, saturated hydraulic conductivity, and infiltrability parameters for September 2005 through December 2005 at station F113.

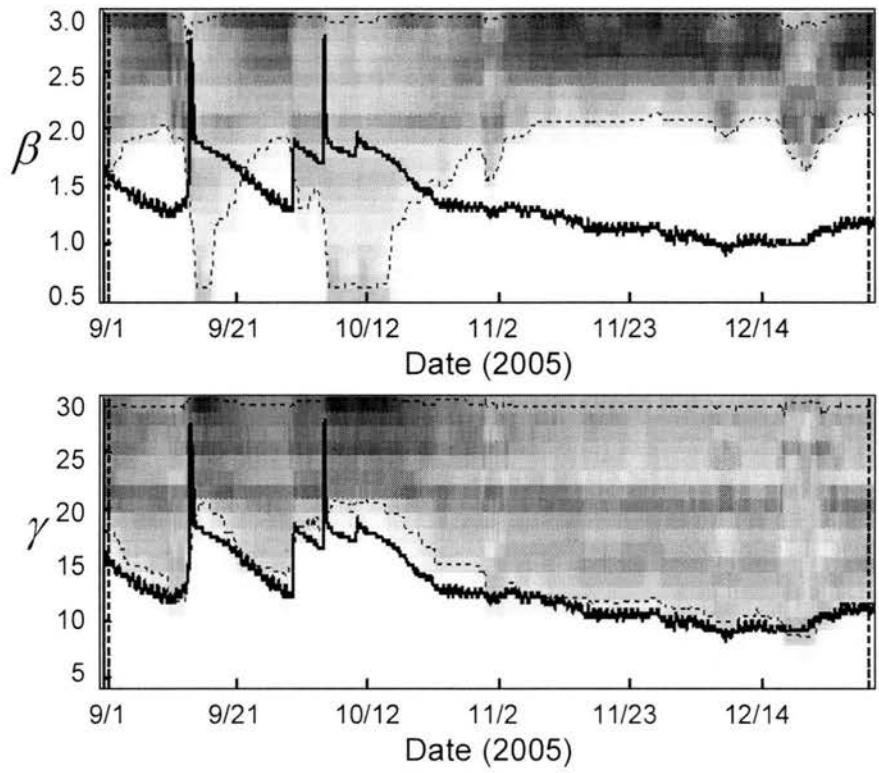


Figure C.2. DYNIA results for the evaporation exponent and recharge exponent parameters for September 2005 through December 2005 at station F113.

Appendix D

DYNIA results for HYDRUS 1D applied at F103 for the 5 cm depth

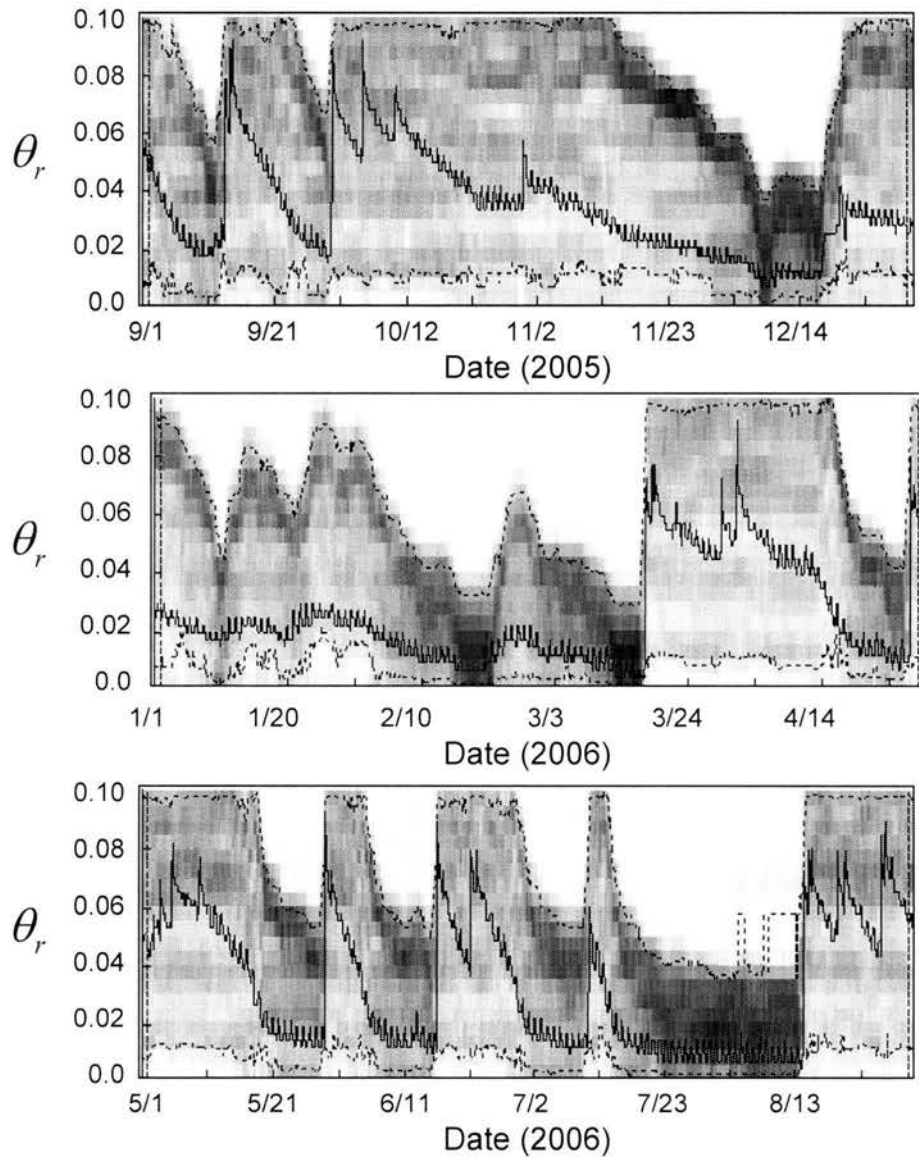


Figure D.1. θ_r parameter DYNIA results for September 2005 through August 2006 for HYDRUS 1D at station F103 at 5 cm.

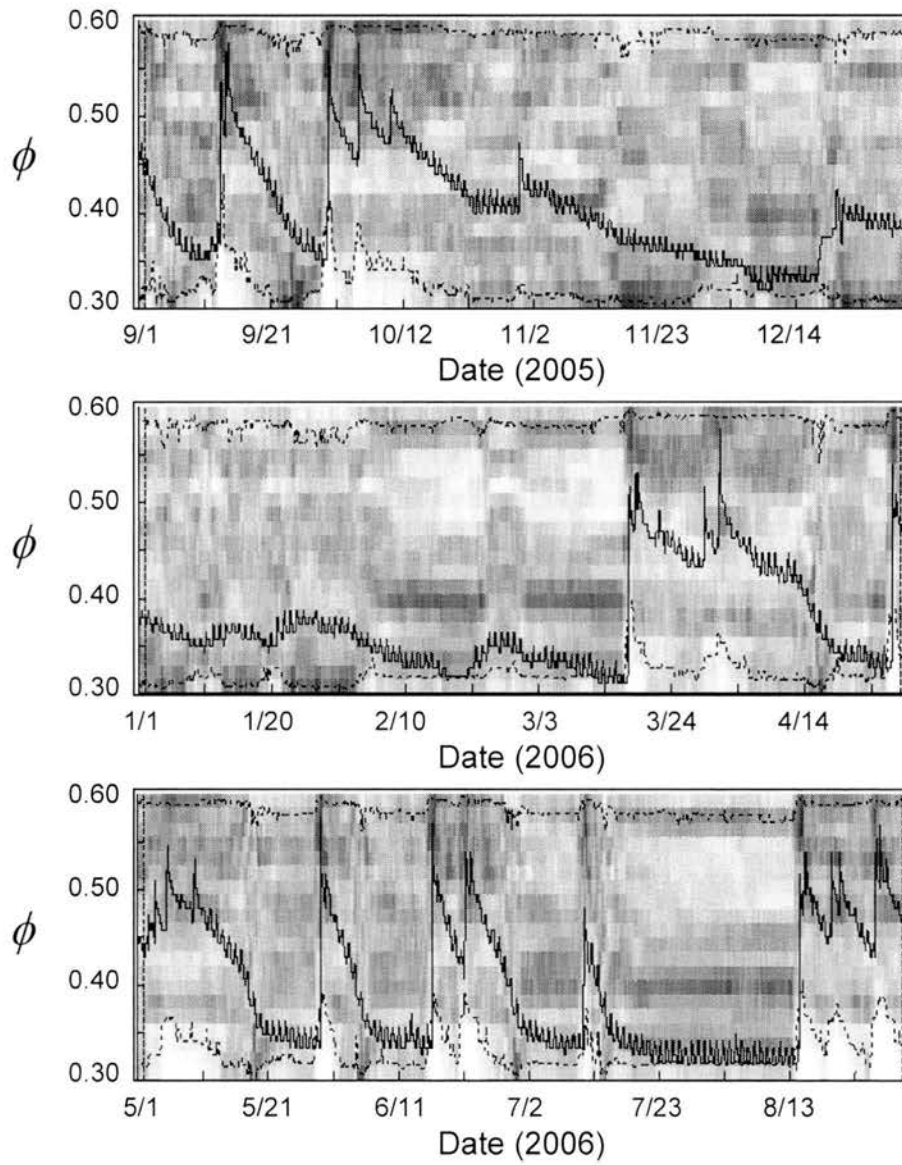


Figure D.2. ϕ parameter DYNIA results for September 2005 through August 2006 for HYDRUS 1D at station F103 at 5 cm.

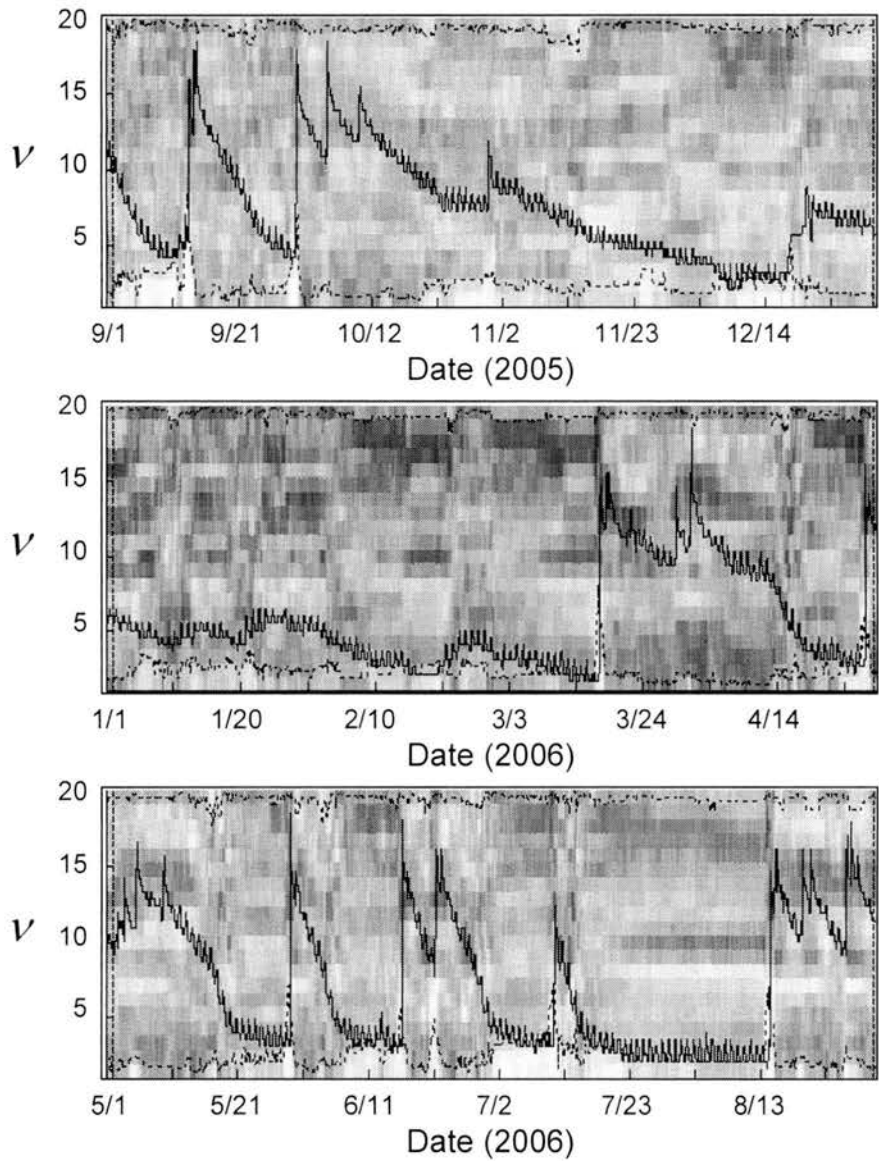


Figure D.3. v parameter DYNIA results for September 2005 through August 2006 for HYDRUS 1D at station F103 at 5 cm.

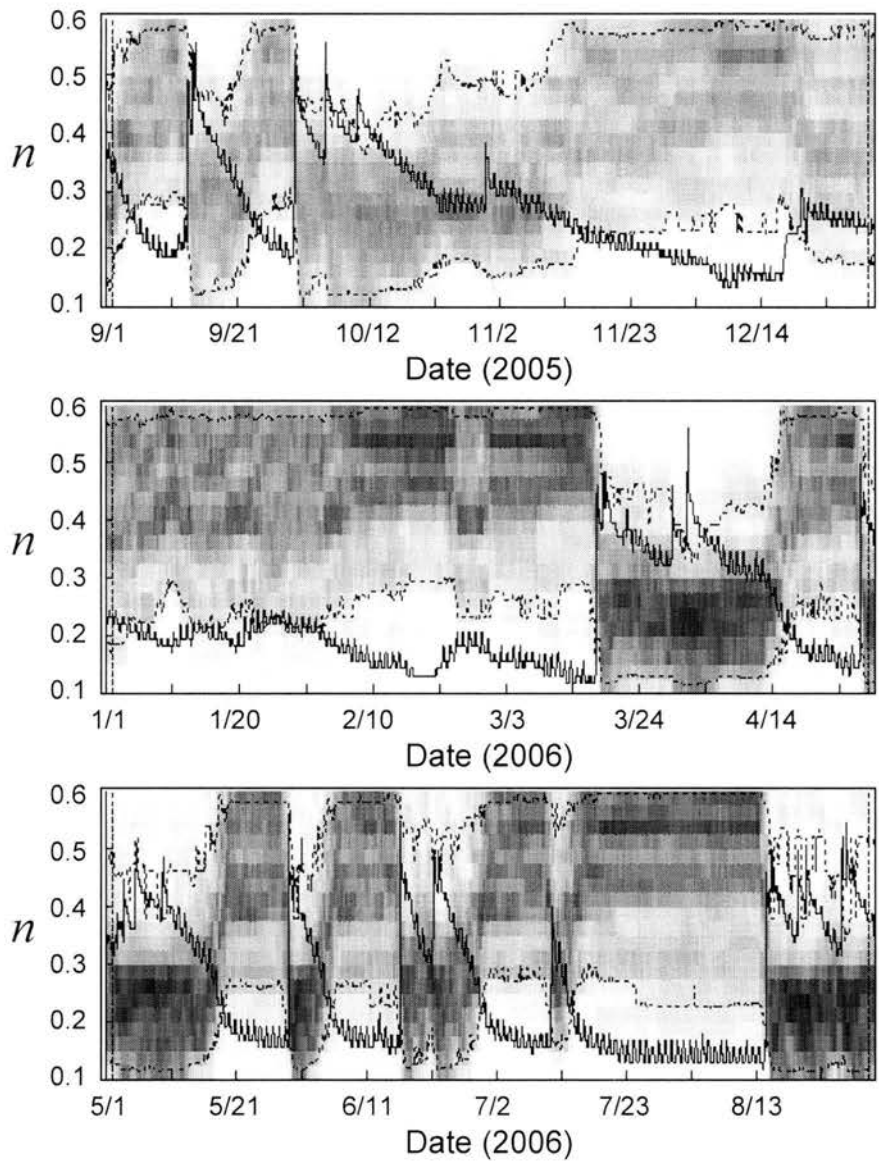


Figure D.4. n parameter DYNIA results for September 2005 through August 2006 for HYDRUS 1D at station F103 at 5 cm.

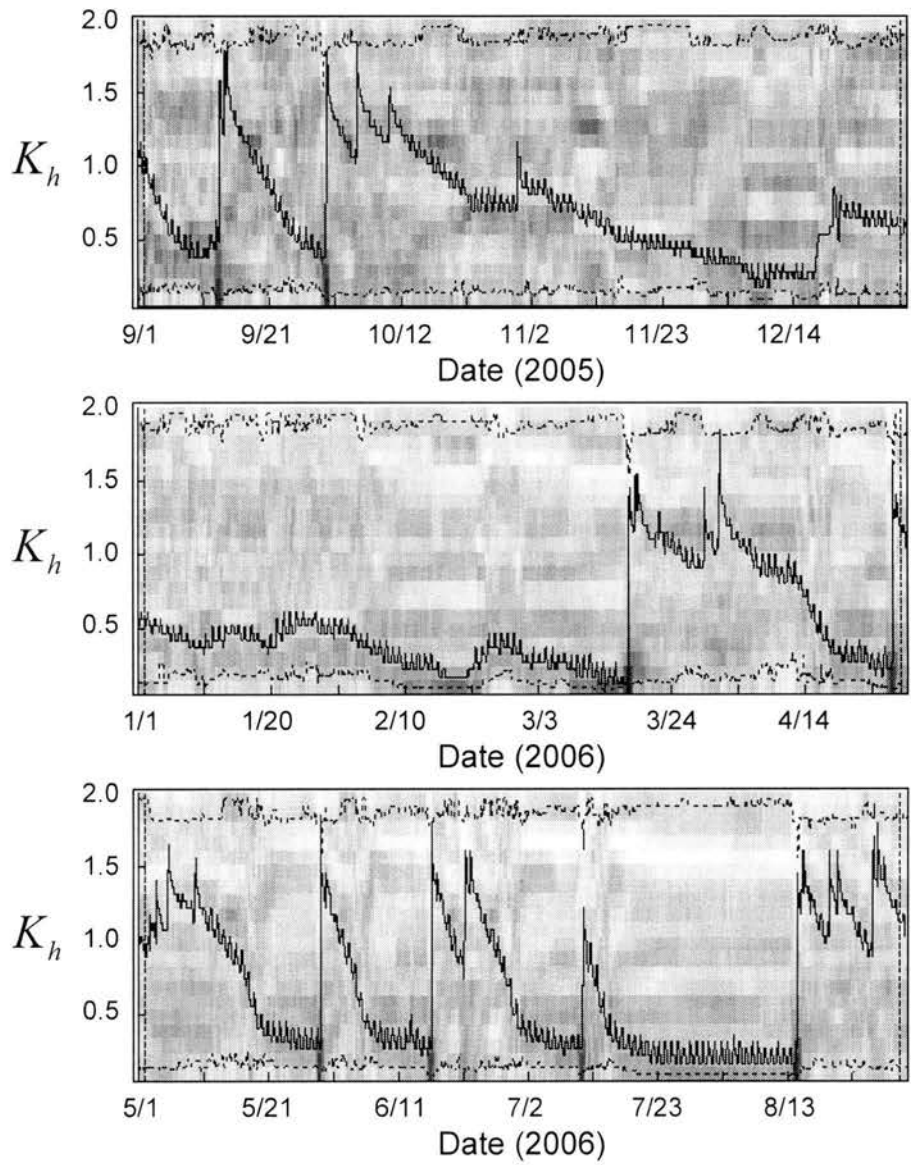


Figure D.5. K_h parameter DYNIA results for September 2005 through August 2006 for HYDRUS 1D at station F103 at 5 cm.

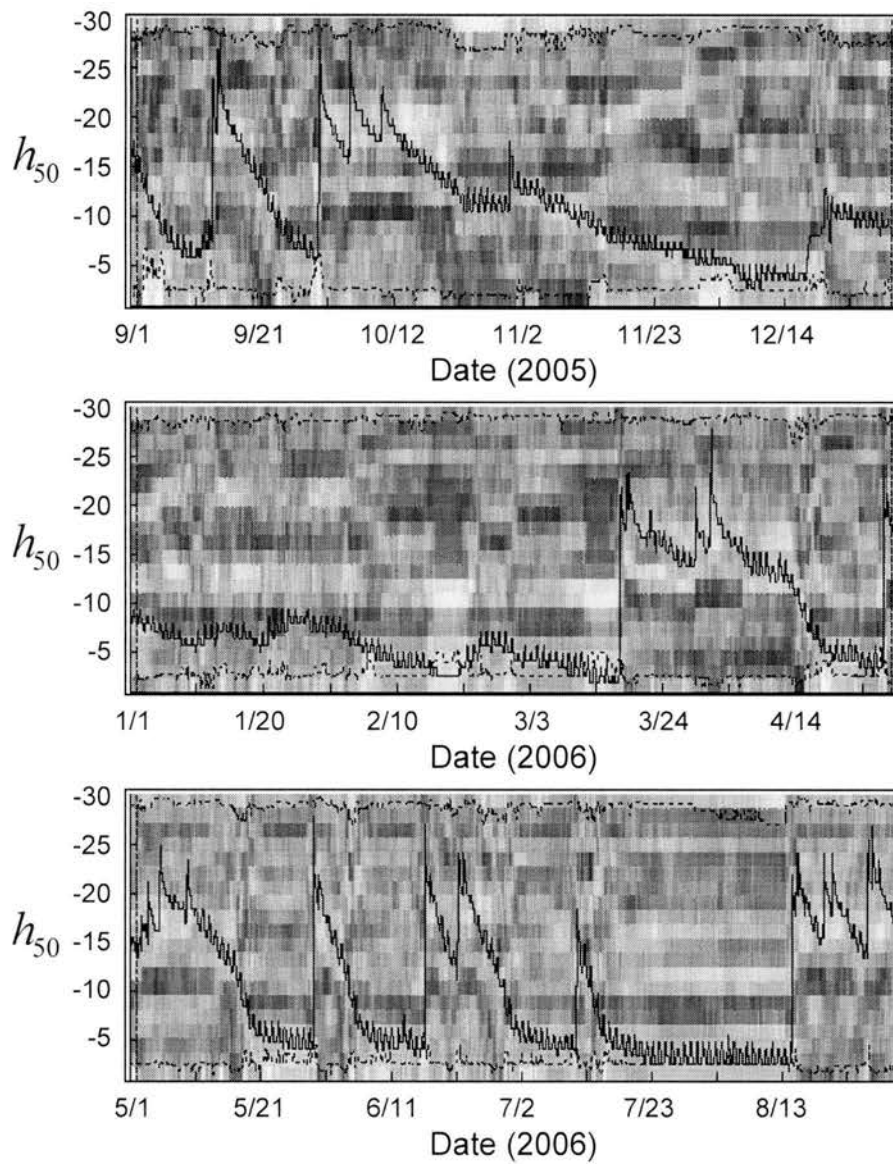


Figure D.6. h_{50} parameter DYNIA results for September 2005 through August 2006 for HYDRUS 1D at station F103 at 5 cm.

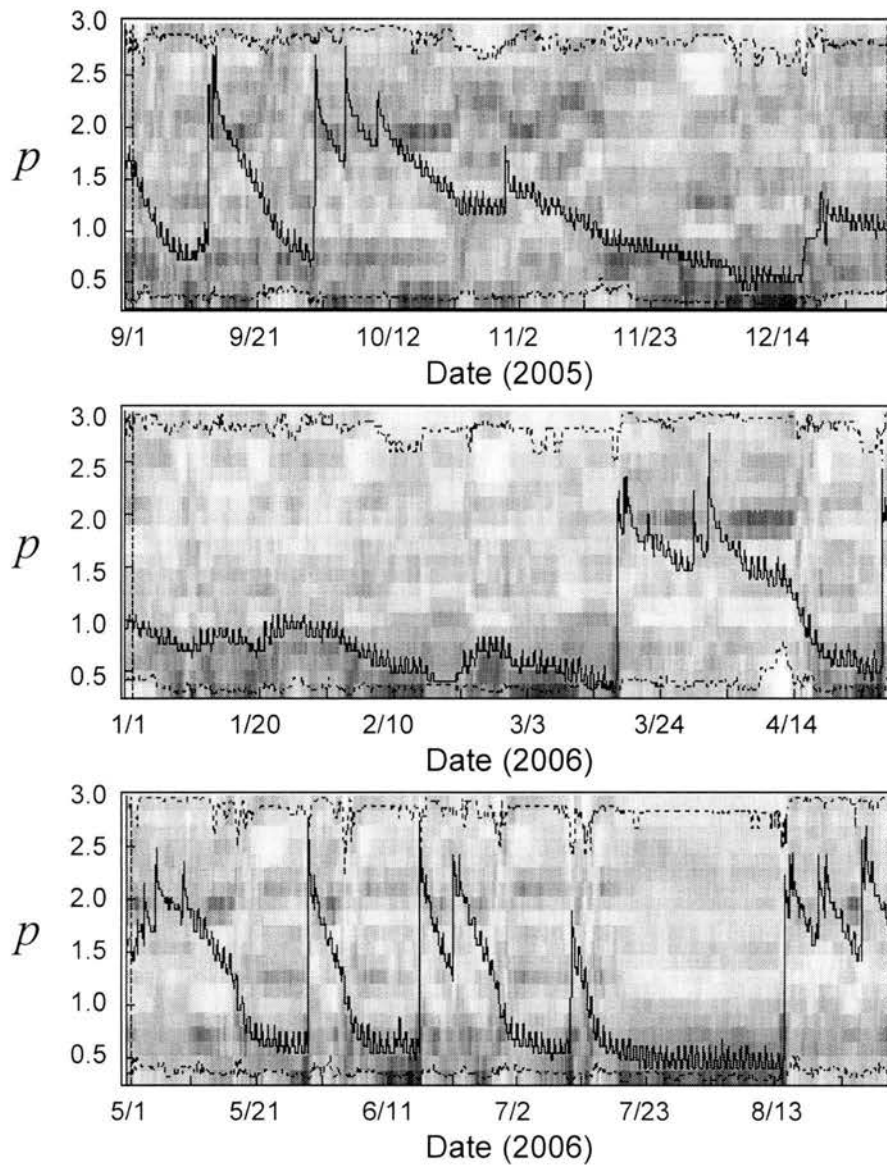


Figure D.7. p parameter DYNIA results for September 2005 through August 2006 for HYDRUS 1D at station F103 at 5 cm.

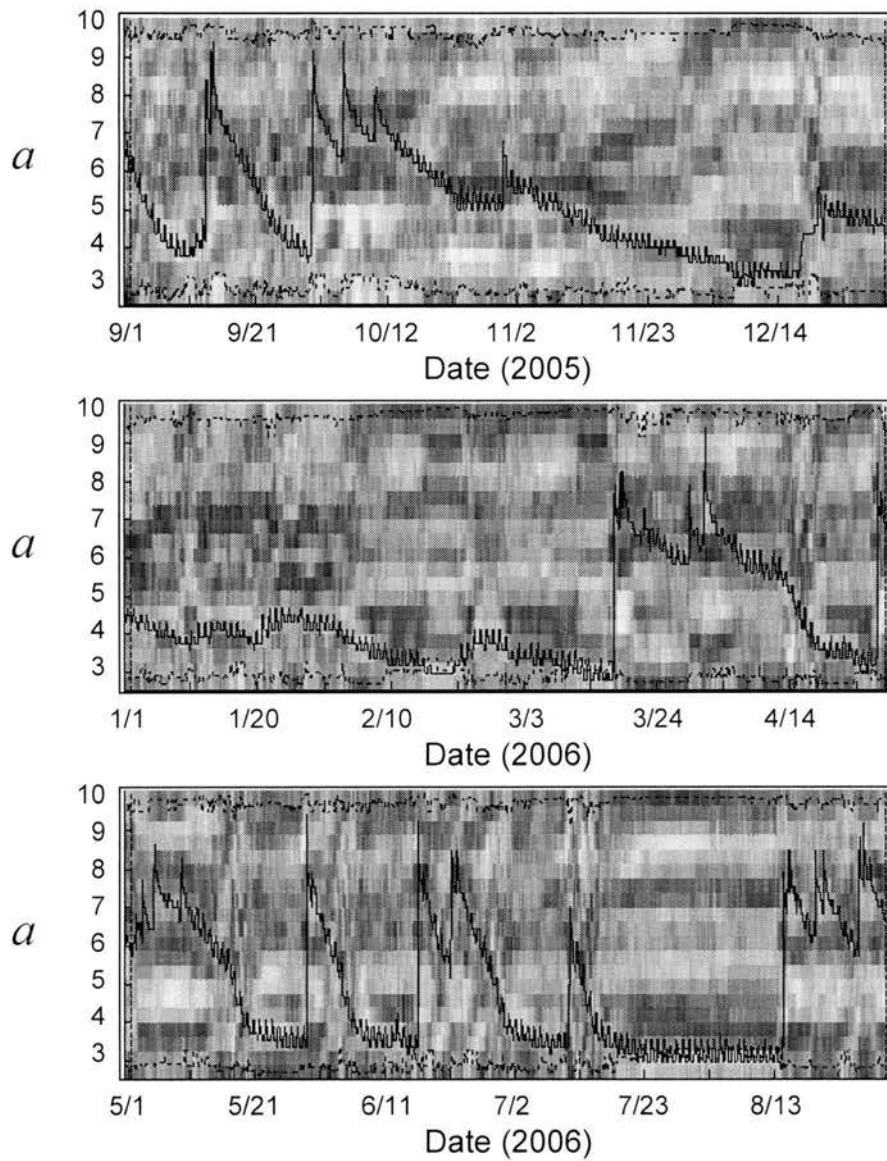


Figure D.8. *a* parameter DYNIA results for September 2005 through August 2006 for HYDRUS 1D at station F103 at 5 cm.

Appendix E

DYNIA results for HYDRUS 1D applied at F103 for the 25 cm depth

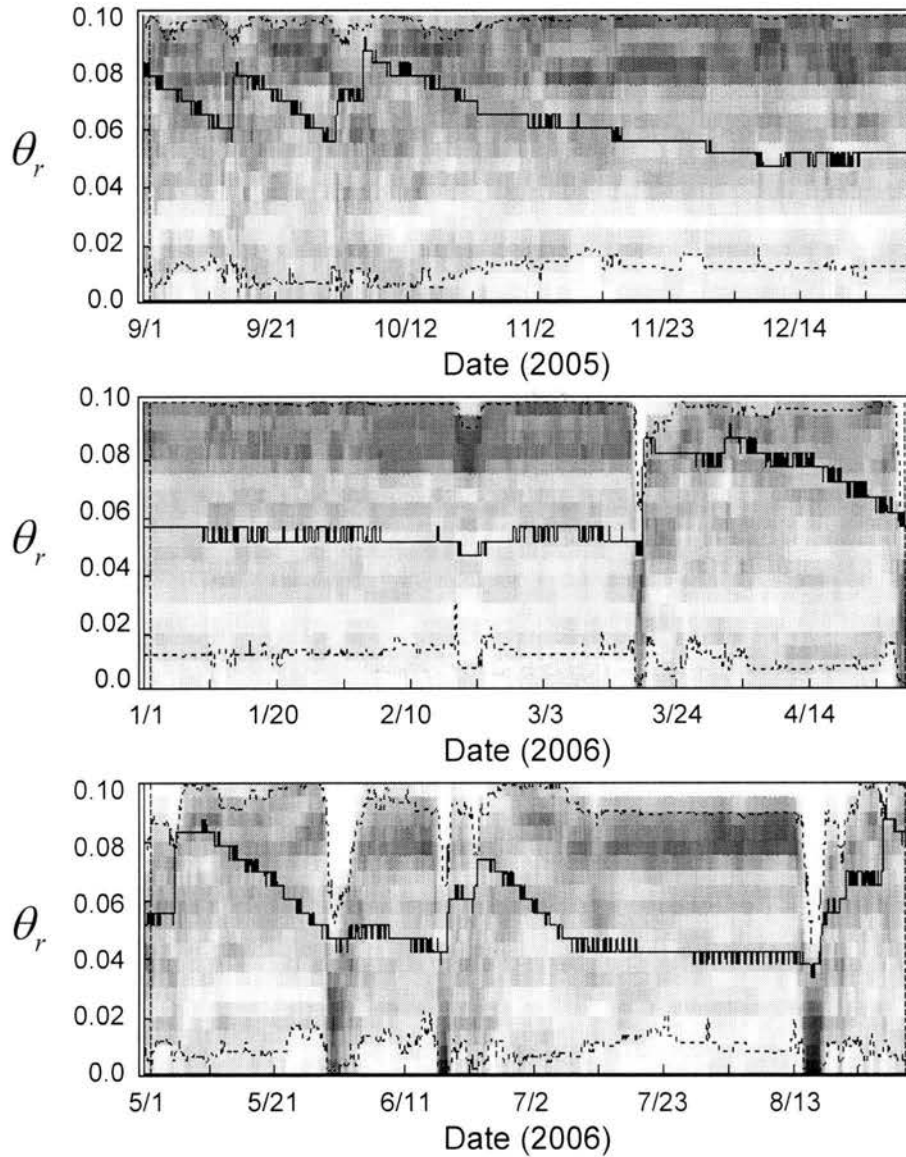


Figure E.1. θ_r parameter DYNIA results for September 2005 through August 2006 for HYDRUS 1D at station F103 at 25 cm.

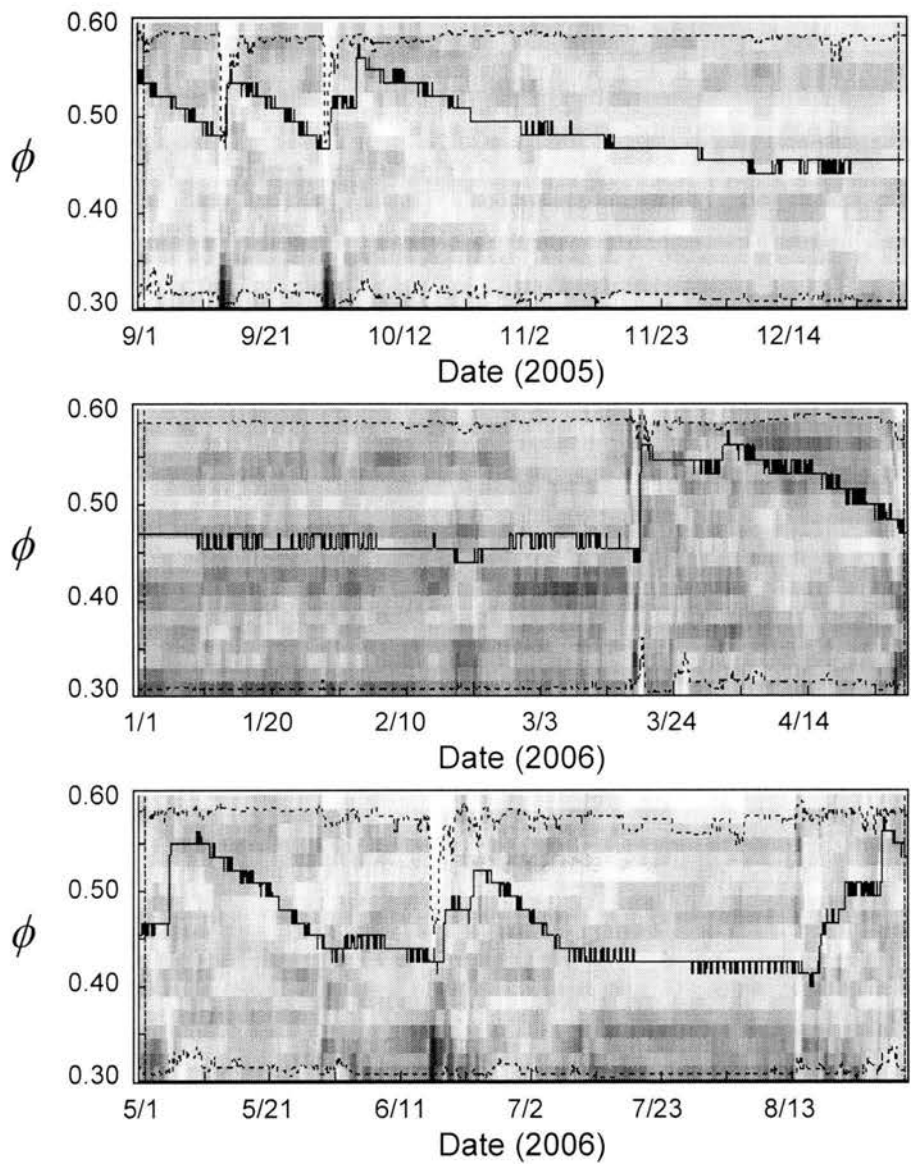


Figure E.2. ϕ parameter DYNIA results for September 2005 through August 2006 for HYDRUS 1D at station F103 at 25 cm.

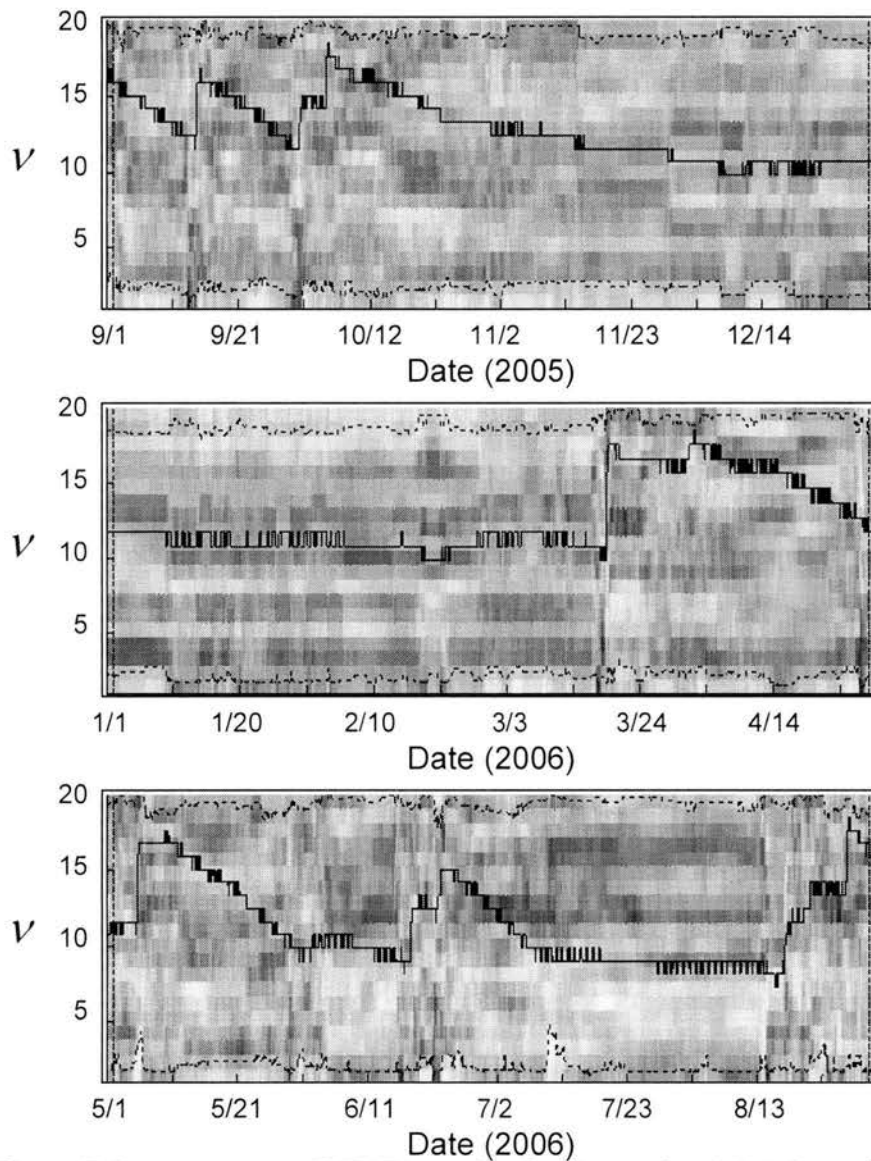


Figure E.3. ν parameter DYNIA results for September 2005 through August 2006 for HYDRUS 1D at station F103 at 25 cm.

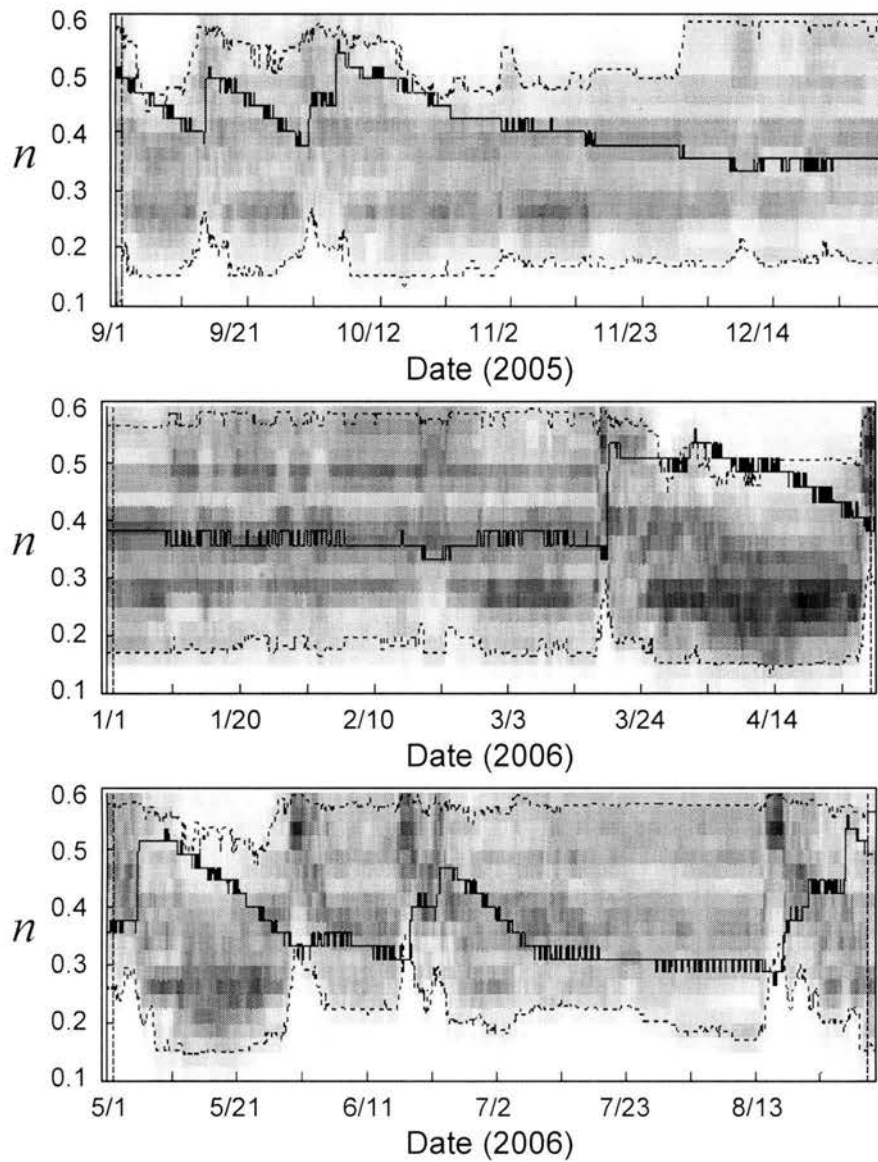


Figure E.4. n parameter DYNIA results for September 2005 through August 2006 for HYDRUS 1D at station F103 at 25 cm.

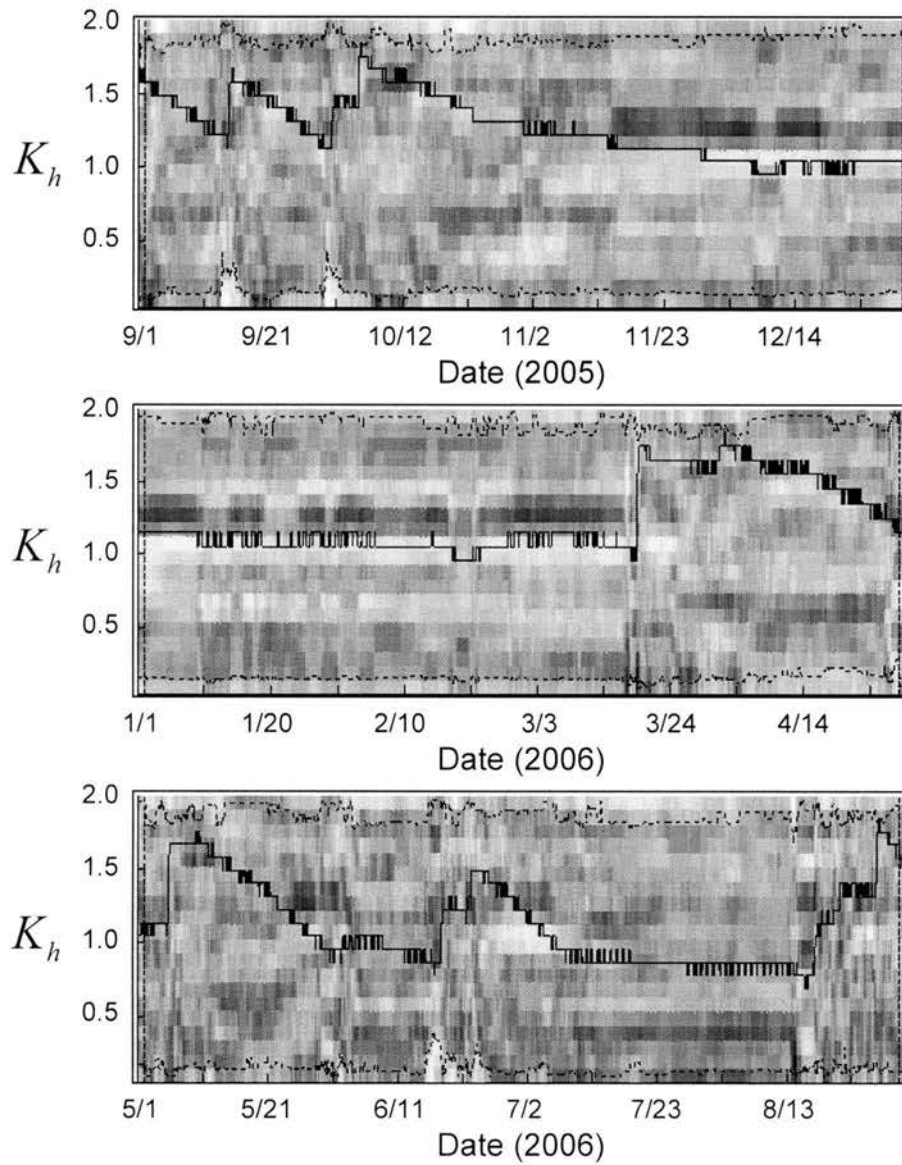


Figure E.5. K_h parameter DYNIA results for September 2005 through August 2006 for HYDRUS 1D at station F103 at 25 cm.

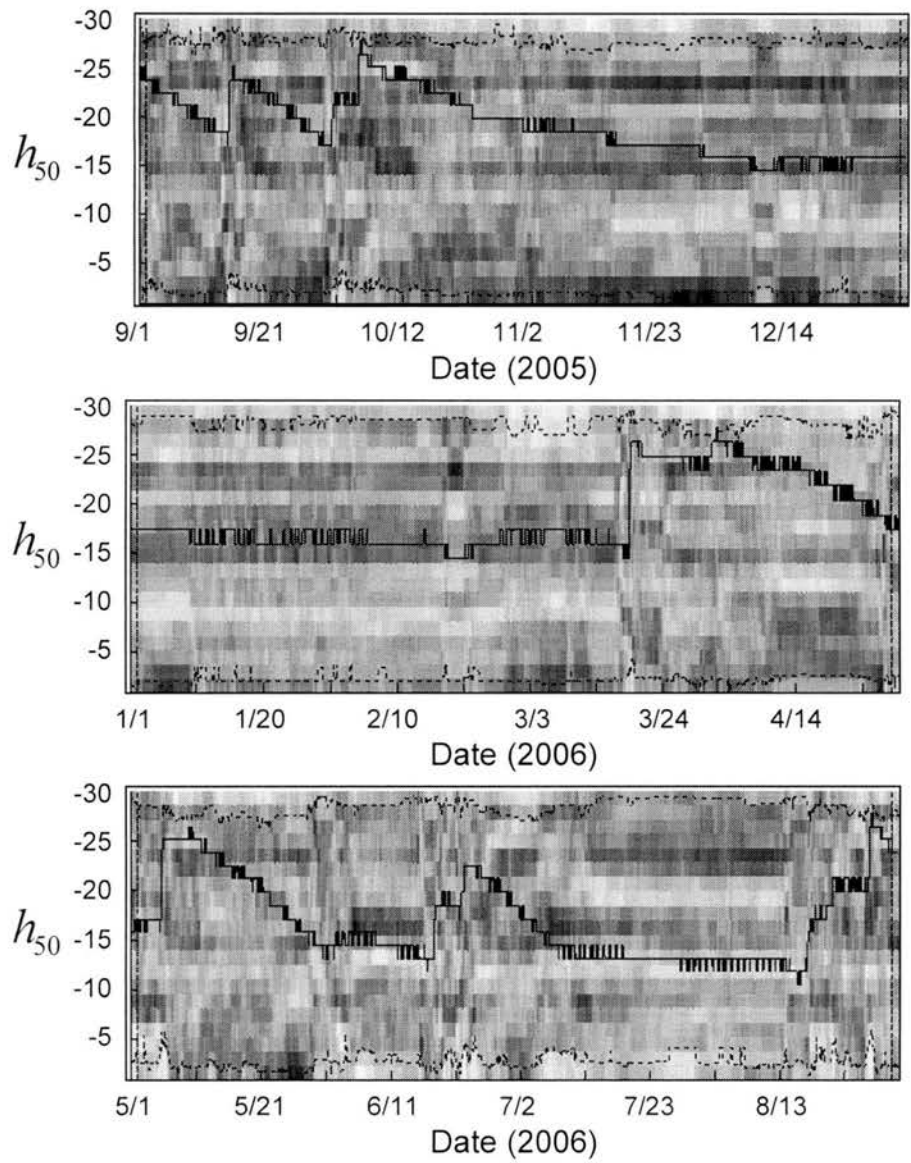


Figure E.6. h_{50} parameter DYNIA results for September 2005 through August 2006 for HYDRUS 1D at station F103 at 25 cm.

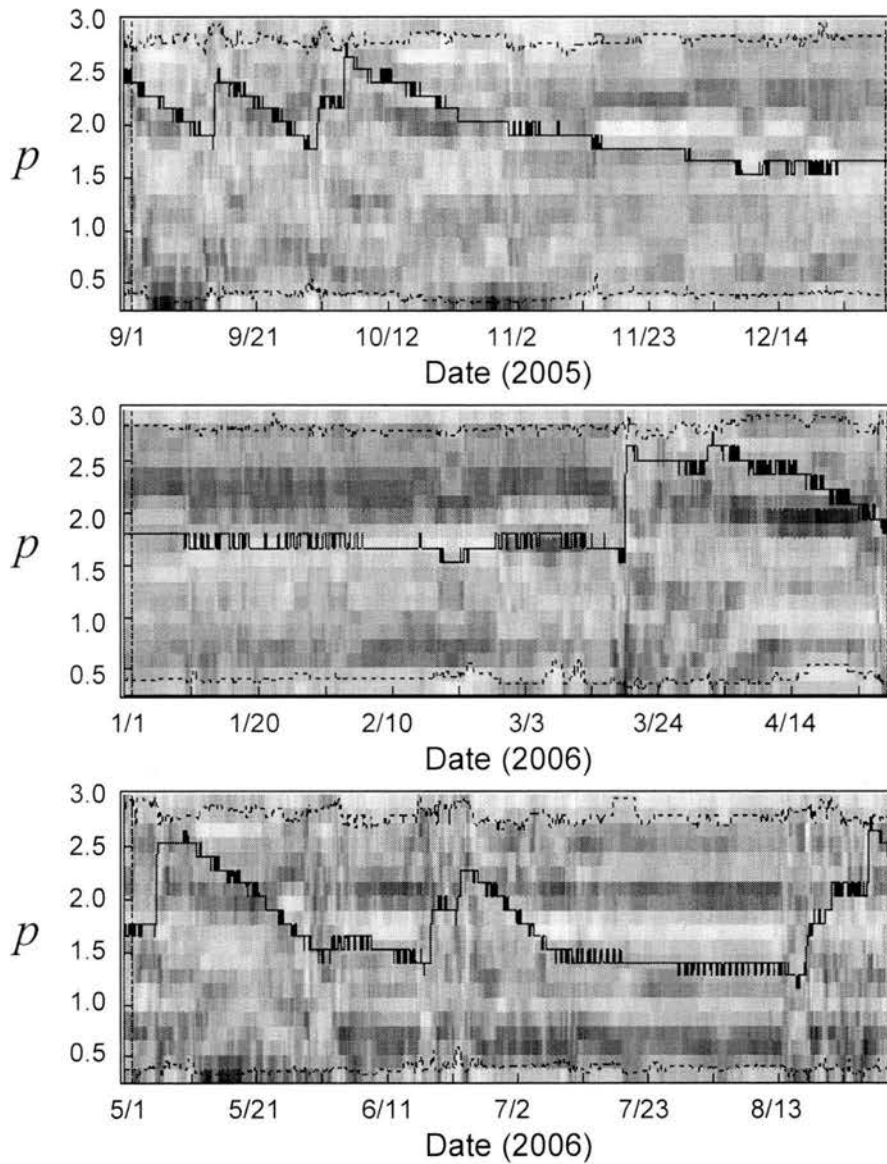


Figure E.7. p parameter DYNIA results for September 2005 through August 2006 for HYDRUS 1D at station F103 at 25 cm.

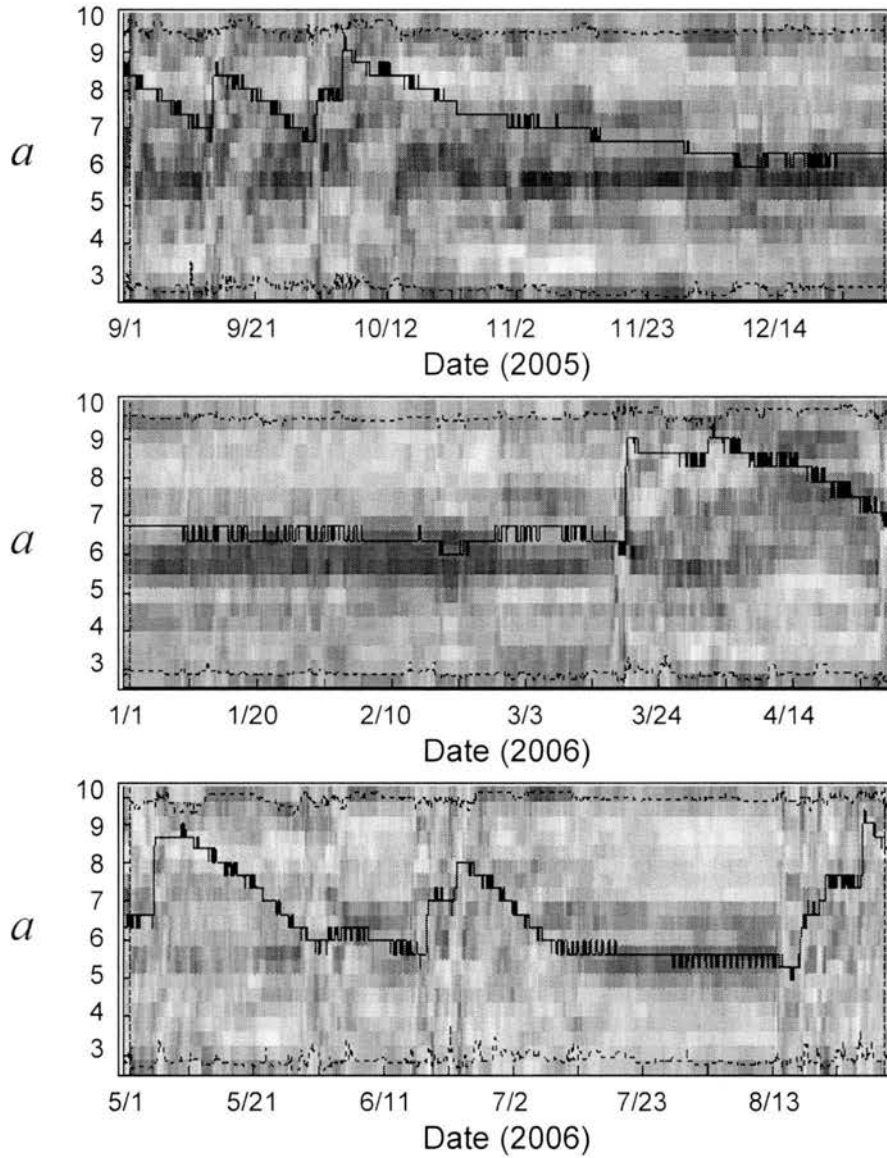


Figure E.8. a parameter DYNIA results for September 2005 through August 2006 for HYDRUS 1D at station F103 at 25 cm.

Appendix F

SIA results for the PDM applied locally at station F103 at 5 cm

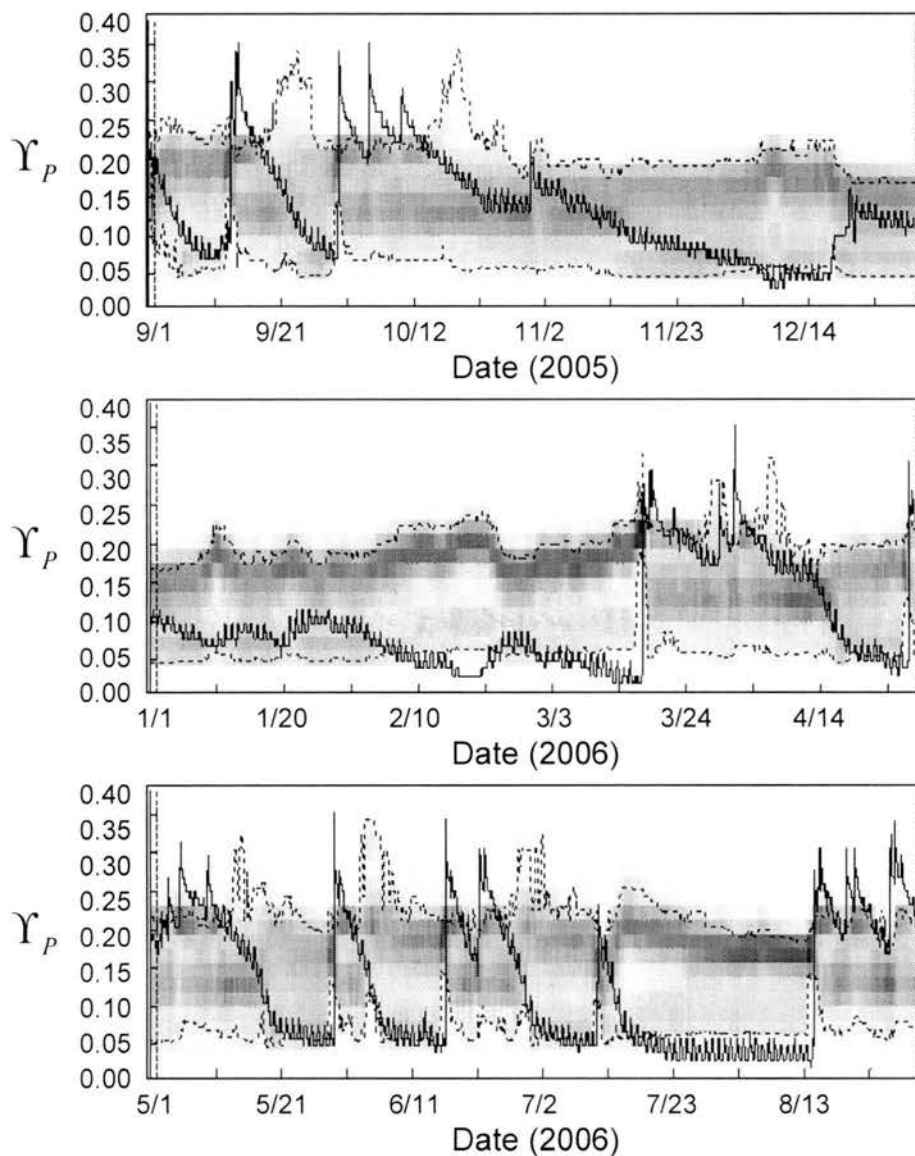


Figure F.1. SIA results from September 2005 through August 2006 for the PDM applied locally by increasing precipitation by 10% at station F103 at 5 cm depth.

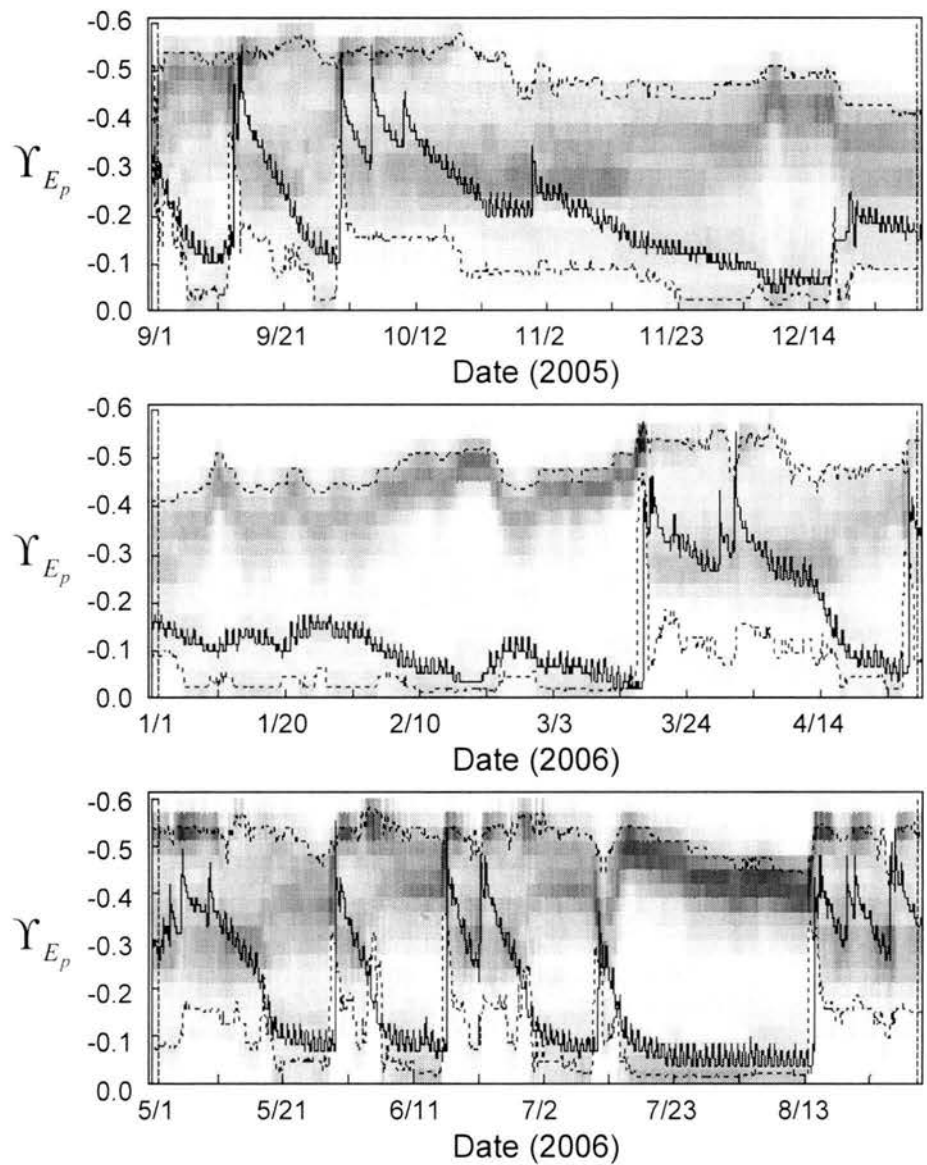


Figure F.2. SIA results from September 2005 through August 2006 for the PDM applied locally by increasing E_p by 10% at station F103 at 5 cm depth.

Appendix G

SIA results for the PDM applied locally at station F103 at 25 cm

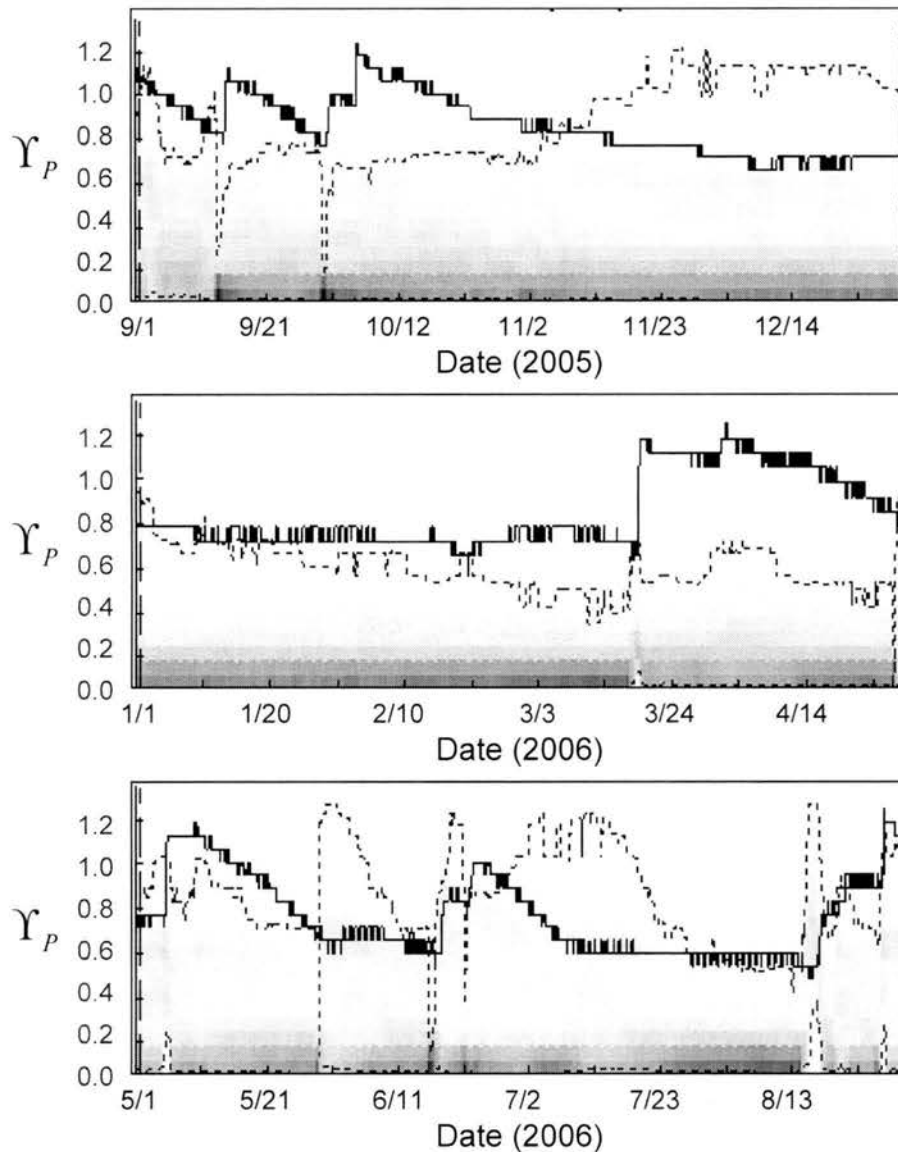


Figure G.1. SIA results from September 2005 through August 2006 for the PDM applied locally by increasing precipitation by 10% at station F103 at 25 cm depth.

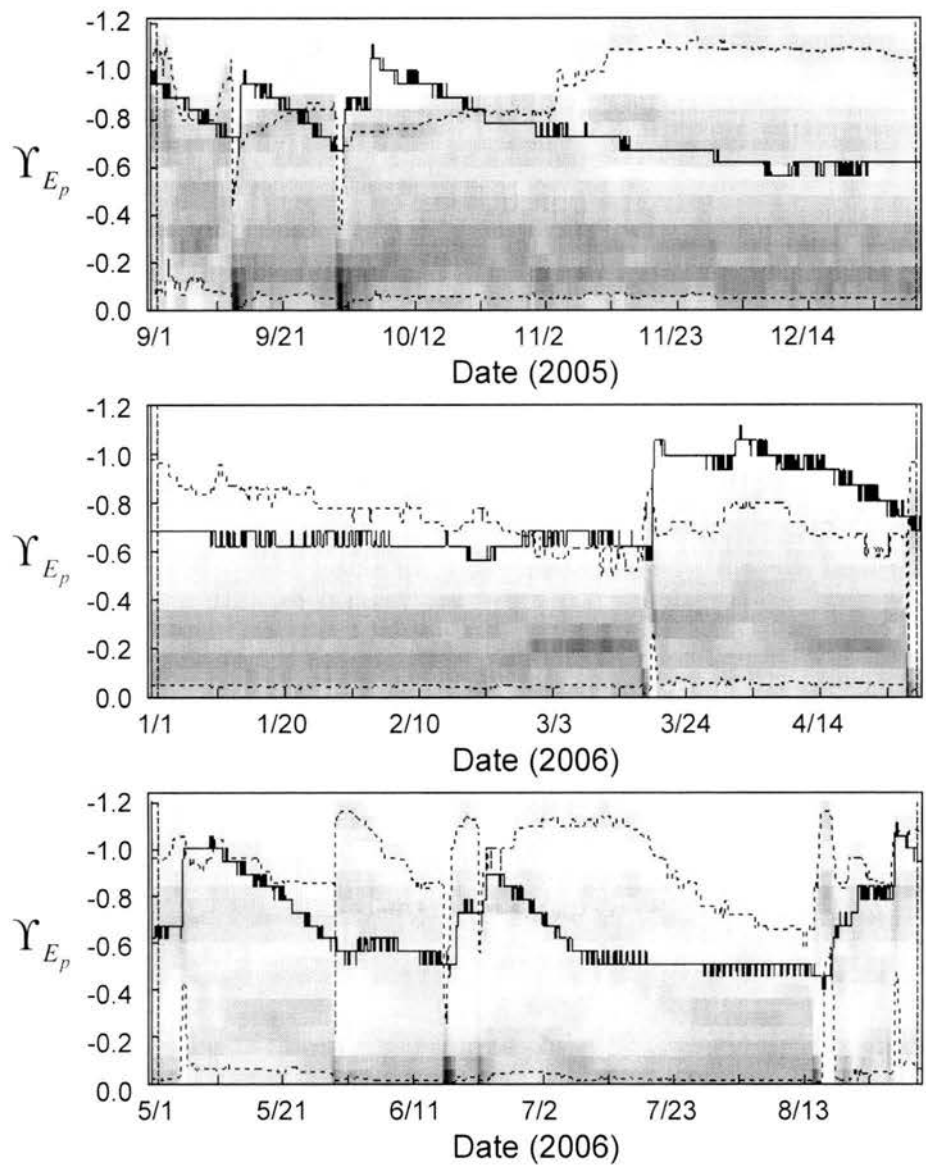


Figure G.2. SIA results from September 2005 through August 2006 for the PDM applied locally by increasing E_p by 10% at station F103 at 25 cm depth.

Appendix H

DYNIA results for the PDM applied to simulate the spatial average at 5 cm.

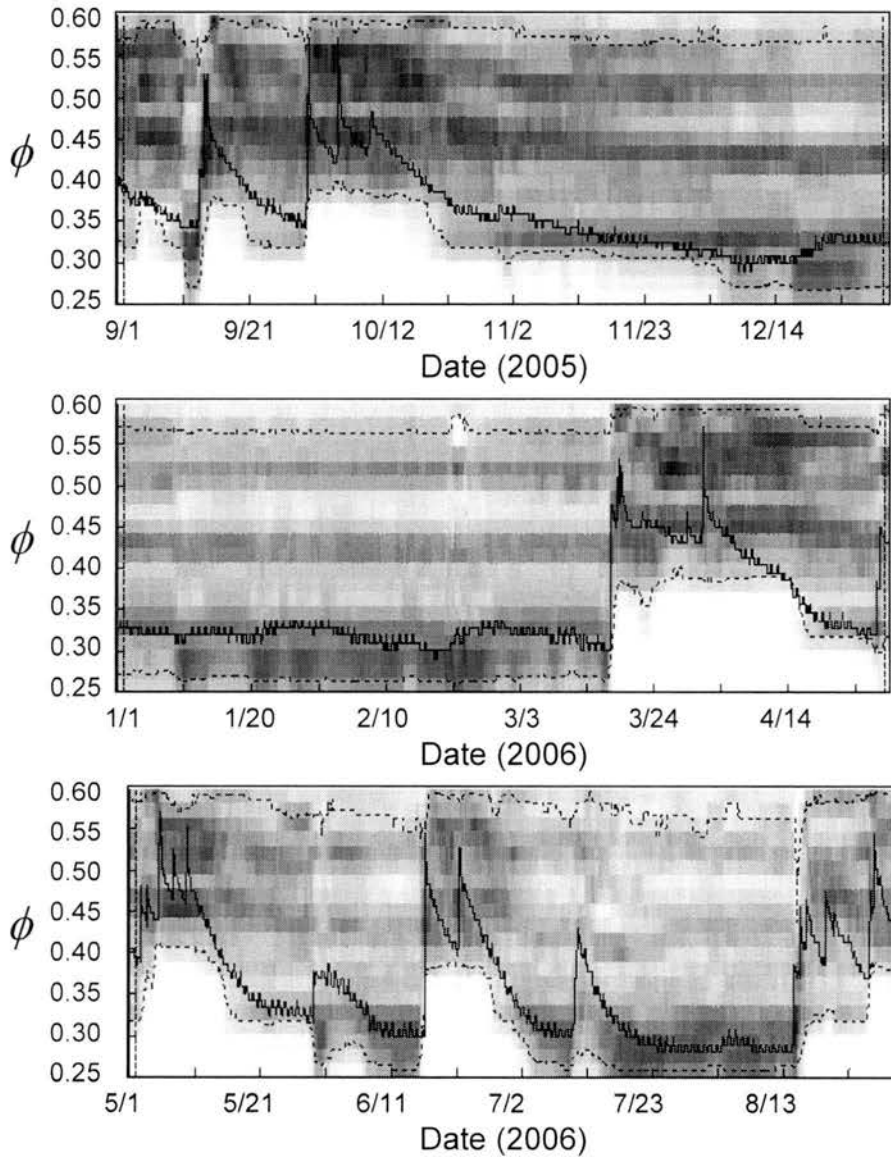


Figure H.1. ϕ parameter DYNIA results for September 2005 through August 2006 for the PDM applied spatially for the 5cm depth.

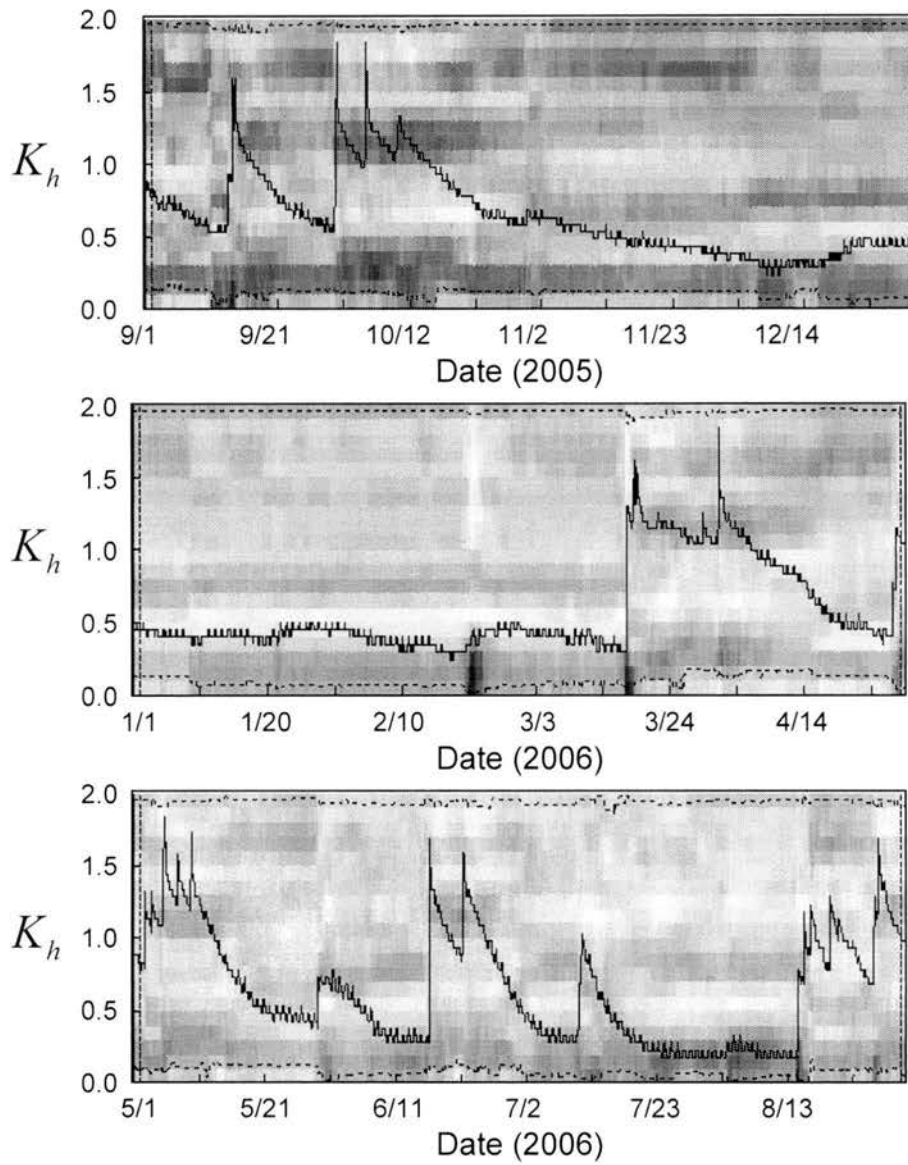


Figure H.2. K_h parameter DYNIA results for September 2005 through August 2006 for the PDM applied spatially for the 5cm depth.

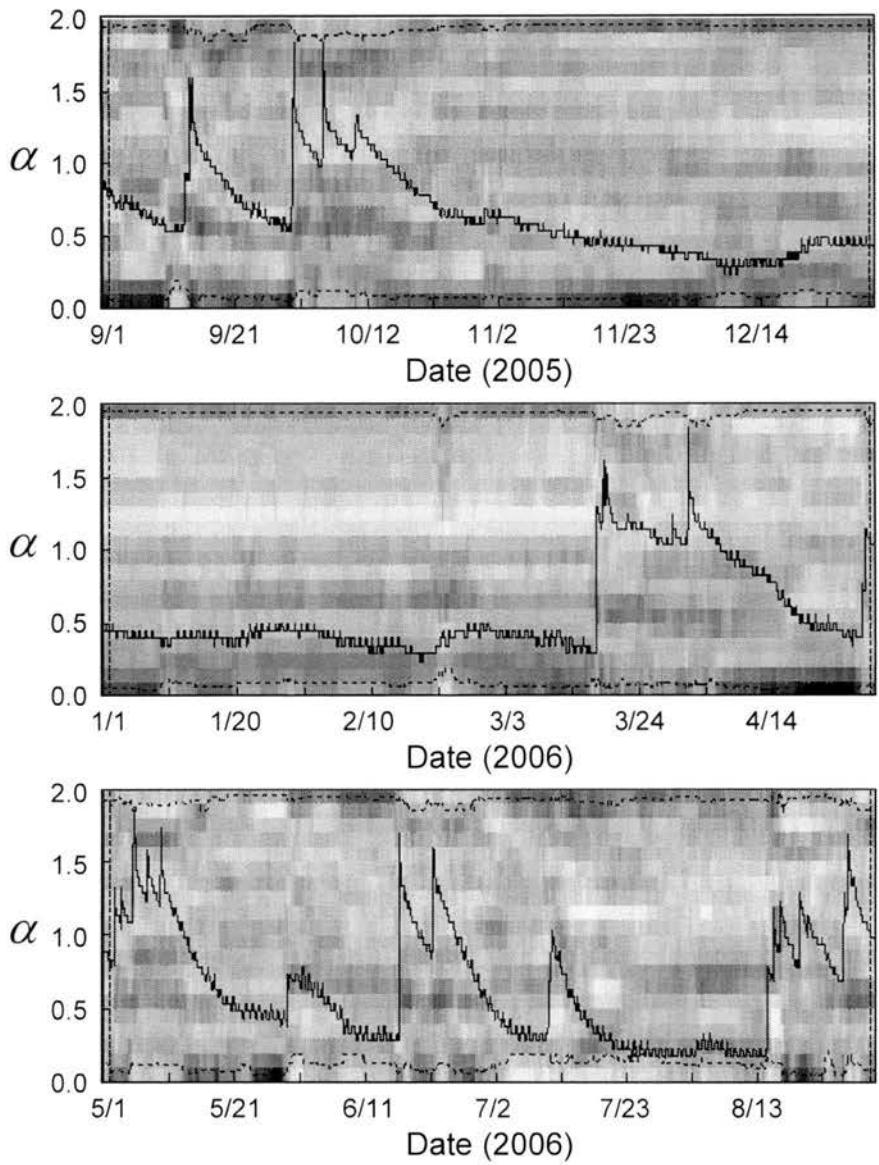


Figure H.3. α parameter DYNIA results for September 2005 through August 2006 for the PDM applied spatially for the 5cm depth.

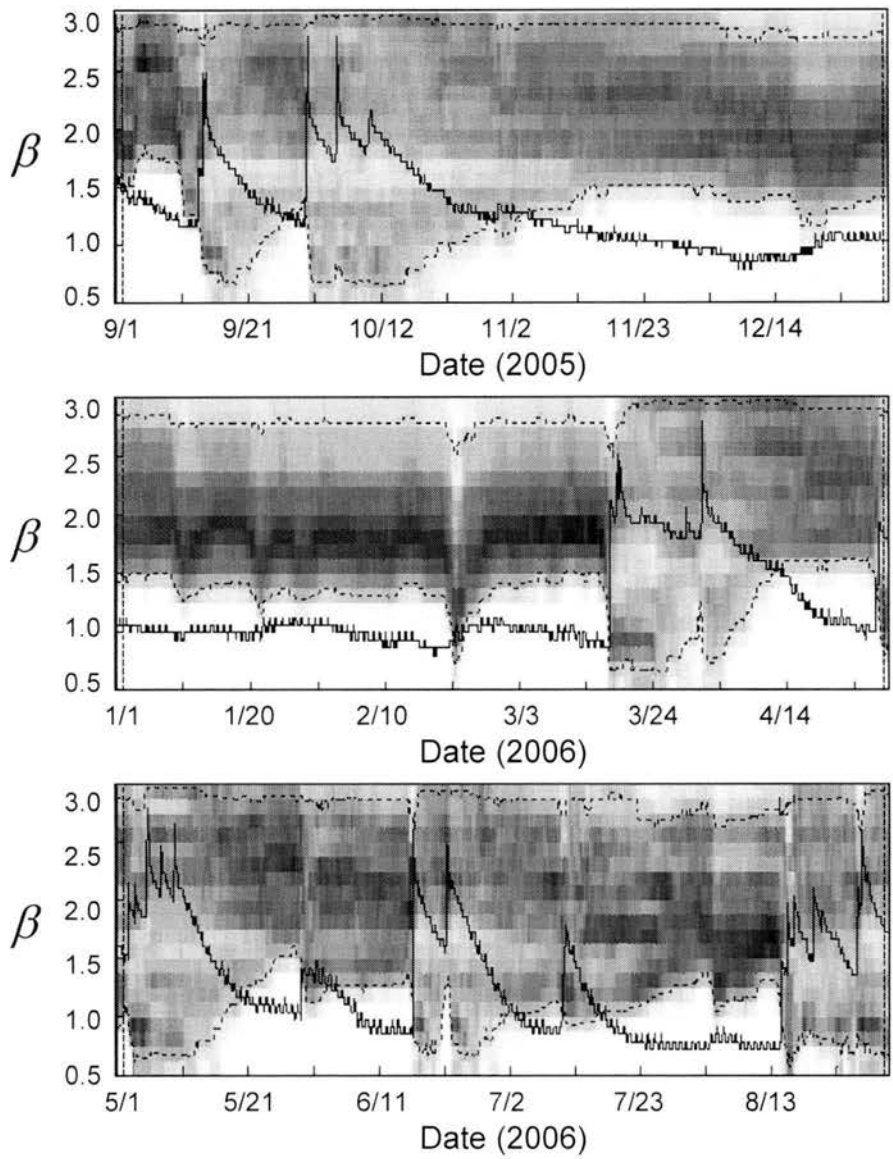


Figure H.4. β parameter DYNIA results for September 2005 through August 2006 for the PDM applied spatially for the 5cm depth.

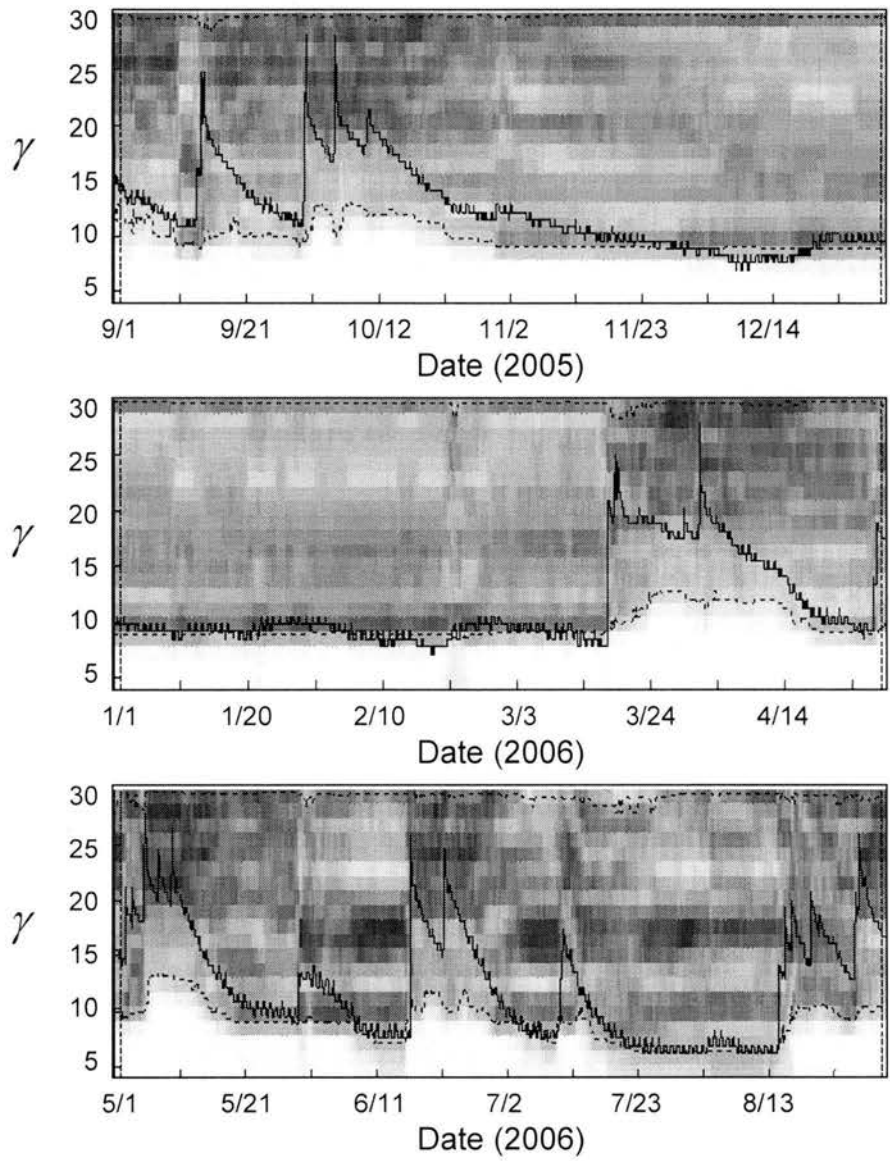


Figure H.5. γ parameter DYNIA results for September 2005 through August 2006 for the PDM applied spatially for the 5cm depth.

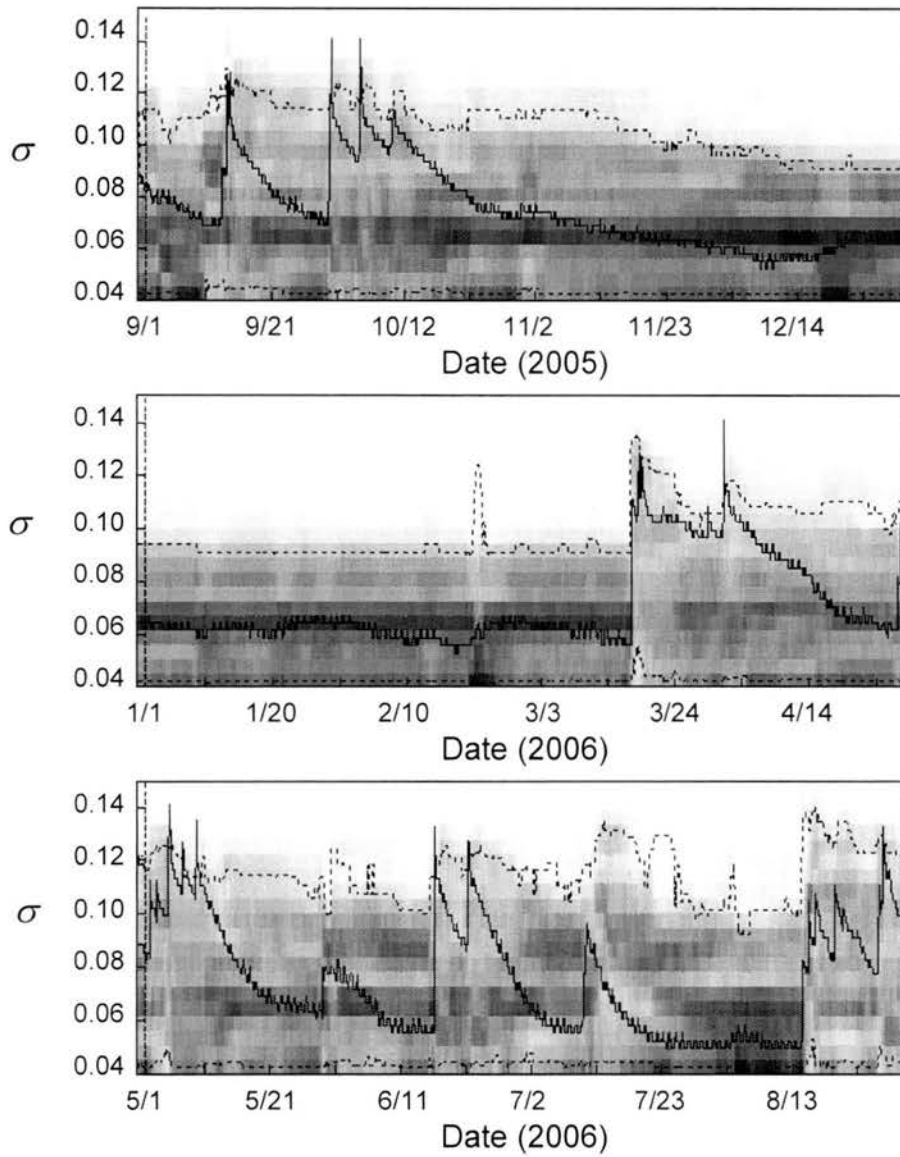


Figure H.6. σ parameter DYNIA results for September 2005 through August 2006 for the PDM applied spatially for the 5cm depth.

Appendix I

DYNIA results for the PDM applied to simulate the spatial average at 25 cm.

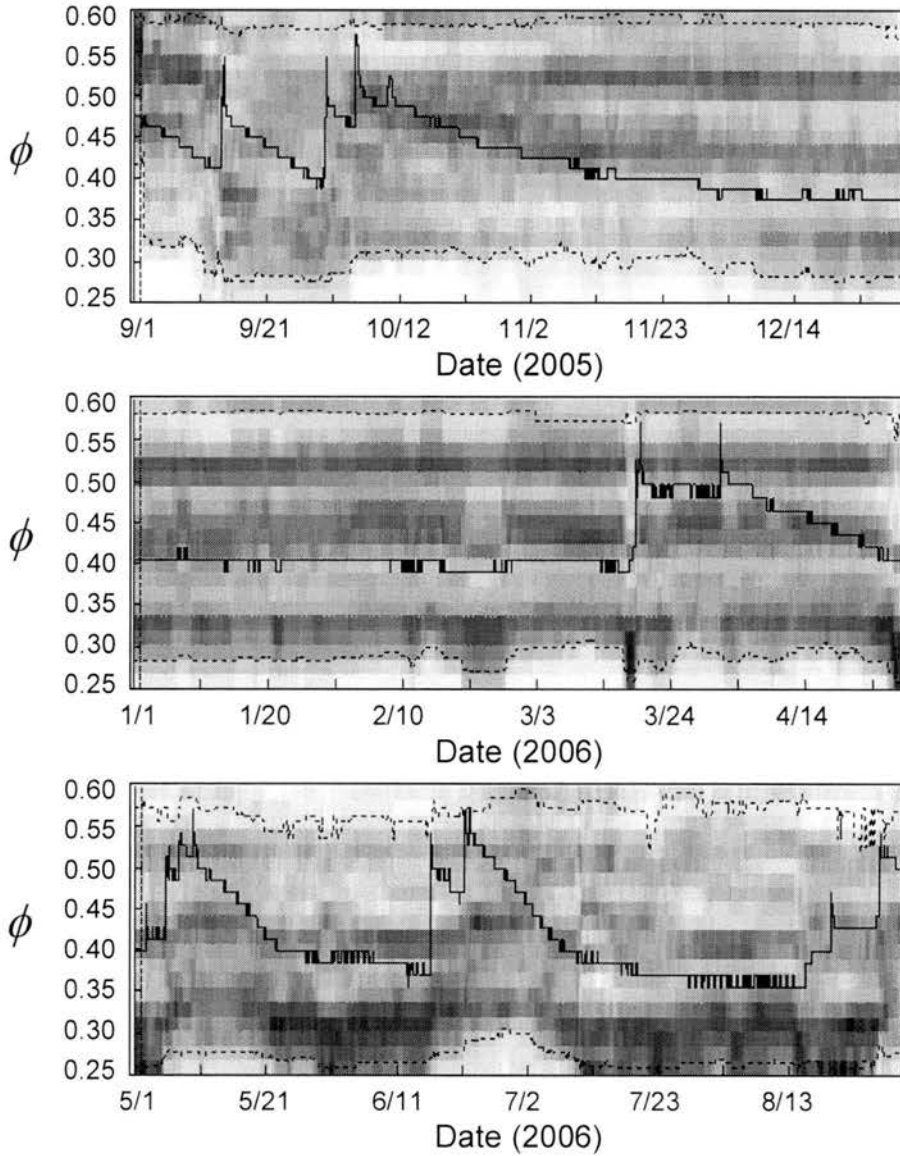


Figure I.1. ϕ parameter DYNIA results for September 2005 through August 2006 for the PDM applied spatially for the 25cm depth.

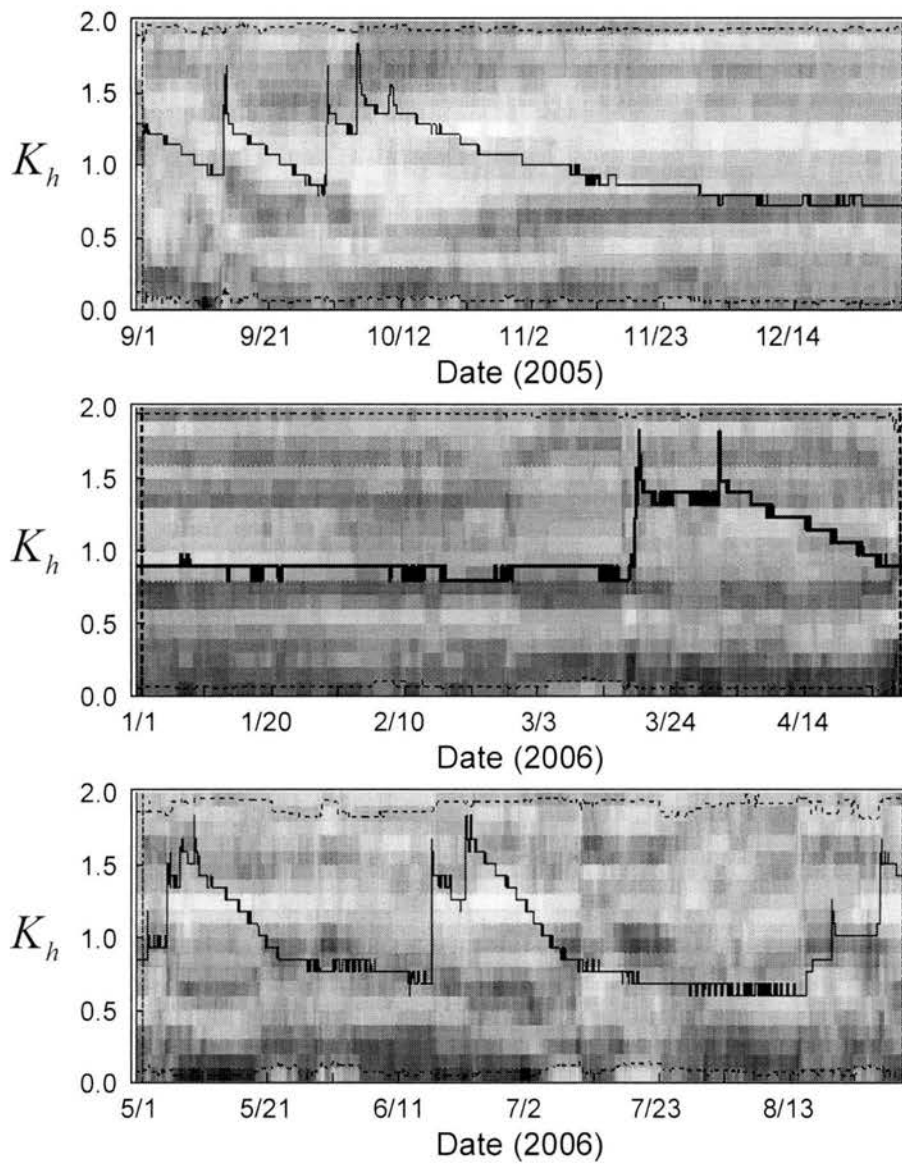


Figure I.2. K_h parameter DYNIA results for September 2005 through August 2006 for the PDM applied spatially for the 25cm depth.

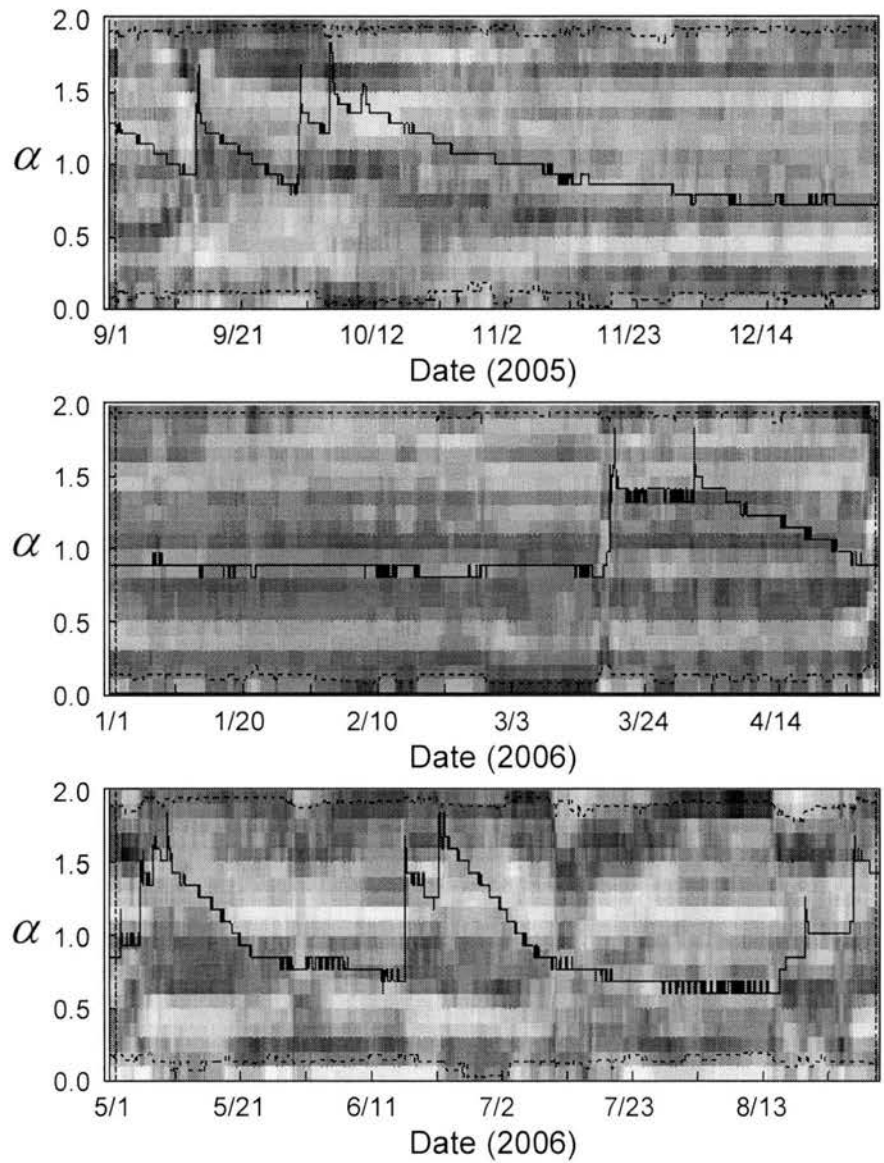


Figure I.3. α parameter DYNIA results for September 2005 through August 2006 for the PDM applied spatially for the 25cm depth.

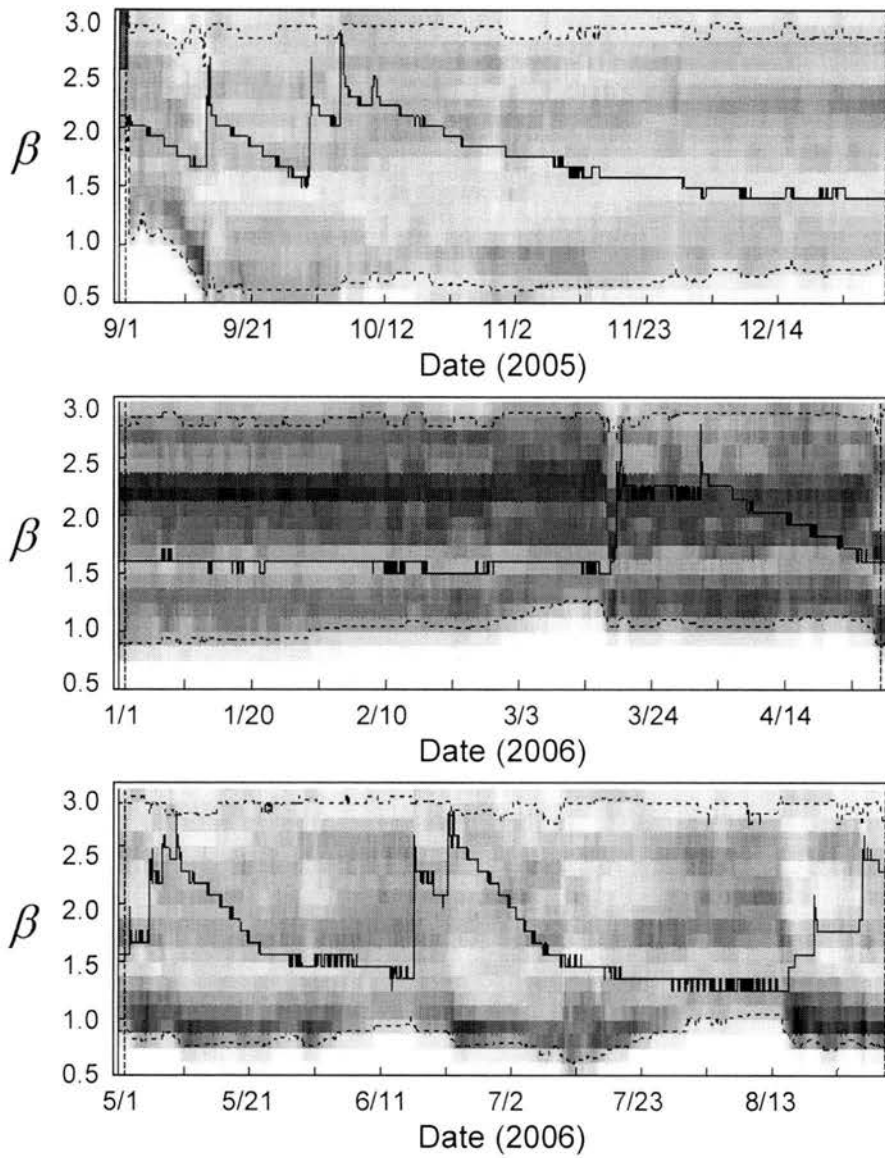


Figure I.4. β parameter DYNIA results for September 2005 through August 2006 for the PDM applied spatially for the 25cm depth.

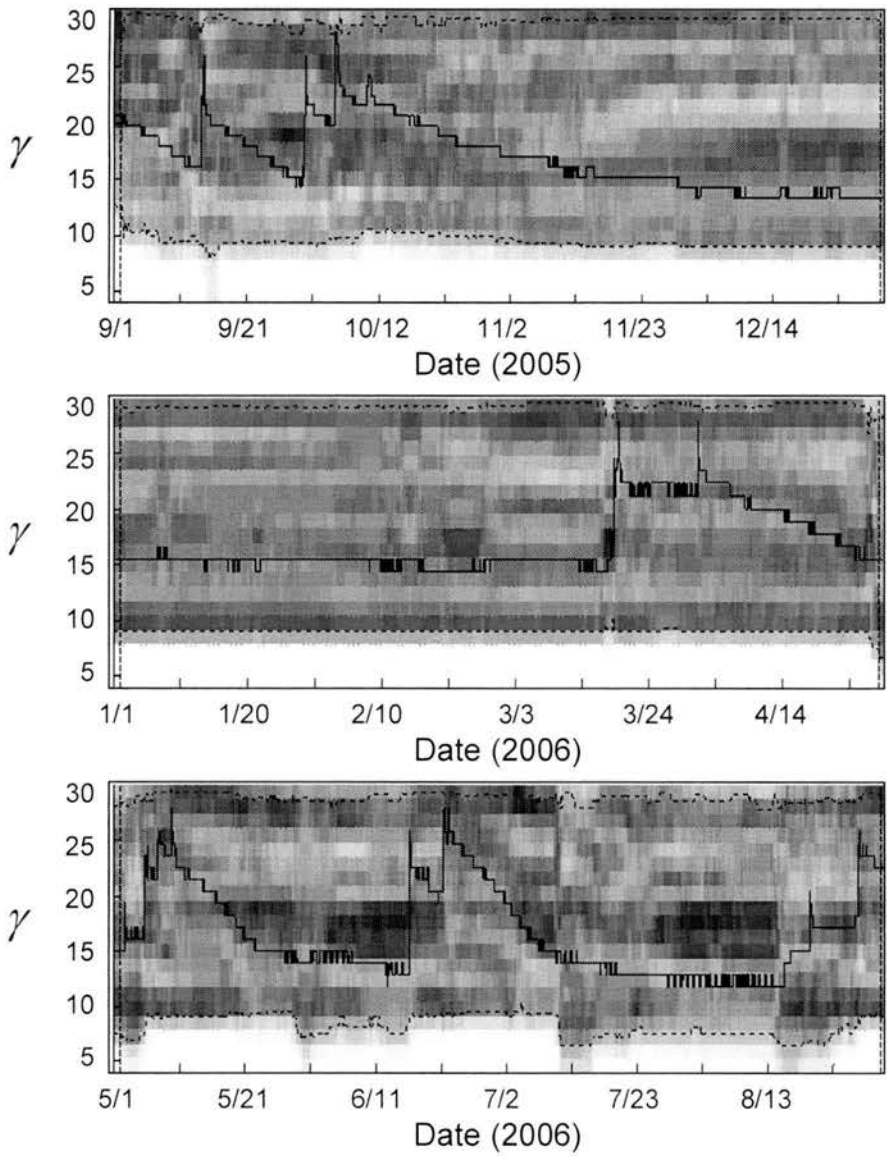


Figure I.5. γ parameter DYNIA results for September 2005 through August 2006 for the PDM applied spatially for the 25cm depth.

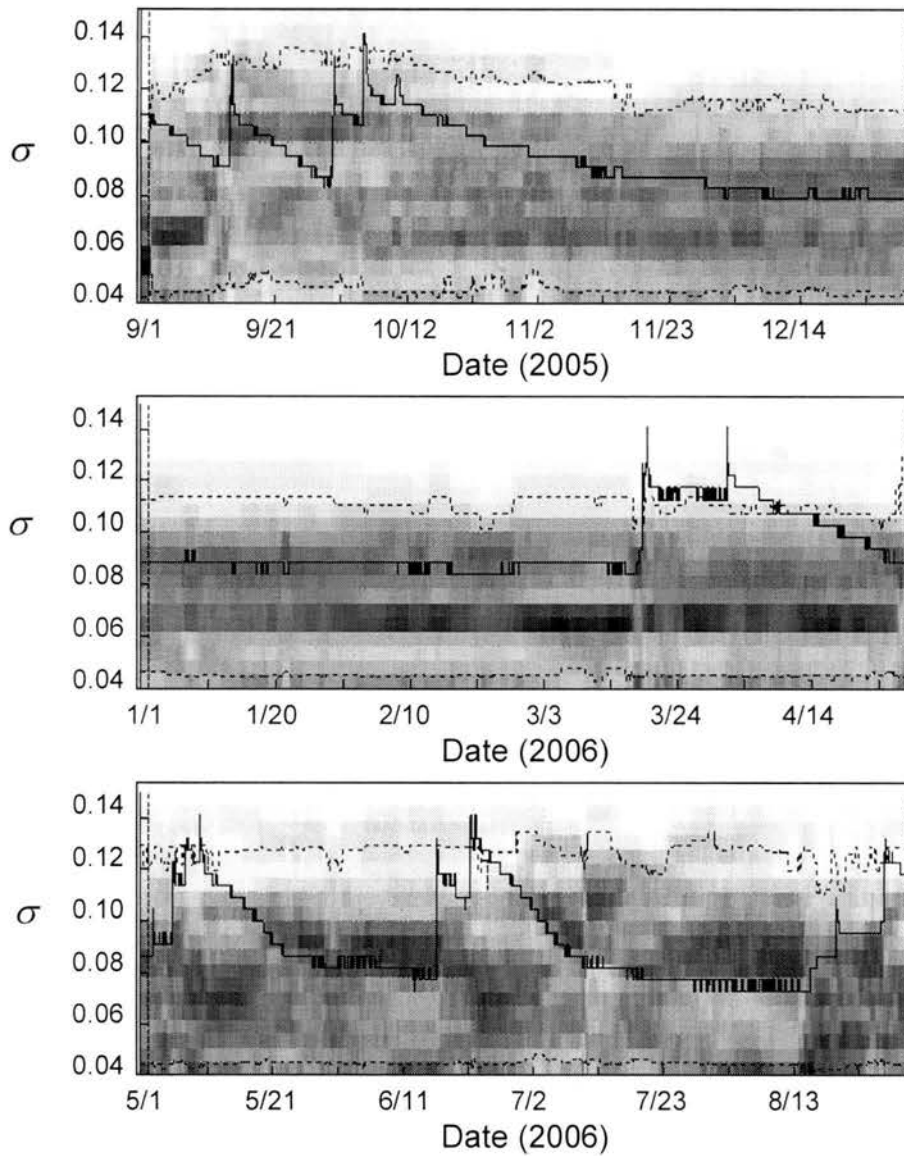


Figure I.6. σ parameter DYNIA results for September 2005 through August 2006 for the PDM applied spatially for the 25cm depth.

Appendix J

SIA results for the PDM applied to simulate spatial average soil moisture at 5 cm depth.

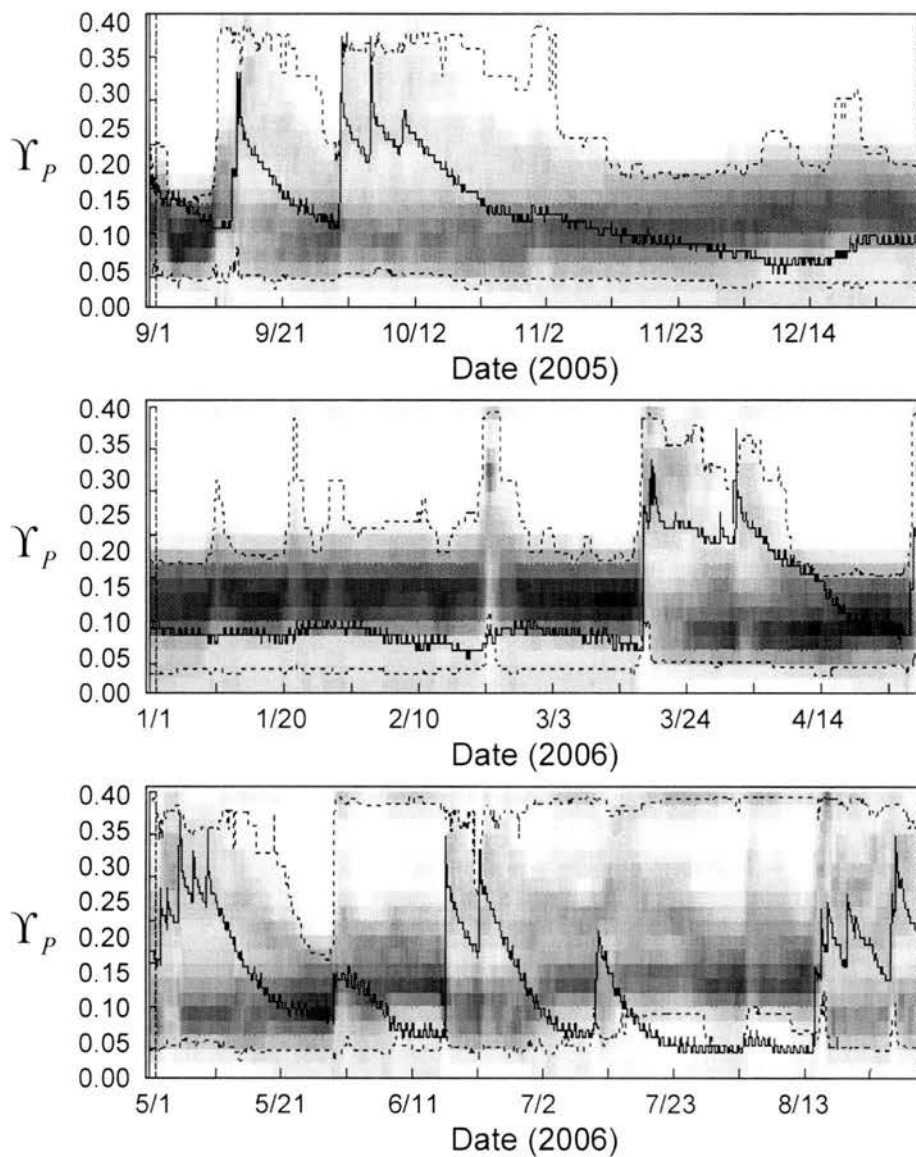


Figure J.1. SIA results from September 2005 through August 2006 for the PDM applied spatially by increasing precipitation by 10% at station F103 at 5 cm depth.

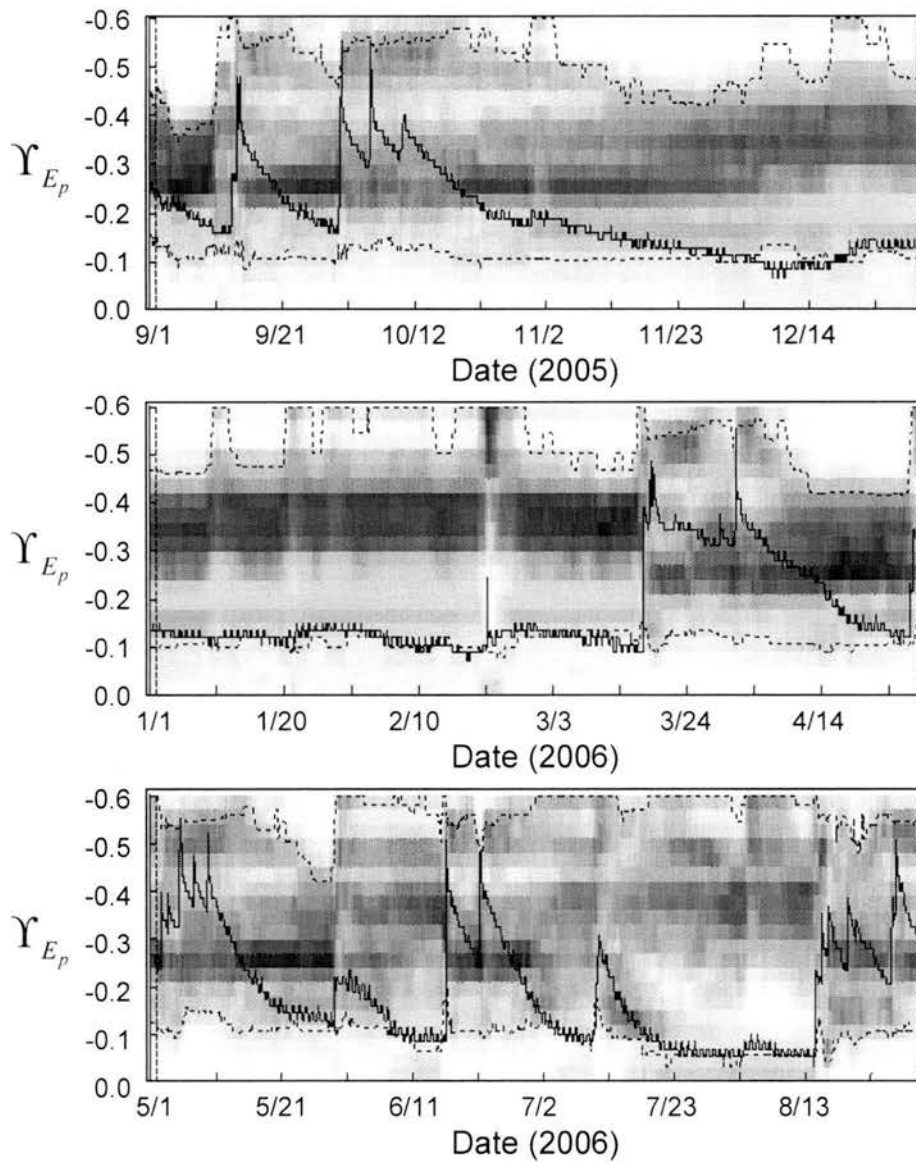


Figure J.2. SIA results from September 2005 through August 2006 for the PDM applied spatially by increasing E_p by 10% at station F103 at 5 cm depth.

Appendix K

SIA results for the PDM applied to simulate spatial average soil moisture at 25 cm depth.

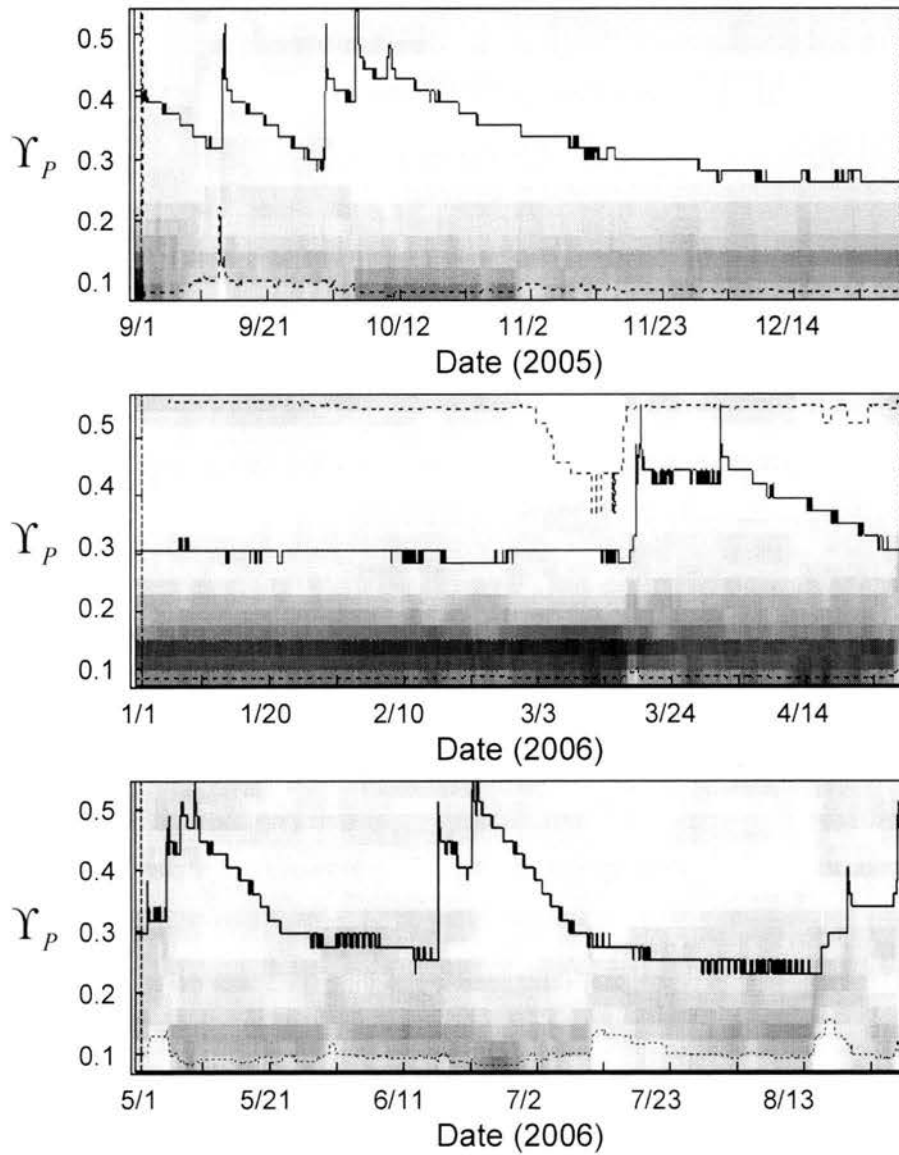


Figure K.1. SIA results from September 2005 through August 2006 for the PDM applied spatially by increasing precipitation by 10% at station F103 at 25 cm depth.

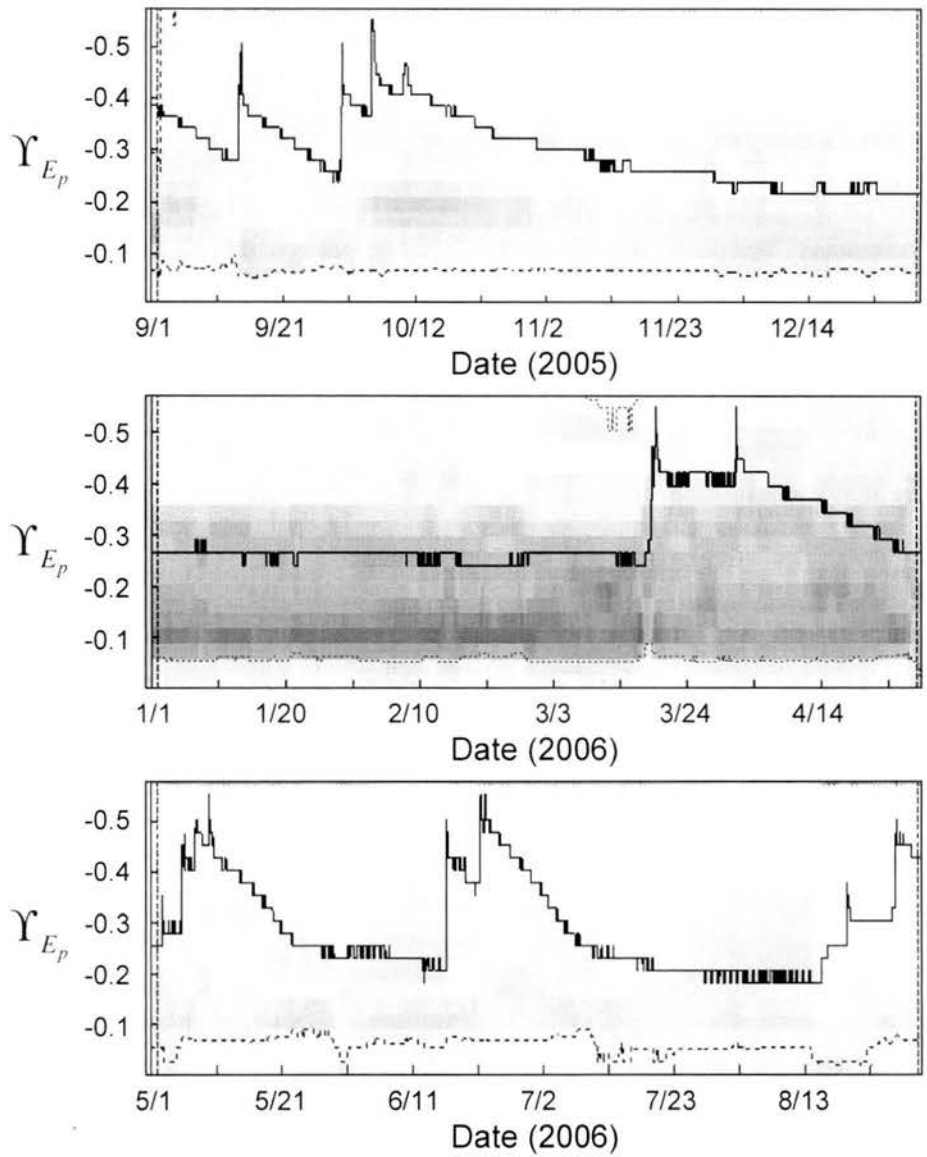


Figure K.2. SIA results from September 2005 through August 2006 for the PDM applied spatially by increasing potential evapotranspiration by 10% at station F103 at 25 cm depth.